BRNO UNIVERSITY OF TECHNOLOGY

Faculty of Mechanical engineering

# PHD THESIS

Brno, 2019 Ing. Erik Bartuli


# BRNO UNIVERSITY OF TECHNOLOGY

VYSOKÉ UČENÍ TECHNICKÉ V BRNĚ

## FACULTY OF MECHANICAL ENGINEERING

FAKULTA STROJNÍHO INŽENÝRSTVÍ

## HEAT TRANSFER AND FLUID FLOW LABORATORY

LABORATOŘ PŘENOSU TEPLA A PROUDĚNÍ


# OPTIMIZATION OF HEAT TRANSFER SURFACES OF HEAT EXCHANGERS

OPTIMALIZACE TEPLOSMĚNNÝCH PLOCH TEPELNÝCH VÝMĚNÍKŮ

DOCTORAL THESIS

DIZERTAČNÍ PRÁCE


AUTHOR — Ing. Erik Bartuli

AUTOR PRÁCE

SUPERVISOR — prof. Ing. Miroslav Raudenský, CSc.

ŠKOLITEL



BRNO 2019

# ABSTRACT

The thesis focuses on metal and plastic heat exchangers. The main object of the research is the optimization of heat transfer surfaces for increase of heat transfer characteristics of heat exchangers. A computer modeling via ANSYS and experimental research were used for this purpose. A cross-wiring technology for plastic hollow fiber heat exchangers (PHFHE) producing was developed based on modeling and experimental results. An experimental setup used for pressure tanks winding was modified for PHFHE mass production.

Heat exchangers for air condition systems were also considered in this work. Example of twisted hollow fiber heat exchanger use in such systems is presented. Influence of thermal cycling test to heat transfer performance of common metal fin-type heat exchanger was also studied.



# ABSTRAKT

Disertační práce je zaměřena na kovové a polymerní výměníky tepla. Hlavním předmětem zkoumání je optimalizace teplosměnných ploch za účelem zvýšení účinnosti výměníku tepla. Tyto cíle byly dosaženy experimentálně a numericky pomocí modelování v ANSYS. Na základě dosažených výsledků byla rozpracována technologie křížového navíjení polymerních výměníků z dutých vláken. Experimentální zařízení původně určené pro navíjení tlakových nádrží bylo modifikované pro automatizovanou výrobu polymerních výměníků z dutých vláken, ježto může být použita při jejich masové výrobě.

Tato práce se také zabývala výměníky tepla pro klimatizační systémy. Byly zkoumány možnosti využití polymerních výměníků z dutých vláken v těchto systémech. Mimo jiné byla provedena studie vlivu cyklického tepelného zatížení standardního kovového žebrovaného tepelného výměníku.

## KEY WORDS

hollow fibers, radiator, heat exchanger, optimization, intensification

## KLÍČOVÁ SLOVA

dutá vlákna, radiátor, tepelný výměník, optimalizace, intensifikace

## CITATION

BARTULI, Erik. *Optimization of heat transfer surfaces of heat exchangers*. PhD thesis. Brno: Brno University of Technology, Faculty of Mechanical Engineering, Heat transfer and fluid flow laboratory, 2019. 92 p. Supervisor: prof. Ing. Miroslav Raudenský, CSc.

# PRONOUNCEMENT

I declare that my thesis for Philosophy Doctor degree on “Optimization of heat transfer surfaces of heat exchangers” I have made independently under the supervision of a doctoral thesis and using specialized literature and other information resources, all of which are quoted in the work and listed in the references at the end of the thesis.

As the author of the doctoral thesis I further declare that in connection with the creation of this doctoral thesis I did not infringe the copyrights of third parties, in particular I did not interfere illegally with foreign copyrights of personality and / or property and I am fully aware of the consequences of violation of S 11 and following Act No. 121/2000 Coll., on copyright, on rights related to copyright and amending certain acts (Copyright Act), as amended, including the possible criminal consequences resulting from the provisions of Part Two, Title VI. Part 4 of the Criminal Code No. 40/2009 Coll.

Brno ……. ……

author signature

# ACKNOWLEDGMENT

I would like to express my gratitude to supervisor of my PhD thesis prof. Ing. Miroslav Raudenský, CSc. and to prof. Ing. Jaroslav Horský, CSc. for their professional guidance, valuable comments and advice.

I am also grateful to my colleagues from the Heat Transfer and Fluid Flow Laboratory for their technical support, discussions and advice.

Last but not least, I would like to thank my wife and my parents for great support and understanding. I am very grateful that you come through this long way with me.

Brno ..... .....

author signature

# CONTENT

# PURPOSES OF WORK

Research and development of polymeric heat exchangers with hollow fibers started at Brno University of Technology, Heat Transfer and Fluid Flow Laboratory in 2008. Topic of this study builds on previous research work and is predominantly aimed to the optimization of geometry of heat transfer surfaces.

The individual objectives of the thesis were formulated on the basis of the state doctoral examination as follows:

Optimization of metal heat transfer surfaces for heat exchangers consisting of a metal tube with pressed ribs. Optimization will be done for the cases of small flow rates. The noise aspects and the influence of cyclic heat pulses on the heat exchanger efficiency will be considered.

Optimization of the polymeric hollow fiber arrangement in the heat exchanger in order to achieve a maximum heat transfer performance of highly compact exchangers. An optimal geometric solution will be considered for fluids and gases flow.

The aims of the thesis will be achieved by combining experimental laboratory research with numerical simulations.

# INTRODUCTION

Devices intended to transfer heat from one fluid to another are commonly called heat exchangers. Different thermal processes such as temperature change, evaporation, boiling, condensation, melting and finally more complex combined processes can occur in heat exchangers. Number of fluids involved in these processes can be more than two, for example, heat can be transferred from one body to another several bodies or conversely from several bodies to the one. These bodies which give and receive heat are called the working fluid. Working fluids may be either gases or liquids.

Heat exchangers are widely used in various industrial manufacturing processes, building heating and conditioning systems, in engines with internal and external combustion, in refrigerating system and in many other fields. The most frequent material from which these devices are manufactured is metal (copper, aluminum and so on). One of the most common type of metal heat exchangers is a heat exchanger made of copper coil pipe with aluminum fins. But these days exist a lot of heat exchangers which are made of other materials such as graphite and polymers. Polymeric heat exchangers become more and more popular in different engineering fields because of their important features to compare with metal heat exchangers.

Polymeric hollow fiber heat exchanger (PHFHE) is a heat exchanger which uses small hollow fibers with outer diameter less than 1.5 mm as a heat transfer aria. The wall thickness of this polymeric fibers is approximately 0.1 mm. Small diameter of the hollow fibers and it thick wall reduces the influence of polymeric thermal resistance on heat transfer performance of all device. Also, these heat exchangers are very compact and have a big heat transfer area to compare with its dimensions.

For improving a heat transfer performance of heat exchangers exist a lot of different methods. Usually they are connected with an optimization of heat transfer surfaces of heat exchangers.

# 1. THEORY OF HEAT TRANSFER

## 1.1 Heat transfer types

Heat transfer is a spontaneous process of heat transfer in the space with the inhomogeneous temperature field. Temperature field is an aggregate of temperature instantaneous values at all points of the considering space. Since the temperature is a scalar value, the temperature field is also a scalar value. Depending on the nature of the thermal motion, the following types of heat transfer are distinguished:

1. thermal conductivity is a molecular heat transfer in a medium with non-uniform temperature distribution by the thermal motion of microparticles;
2. convection is a heat transfer in a medium with non-uniform temperature distribution taking place at medium motion;
3. radiation is a heat transfer, including a transition of the body internal energy to the radiation energy, transport of the radiation and conversion of the radiation energy to the internal energy of another body.

Simultaneous combined effect of three basic types of heat transfer is called a complex heat exchange. However, very often the role of one or another constituent in the overall heat balance is slight, and then heat transfer processes receive separate, special names.

This work deals with metal and polymeric heat exchangers intended for air-water and water-water applications and operated at natural or forced convection. Therefore, the focus was made on this type of heat transfers. In further part a theoretical description of several special cases, connected with investigated heat exchangers, will be presented.

## 1.2 Convection

In liquids and gases, a convective heat transport due to the motion of medium volumes is imposed upon the thermal conductivity process. The inhomogeneous temperature field leads to the appearance of inhomogeneous densities field: in areas with a higher temperature density of the medium due to thermal expansion is reduced, and vice versa. Non-uniform field of gravitational mass forces appears. So, a difference in densities connected with the temperature gradient is equal to

$$\frac{\rho}{\rho_0} = 1 + \beta \Delta T \qquad (1)$$

where $\beta = -\frac{1}{\rho}\left(\frac{d\rho}{dT}\right)_p$ is a coefficient of volume expansion.

Lifting force of volume unit (Archimedean force) is equal to

$$g(\rho - \rho_0) = -g\rho\beta\Delta T \qquad (2)$$

Heat transfer during medium motion due to Archimedean force is called free or natural convection. In general, free convection can take place during the liquid motion under the non-uniform field of not only gravity, but other mass forces [1].

If the medium motion is caused by the action of external forces, applied on the system boundary, or due to the kinetic energy, forced to the liquid from the outside of system, such heat transfer process is called a forced convection. The heat transfer intensity during the forced convection is significantly higher than at free convection.

In the most cases of convective heat transfer characteristic dimensions of the working fluid flow area are significantly higher than the free path length of structural particles (atoms and molecules). This allows to consider liquids and gases as a continuous medium with the use of such statistical concepts as temperature, pressure, viscosity and heat transfer rate even for very small their volumes. The temperature field in such mediums can also be considered as a continuous and all of the concepts discussed above can be applied.

Heat transfer due to the medium motion cab be described by the equation

$$\vec{q} = -\lambda_f grad T + c_p \rho_f \vec{w} T \qquad (3)$$

Here$\lambda_f$,$c_p$,$\rho_f$ are the thermal conductivity, the heat transfer rate and the medium density at *p=const*. On the right side of this equation the first term takes into account the molecular heat transfer and the second - the convective (molar) heat transfer. When exists the convective heat exchange of the medium with a surface, this equation can be transformed upon the condition that on the surface the tangent velocity of medium motion is equal to zero.

The velocity component normal to the surface depends on the presence of material flows on the surface. In the case of such flows presence the medium motion normal to the surface occurs.

During "pure" heat transfer the velocity normal component is also equal to zero. At $n \to 0$, $w=0$, $grad T = grad T|_{n\to 0}$ the equation takes the form

$$\vec{q} = -\lambda_f grad T|_{n\to 0} \qquad (4)$$

When calculating the heat transfer between the surface and the environment equation (4) is usually used in the form of Newton's law, introducing a convective heat transfer coefficient h (W/m²K)

$$h = \frac{-\lambda_f grad T|_{n\to 0}}{\Delta T} \qquad (5)$$

and

$$q = h\Delta T \qquad (6)$$

where $\Delta T$ is a temperature difference between the surface and the environment.

Equation (6) is called Newton's law for heat transfer. The convective heat transfer coefficient h, as opposed to the thermal conductivity λ, is not a physical characteristic of the body. The convective heat transfer coefficient h can be regarded as a function of the process, which depends on many different factors: body shape and size, temperature, pressure and velocity of the medium, physical properties of the medium and so on. The approximate range of numerical values of h is shown in Tab. 1.

*Tab. 1 The range of numerical values of the convective heat transfer coefficient, depending on the motion regime [1].*

| Motion regime | Convective heat transfer coefficient h, (W/m²K) |
|---|---|
| Free gas convection | 5...50 |
| Forced gas convection | $30...5 \cdot 10^2$ |
| Free water convection | $10^2... 10^3$ |
| Forced water convection | $5 \cdot 10^2... 2 \cdot 10^4$ |

### 1.2.1 Thermal boundary layer

Let's say that there is a conditional layer near the surface with a thickness $\delta_T$, wherein temperature changes from the surface temperature ($T_w$) to the ambient temperature ($T_f$) (see Fig. 1) and the heat transfer occurs due to liquid thermal conductivity. Then the average temperature gradient in this layer is equal to $\left(\frac{\Delta T}{\Delta n}\right)_{ave} = \frac{T_w - T_f}{-\delta_T}$. Sign "minus" appears, as in Fig. 1 the thickness $\delta_T$ is measured from the surface in a direction opposite to the positive direction of the normal.

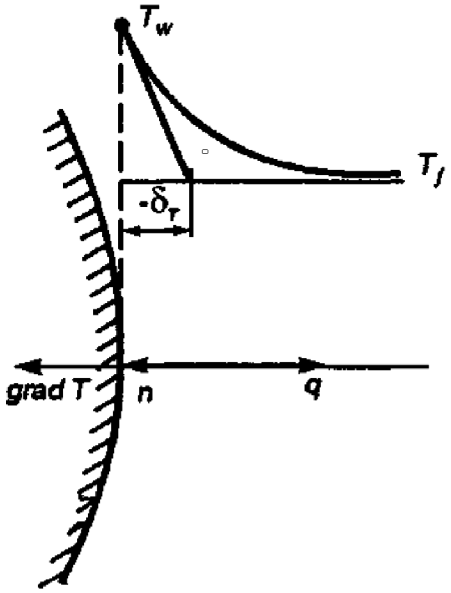


*Fig. 1 Thermal boundary layer [1].*

Then, if written approximately $\frac{\partial T}{\partial n}\Big|_{n\to 0} \approx \left(\frac{\Delta T}{\Delta n}\right)_{ave} = \frac{T_w - T_f}{-\delta_T} = \frac{\Delta T}{\delta_T}$, where $\Delta T$is a positive temperature drop. Then from equation (5) we find:

$$h = \frac{-\lambda_f grad T|_{n\to 0}}{\Delta T} = \frac{\lambda_f}{\delta_T} \tag{7}$$

Hence, we obtain the expression for the boundary layer thickness

$$\delta_T = \frac{\lambda_f}{h} \tag{8}$$

Then the equation (4) takes the view

$$q = h\Delta T = \frac{\lambda_f}{\delta_T}\Delta T \tag{9}$$

The modern theory of convective heat transfer is mainly based on the boundary layer theory. For the simplest cases an analytical solution can be given.

### 1.2.2 Heat transfer during flow around the flat surface

During the calculations for the laminar boundary layer allow the similarity of velocity and temperature fields (see Fig. 2). The average heat transfer coefficient for a plate of length *l* is equal to

$$\bar{h} = 0{,}664\frac{\lambda_f}{l}\sqrt[3]{Pr}\sqrt{\overline{Re}} \tag{10}$$

and in dimensionless quantities

$$\overline{Nu} = 0{,}664\sqrt[3]{Pr}\sqrt{\overline{Re}} \tag{11}$$

where $\overline{Nu} = \frac{\bar{h}l}{\lambda_f}$ and $\overline{Re}\frac{wl}{v}$.

In these equations the average liquid temperature ($T_f$) is taken as a determining temperature and the longitudinal coordinate or the plate length *l* is taken as a determining size. This equation can also be used for the calculation of heat transfer during axial flow around the horizontal pipe.

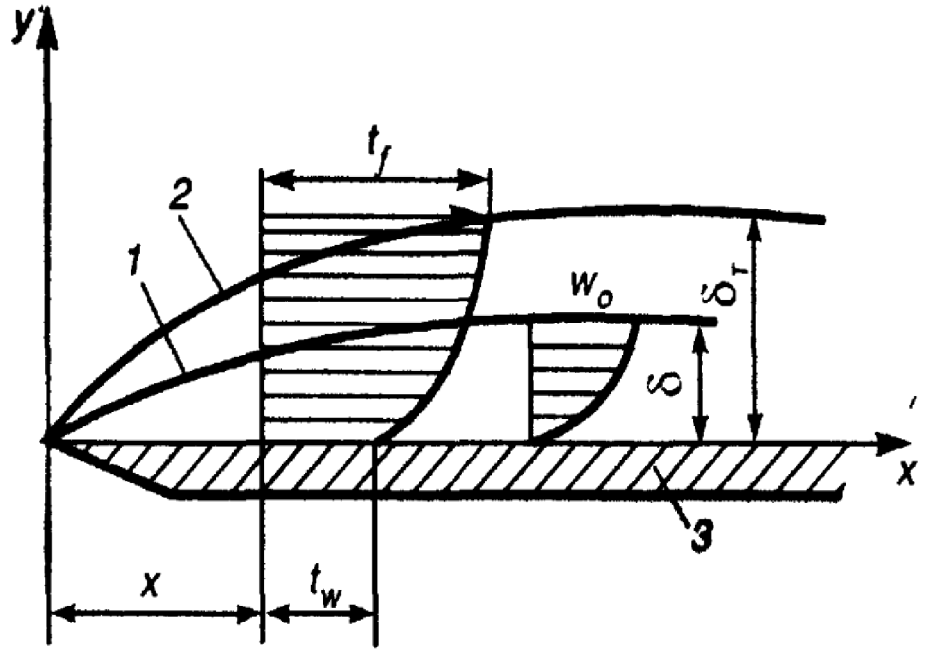


*Fig. 2 Distribution of velocity and temperature fields in the laminar boundary layer: 1 – velocity field, 2 – temperature field, 3 - body surface. δ - hydrodynamic boundary layer, $\delta_T$ - thermal boundary layer, $w_0$ – velocity of core flow, δT - thermal boundary layer, $t_w$ - surface temperature, $t_f$ - undisturbed flow temperature [1]*

More difficult task is to calculate convection between two walls. In the article [2] a thermal field and heat transfer characteristics of a system consisting of two staggered vertical plates cooled by air in free convection were experimentally studied. The stability of buoyancy-driven convection in a vertical infinite fluid layer between two rigid walls with different thermal conductivities and thicknesses is presented in the article [3]. It is shown in the article that the thermal conductivity and thickness of the walls has a weak influence on hydrodynamic modes but a strong influence on thermal modes which become critical for lower values of Prandtl number than in the case of perfect conducting walls.

### 1.2.3 Heat transfer during crossflow of a single cylinder

Scheme of an unrestricted cylinder streamlining by a liquid cross-flow is given in Fig 3. The boundary layer has a minimum thickness in the frontal part (φ = 0) and increases to the middle section (φ = 90°). The heat transfer coefficient has its maximum value at the smallest thickness of the boundary layer.

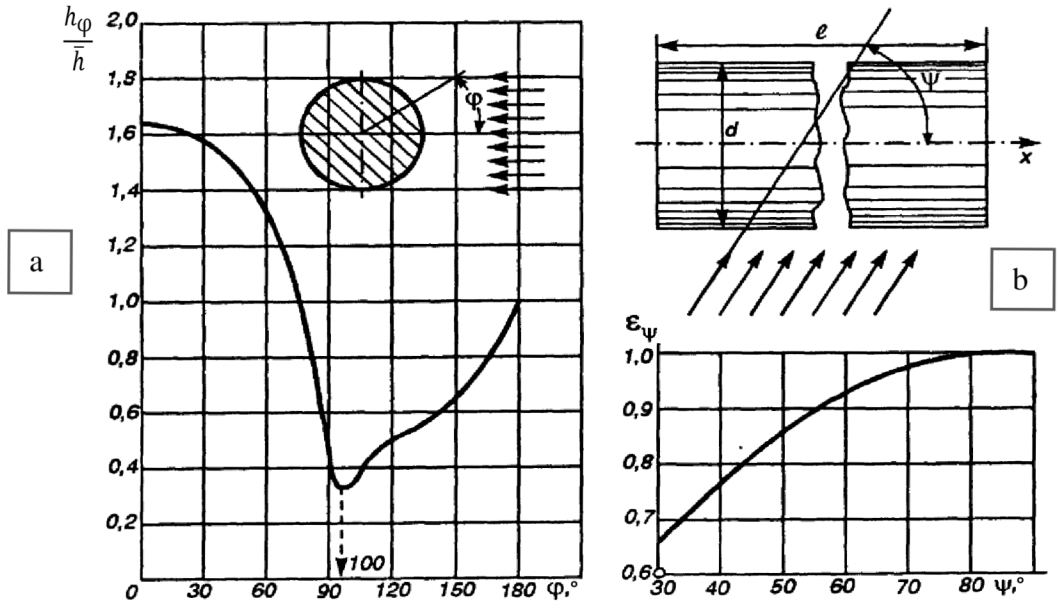


*Fig. 3 Cylinder streamlining by a liquid cross-flow [1]. a) Changing in the relative local heat transfer coefficient $h_\varphi$ around the circumference of the cylinder. b) correction factor taking into account the effect of the angle of attack $\psi$ on h*

In the rear part of the cylinder (φ = 180°) attached flow takes place at Reynolds numbers less or equal to 5. At higher Reynolds numbers the velocity in the rear part reduces, arise reversal flows and eddies, which cause a boundary layer separation from the cylinder and result in some increase in the heat transfer coefficient. The average over the cylinder perimeter Nusselt number is determined by the attack angle ($\psi$) and by criteria Re and Pr. At 0,6<Pr<800

Re= $5\ldots10^3$

$$\overline{Nu} = 0{,}5\, Re^{0{,}5}\, Pr^{0{,}37}\, \varepsilon_t\, \varepsilon_\psi \qquad (12)$$

Re= $10^3\ldots2\cdot10^5$

$$\overline{Nu} = 0{,}25\, Re^{0{,}6}\, Pr^{0{,}37}\, \varepsilon_t\, \varepsilon_\psi \qquad (13)$$

Re= $10^3\ldots2\cdot10^5$

$$\overline{Nu} = 0{,}023\, Re^{0{,}8}\, Pr^{0{,}4}\, \varepsilon_t\, \varepsilon_\psi \qquad (14)$$

During liquid heating $\varepsilon_t = \left(\frac{Pr_f}{Pr_w}\right)^{0{,}25}$ and during liquid cooling $\varepsilon_t = \left(\frac{Pr_f}{Pr_w}\right)^{0{,}2}$

For the air

Re= $10\ldots10^3$

$$\overline{Nu} = 0{,}43\, Re^{0{,}5}\, \varepsilon_\psi \qquad (15)$$

Influence of the attack angle on $\varepsilon_\psi$is shown in Fig 3. In the region of$30° \le \psi \le 90°$ $\varepsilon_\psi = 1 - 0{,}54\, cos^2\, \psi$.

These formulas are valid for convective heat transfer of fluids without changing their aggregate state. Indexes *w* and *f* refer to the thermo-physical parameters, to the temperature of the cylinder wall $t_w$ or to the liquid temperature $t_f$. The determining size is a cylinder diameter; $t_f$ is taken as a determining temperature.

### 1.2.4 Heat transfer during crossflow of tube bundle

Tube arrangement in bundles or packages has found widely application in constructions of heat exchangers and radiators. The most commonly used location of tubes in the bundle are staggered and in-line (see Fig. 4). Bundle geometry is set by tube diameter *d* and by relative transverse (perpendicular to the flow direction) $s_1/d$ and relative longitudinal (in the flow direction) $l_2/d$ pipe steps.

The heat exchange of tubes in the front row can be considered as a flow around the single cylinder regardless of the bundle geometry. Tubes in second and subsequent rows lay in a vortex wake, generated by the first-row tubes. Therefore, a heat transfer coefficient of the tube bundle is higher than of one tube. From the third row a flow regime and heat exchange are stabilized. Heat transfer of the third row is higher than the first and second rows.

Subsequent tube rows of in-line bundles are in the vortex area of ahead standing tubes, that is why the local maximum values of heat transfer coefficients are moved downstream the flow to φ≈50°. For staggered bundles of all tubes rows local heat transfer coefficients have the greatest value at φ≈0°.

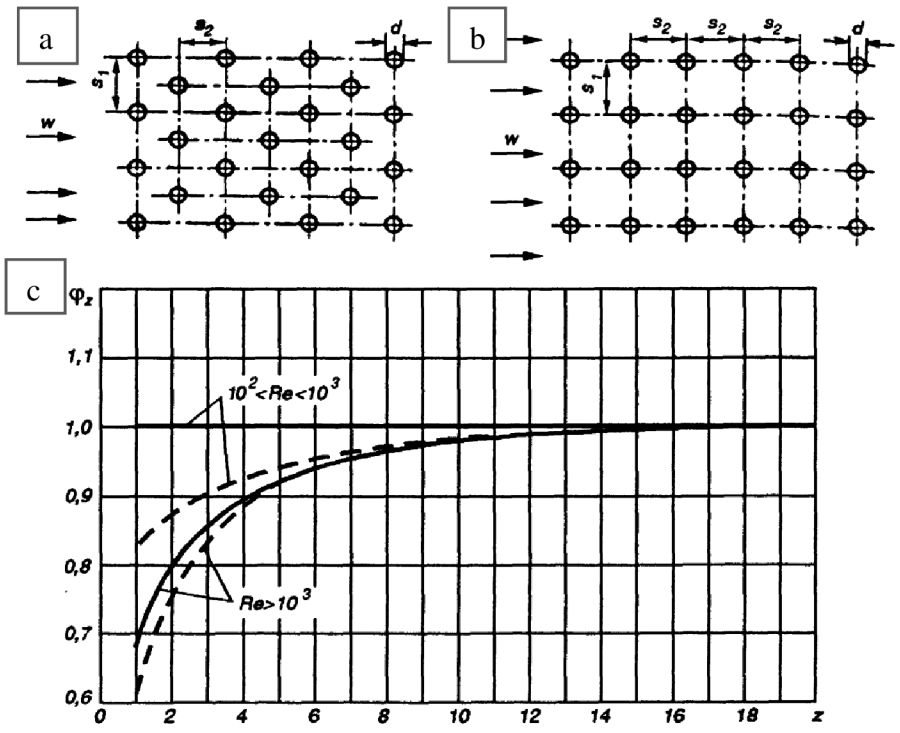


*Fig. 4 Staggered and in-line tube arrangement and correction factor for the number of rows in the bundle [1]*

The average heat transfer coefficient can be found by the following dependence, for pipes of third row and higher:

$$\overline{Nu} = C\,Re^{n}\,Pr^{0,33}\left(\frac{Pr}{Pr_w}\right)^{0,25}\varepsilon_s\varepsilon_\psi \qquad (16)$$

The coefficients for equation (16) are shown in Tab. 2.

*Tab. 2 Coefficients C depending on Re [1]*

| Bundles | $Re<10^3$ | $10^3<Re<10^5$ |
|---|---|---|
| Staggered | C=0,56; n=0,5 | C=0,35; n=0,6 |
| In-line | C=0,56; n=0,6 | C=0,26; n=0,65 |

Influence of bundle layout characteristics is determined by a correction factor$\varepsilon_s$, which is calculated for staggered bundle at $l_1/l_2<2$ by the formula $\varepsilon_s=(l_1/l_2)^2$ and at $l_1/l_2\geq 2$ is equal to $\varepsilon_s=1.12$. For in-line tube bundle $\varepsilon_s= 1$.

For the first row the heat transfer coefficient is equal to $h_1 = 0,6h_3$; for the second staggered row - $h_2=0,7h_3$ and the in-line row - $h_2=0,9h_3$. The average flow temperature is accepted as a determining temperature, the determining size is an outer diameter of the tube.

Velocity is calculated in the narrowest cross-section of the channel using on the approach flow velocity $w_0$. The value of$\varepsilon_\psi$can be taken from Fig. 4b.

The average heat transfer coefficient for the whole bundle is determined by the average heat transfer coefficients for individual rows:

$$h_П = \frac{\sum_{i=1}^{Z} h_i S_i}{\sum_{i=1}^{Z} S_i} \qquad (17)$$

where $z$ is a number of rows in the bundle; $S_i$ is a heat exchange surface if the i-row.

Value can also be found from the relation:

$$\overline{Nu}_П = \phi_Z\overline{Nu} \qquad (18)$$

where $\phi_Z< 1$ for number of rows $z < 16$ and is determined from the Fig. 4c.

Perfection of bundle geometry can be estimated by the ratio of heat transferred from liquid to surface to the value of energy consumption for the liquid motion near the surface with the velocity $w_0$

$$\phi_E = \frac{hS}{w_0 S_f \Delta p} \qquad (19)$$

where $S_f$is a flow cross-section area, $\Delta p$ is a pressure drop at the liquid motion.

Article [4] describes universal methods of calculating convective heat transfer of smooth and finned tube bundles in the crossflow. These methods were developed basing on analysis of experimental data for Reynolds number $3\times10^3\ldots1\times10^5$ and provide a high accuracy of calculation of convective heat transfer of smooth and transversely finned tube.

# 2. INTENSIFICATION OF HEAT TRANSFER

Intensification of heat transfer is an effective method to solve the problem of reducing the weight and dimensions of heat exchangers and devices. By now, various methods of convective heat transfer intensification have been proposed and investigated.

With regard to a single-phase working fluid flow such methods of heat transfer intensification are used:

1. turbulators on heat-exchange surface [5],
2. rough surfaces [6],
3. developed surface due to finning, flow swirling by spiral fins [7],
4. screw devices,
5. swirlers, installed at the channel inlet [8],
6. gas bubbles admixing to the liquid flow and admixing of solid particles and liquid droplets to the gas flow [9], [10]
7. rotation of heat transfer surface [11],
8. surface vibration [12],
9. working fluid pulsation [13],
10. impact on the flow of electrostatic fields [14],
11. suction flow from the boundary layer [15], [16].

A combination of number of intensification methods is often highly effective.

It should be noted that when choosing a heat transfer intensification method for the practical application it is necessary to take into account not only the effectiveness of the heat-exchange surface, but also its adaptability to manufacture, adaptability to assembly the heat exchanger, strength requirements, surface dirt retention, operational features and so on. All these factors essentially reduce the possibility of choosing one of the numerous investigated intensification methods.

The use of artificial flow turbulence is one of the most effective method of heat transfer intensification in channels with a single-phase working fluid [17].

In some applications other heat transfer intensification methods can also be effective, for example, the use of spiral or helical tubes at the laminar flow of the working fluids, the use of multiple-flighted screws swirling the flow before the channel part in which an increased heat dissipation is. In curvilinear channel under the influence of centrifugal forces are developed helical structures, covering all the channel section. Furthermore, at sufficient sharp turnings can appear separate zones with two- and three-dimensional system of vortices. A system of helical vortices with opposite rotation directions can appear on the concave wall. In turbulent flows all this leads to additional turbulization, increase in the heat transfer and the hydraulic resistance. The use of

channels and pipes finned inside and outside is advisable at low heat fluxes, especially at laminar flow of the working fluid.

The use of finned surfaces in the cooling systems of electronic equipment allows in a number of cases ensuring of acceptable cooling in the presence of free convection only, without organization of the forced cooling which significantly simplifies the design [18].

# 3. INVESTIGATION OF HEAT PULSES INFLUENCE ON METAL HEAT EXCHANGER

Several examples of fin geometry optimization were presented in Chapter 2. But in many cases, for factories producing heat exchangers, change of the fin geometry is a quite difficult task that requires serious changes in the production process. However, not only the fin geometry effects on thermal characteristics of the heat exchanger, but also the quality of the contact between fin and tube plays significant role.

One of the most common types of heat exchangers used in air conditioning systems of buildings are heat exchangers made of copper coil pipe with aluminum fins. These heat exchangers can operate in heating mode in cold seasons and in cooling mode in warm seasons. Due to such a temperature cycles and the difference in thermal expansion coefficients of copper and aluminum the relative dimensions of the tube and fins can change. It can lead to a deterioration in the thermal contact between tube and fin, which leads to deterioration of the heat exchanger thermal characteristics and the possible occurrence of noise due to ribs vibrations on the tube.

The purpose of this work was a study of heat pulses influence on the heat exchanger efficiency reduction. A thermal cycling tests of a metal heat exchanger were carried out to simulate its actual operating conditions and find out a potential deterioration of contact between fins and the coil pipe. Using achieved data to find a way for design optimization and a method of fins fixing.

In this work, the commercial fancoil that is used in building air-conditioning systems was studied (seen in Fig. 5). Overall view of a metal finned tube heat exchanger placed under the fancoil external casing is presented in Fig. 6. Heat exchanger consists of 3 rows of copper tubes with an external diameter of 10 mm. Aluminum fins were pressed on copper tubes with the fin pitch of 2 mm. The overall heat exchanger dimensions were 250x250x65 mm. A fan was installed at the bottom of the heat exchanger to provide a directed air flow throw the radiator.

*Fig. 5 Overall view of the fancoil installed in calorimeter chamber*

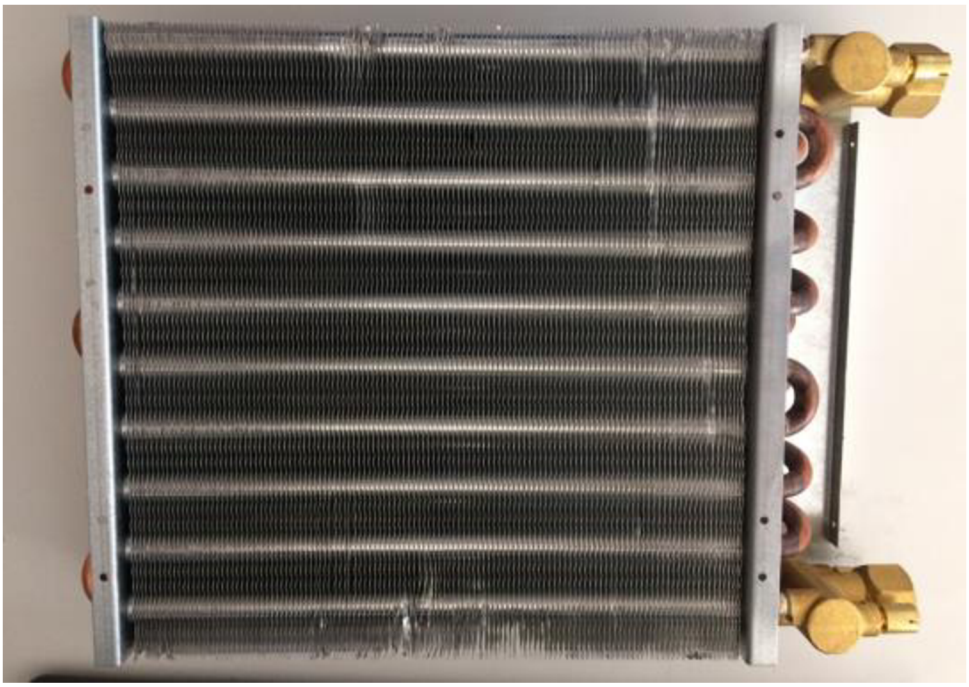

*Fig. 6 Overall view of the metal finned tube heat exchanger inside the fancoil*

According to technical characteristics of the heat exchanger, specified by the manufacturer in the device certificate, in the heating mode this heat exchanger has a heat transfer rate of 1000 W at the water inlet temperature to the heat exchanger equal to 50 °C, the water flow rate through the heat exchanger equal to 136 l/h and the ambient air temperature equal to 20 °C.

The working body of the fancoil is made of two different materials: the radiator coil pipe is made of copper and fins are made of aluminum plates. The thermal expansion coefficient for copper is $16{,}6*10^{-6}\ °C^{-1}$ and for aluminum is $22{,}2*10^{-6}\ °C^{-1}$. It means that during cooling and heating these two metals will expand differently. It can impair the contact between fins and copper coil pipe of the heat exchanger. This can lead to increase in thermal resistance in the contact area between fins and pipe, which will decrease the heat transfer rate of the heat exchanger.

To evaluate the influence of thermal stress on the fin-coil contact the following experiments were conducted:

1) heat transfer rate of the new fancoil sample was measured;
2) thermal cycle tests were conducted;
3) heat transfer rate of tested fancoil was measured to compare with initial values.

All the tests were conducted in the calorimetric chamber.

## 3.1 Calorimetric chamber

For measuring the thermal characteristics of the heat exchanger a unique testing equipment was used - a testing calorimetric chamber for measuring the thermal output of heating/cooling equipment. The chamber shown in Fig. 7 allows precise control and measurement of all parameters (temperature, flow rate, etc.) and simulate a real working conditions of heat exchangers.

From the structural point of view the calorimetric chamber consists of 3 parts: a working chamber, an automatic control system and a cooling/heating system.

The working chamber is a room with internal dimensions of 4x4x3 m and allows for measurement of heat transfer rate from between 200 W to 4.5 kW. The room has two main circuits for setting the test conditions. The first is the external circuit, which is used to setup environmental conditions for the experiment. The external circuit system includes pumps, heat and cold storage, heaters, air conditioning, flow meters, temperature sensors. Maintaining a constant air temperature inside the calorimetric chamber is provided by controlling a temperature of walls, floor and ceiling by flowing water with given temperature and flow. The second circuit is the internal, going through the test sample, also allows to set the temperature and the water flow rate through the heat exchanger. With the help of these circuits and a special computer program it is possible to provide automatically measurements and evaluate the heat power of the measured heat exchanger. The power of the heat exchanger is determined by measuring the mass flow rate of the working fluid passing through the heat exchanger and the difference in the enthalpy of the working fluid in the inlet and outlet of the heat exchanger.

*Fig. 7 Testing calorimetric chamber*

The testing calorimetric chamber was made in accordance with the Czech Technical Standard ČSN EN 442-2 "Otopná tělesa: zkoušky a jejich vyhodnocování", which is the Czech equivalents of the European standard EN 442-2: 1996. To measure the heat transfer rate of heat exchangers in accordance with this standard, the temperature of the working fluid in the inlet to the heat exchanger should be 75 °C, and in the outlet – the working fluid temperature should be equal to 65 °C, while the air temperature in the chamber is 20 °C. However, the calorimeter chamber allows to set working fluid temperature of the test circuit in the range from 6 °C to 95 °C, and the temperature of ambient air in the range from 10°C to 40 °C. The accuracy of temperature measurement is ±0.1 °C. So, the calorimetric chamber can also be used for other measurements not related to the ČSN EN 442-2 standard. In addition, it is possible to work in cooling mode and to measure cooling heat transfer rate, and to solve problems of condensation and its influence on heat exchanger performance.

Measurements in the chamber allow for the rapid acquisition of information, characterizing the tested heat exchanger, and the ability to easily change operating parameters. If necessary, a numerical simulation can be used to achieve optimal parameters. An example of temperature distribution in the volume of a chamber, obtained as a result of computer simulation of the heat exchange process, is shown in Fig. 8.

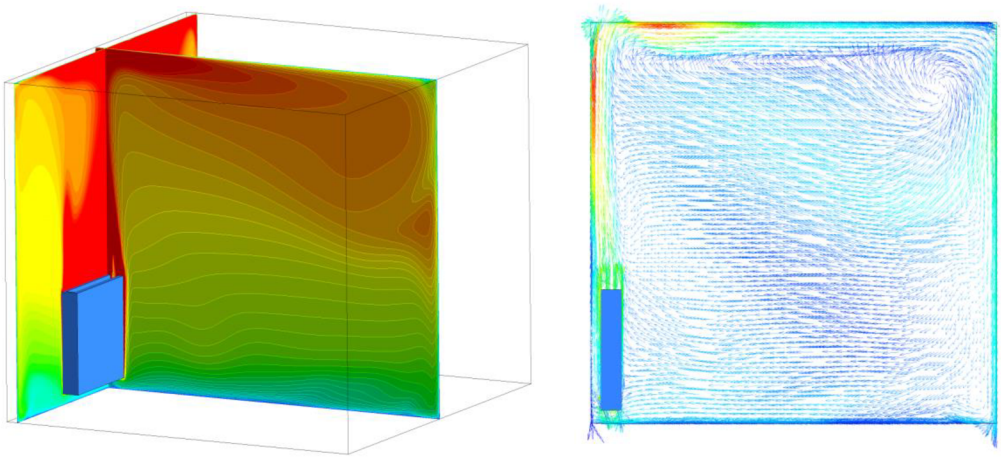

*Fig. 8 Computer simulation of the heat exchange process inside of calorimetric chamber*

## 3.2 Heat transfer rate measurement of the fancoil

At the first step of experiments with the fancoil, tests to measure its heat transfer rate in the calorimeter chamber were performed for its further comparison with the characteristics declared by the manufacturer.

For testing in heating mode, the inlet water temperature of the heat exchanger was 50 °C, the water flow rate through the heat exchanger was 136 l/h and the ambient air temperature was 20 °C. For testing in cooling mode, the inlet water temperature of the heat exchanger was 7 °C, the water flow rate through the heat exchanger was 136 l/h and the ambient air temperature was 27 °C.

The measured data in comparison with the certificate data of the device are presented in Tab. 3.

*Tab. 3 Heat transfer rate comparison between measured data and manufacturer's data.*

| Heat transfer rate, heating mode, certificate | Measured heat transfer rate, heating mode | Heat transfer rate, cooling mode, certificate | Measured heat transfer rate, cooling mode |
|---|---|---|---|
| 1000 W | 942 W | 790 W | 602 W |

The table shows that the heat transfer rate in heating mode agrees with the manufacturer data, however, in cooling mode, these two values had a difference of 24%. This is primarily because the manufacturer had his data for a relative air humidity of 45%, but in our measurements the air humidity was 13-14%, which leads to a decrease heat transfer rate of heat exchanger.

## 3.3 Thermal cycle tests of metal heat exchanger

The second stage of experimental research was to conduct thermal cycle tests with switching between heating and cooling modes. The purpose of these tests was to determine the effect the useful life of a copper heat exchanger with aluminum fins on its thermal performance.

For providing a life-tests a special stand was developed and assembled. This stand allows to carry out thermal cyclic tests. One cycle consists of a quick heat exchanger heating and then its rapid cooling. Duration of one cycle is regulated by the water flow rate. Experimental setup allows to make tests at pressures up to 10 bar.

The scheme of the developed stand is shown in Fig. 9. The stand had two circuits of water flow– closed for hot water and open for cold. In heating mode, electric valves 3 and 6 were closed, and valves 2 and 5 were open. Hot water from the boiler with the help of the pump 9 flowed through the heat exchanger. The heat exchanger temperature was measured at three points: inside the inlet pipeline 1 of heat exchanger and inside outlet pipeline 3 and one thermocouple was put on the outer surface of radiator 2. When thermocouple 2 reached the required temperature, valves 2 and 5 are closed, valve 4 is opened and the hot water circuit switched to the stirring mode, hot water flows along the circuit not connected to the measured heat exchanger. At this moment valves 2 and 6 were opened, putting the stand into cooling mode. Cold water flowed through the water filters, electric valve 3, radiator, electric valve 6, valve 7 and the drain, cooled the heat exchanger to the required temperature. After reaching set temperature, cold circuit closed and the hot one opened again.

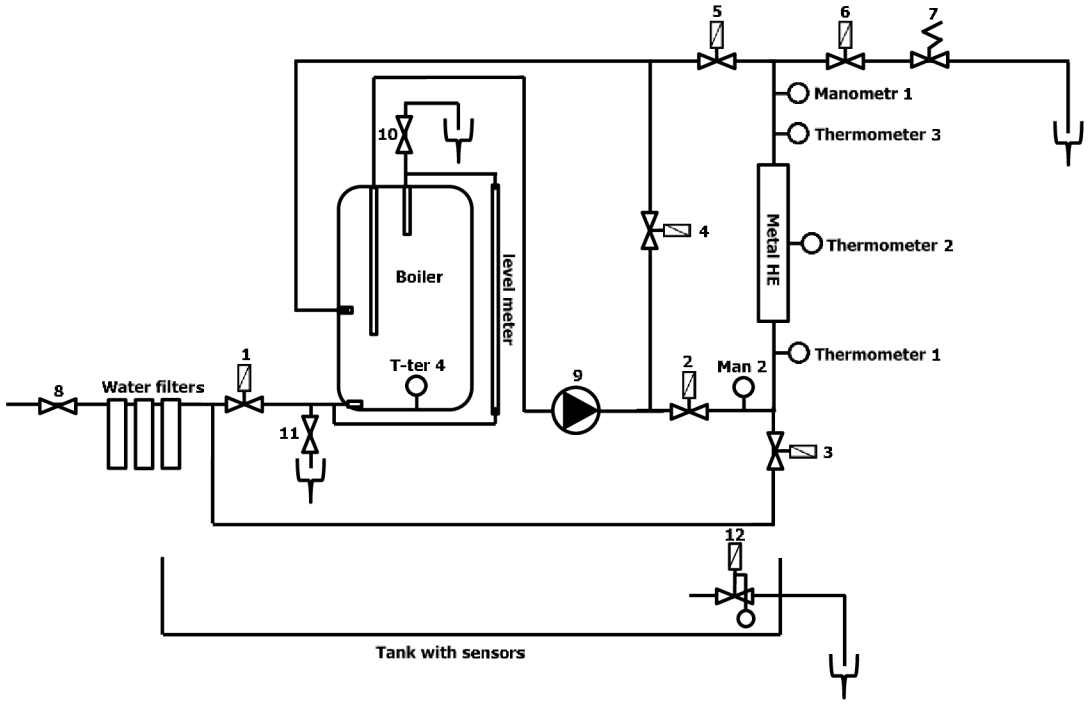


*Fig. 9 Scheme of the thermal cycling stand*

The experimental setup was equipped with resistance thermometers Pt 100 that transmitted data to a computer using datalogger National Instruments, which allowed real-time monitoring of the temperature level in the radiator, and also saved necessary data to the computer. Using electric valves the experimental setup was fully automatic and controlled by a program Labview. The program allowed to set the cycle time in two ways: first, by setting the maximum and minimum temperature on the outer surface of the heat exchanger (resistance thermometer 2). The second method allowed setting the cycle time directly, determining the response time of the electric valves, regardless of the resistance thermometer 2.

Cycling on the experimental setup was carried out 24 hours a day. For this reason, a safety system was developed. This system allows to automatically shut down experimental setup in case of measurement device leaking. An empty tank was located under the tabletop of the setup, directly under the hole to drain the water. In this reservoir sensors registering the position of the water surface were installed. In case of a leaking, all water flowed into the tank, where the sensors registered water. This data came from the sensors to the computer and the entire experimental setup was instantly deenergized and all valves become closed.

An experimental setup with connected heat exchanger is shown in Fig. 10. For simplification of installation and conducting experiments during heating and cooling cycles, the upper case was removed from the radiator.

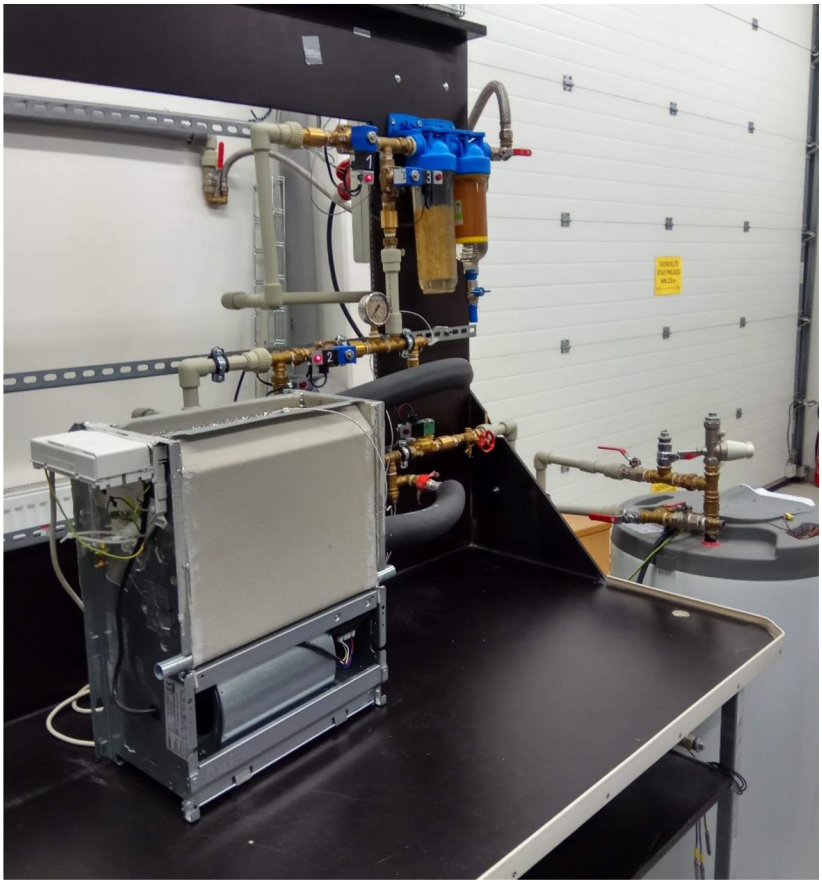

*Fig. 10 Experimental setup with a connected fancoil*

The temperature plot of resistance thermometer 2 on the outer surface of the radiator for several cycles is shown in Fig. 11. The heat exchanger was heated up to the temperature of 76 °C and then rapidly cooled to a temperature of 17 °C. Duration of one cycle was about 35 seconds. The pressure in the system was equal to atmospheric. To identify the effect of different thermal expansion coefficients on the heat exchanger heat transfer rate 100000 heating and cooling cycles of the metal heat exchanger were carried out.

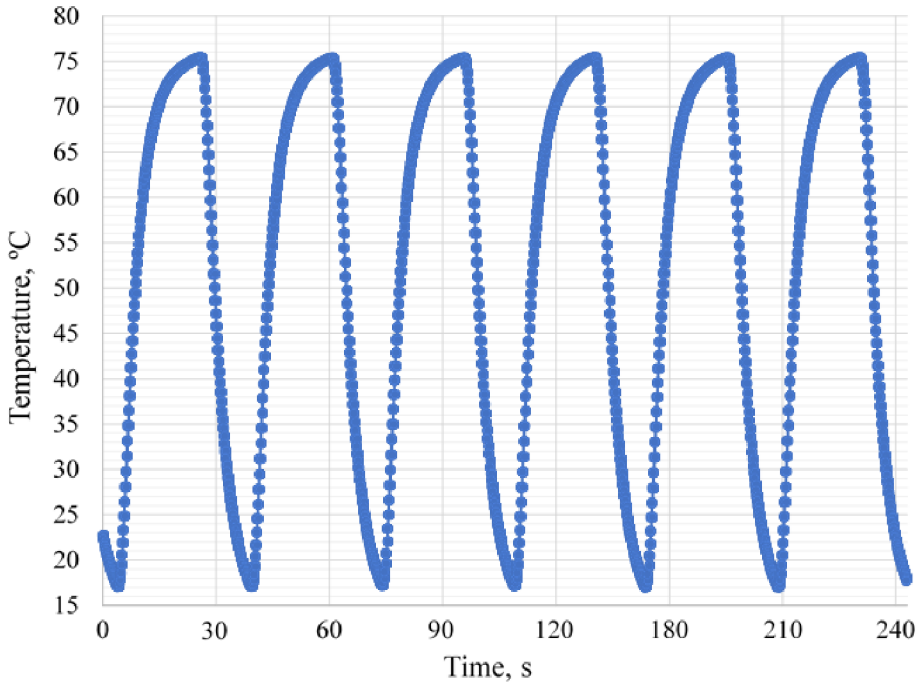


*Fig. 11 Thermal cycles of tested heat exchanger*

## 3.4 Heat transfer rate measurement of the fancoil after thermal cycle tests

The third stage of the study was to conduct tests to re-measure the power of the heat exchanger using a colorimetric room in order to find out how thermal cycles, typical for actual operating conditions, influence on operating characteristic of the metal heat exchanger.

Heat transfer rate of the heat exchanger was measured in a calorimeter chamber under the same conditions as the original measurements, i.e. for testing in the heating mode, the water temperature at the inlet to the heat exchanger was 50 °C, the flow rate of the liquid through the heat exchanger was 136 l/h and the ambient air temperature was 20 °C. For testing in cooling mode, the water temperature at the inlet to the heat exchanger was 7 °C, the flow rate through the heat exchanger was 136 l/h and the ambient air temperature was 27 °C. The obtained data are presented in Tab. 4.

*Tab. 4 Comparison of heat transfer rate measurements before and after thermocycles.*

| Measured heat transfer rate, heating mode before cycling | Measured heat transfer rate, heating mode after cycling | Measured heat transfer rate, cooling mode before cycling | Measured heat transfer rate, cooling mode after cycling |
|---|---|---|---|
| 942 W | 945 W | 602 W | 593 W |

The experimental data showed that the thermal characteristics of the fancoil after thermocycling remained the same under measurement accuracy. According to this data can be concluded that the contact between aluminum fins and the copper coil pipe of the heat exchanger created by pressed method remained the same and the longtime of using does not have influence on heat exchanger. Since the contact between the fins and the tube has not changed, therefore, the occurrence of additional vibration of finning is excluded. Due to this fact there is no need to conduct noise tests.

## *Intermediate conclusion*

In this work was experimentally shown that the technology of manufacturing metal-heat exchangers with a copper coil pipe with pressed aluminum fins is optimal. Even 100000 cycles of heat exchanger heating and its subsequent rapid cooling doesn't have negative effect on the fancoil heat transfer rate. The contact between the fins and the tube remain constant during all its useful life. Since the contact between the fins and the tube has not changed, therefore, the occurrence of additional vibration of finning is excluded. In this regard, it was decided that further optimization of this metal heat exchanger is inappropriate. Therefore, the main focus of this work was on plastic heat exchanger investigation.

# 4. OPTIMIZATION OF AIR-WATER PHFHE

Despite all the advantages of metal heat exchangers, there fields of application where due to several restrictions (weight, aggressive environment, impossibility of shaping, etc.) metal heat exchangers can't be used. For such applications heat exchangers made of non-metal material play significant role. Most common materials for non-metal heat exchangers manufacturing are polymers and graphite (Fig. 12).

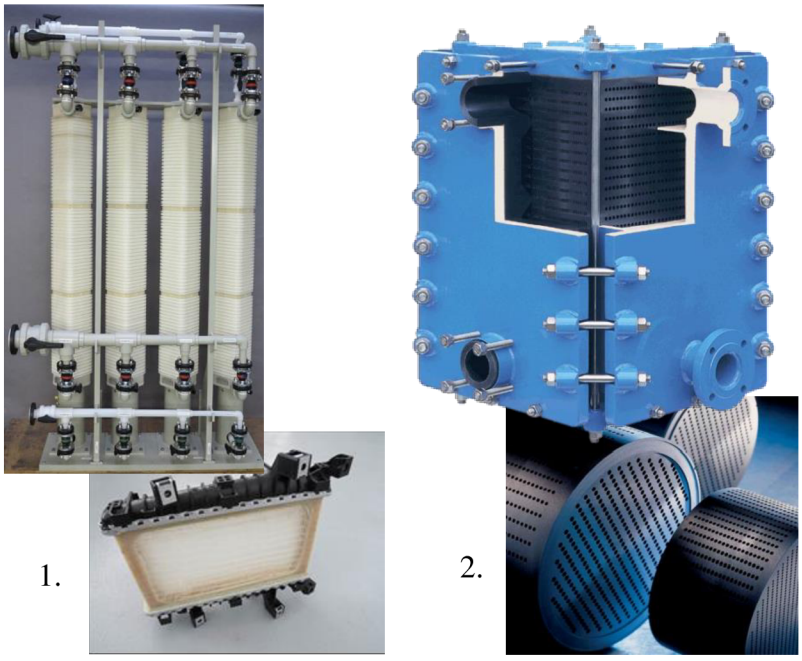

*Fig. 12 Types of heat exchangers by the material: 1 - polymeric, 2 - graphitic [19], [20].*

In this work will be considered polymeric heat exchangers which are becoming more and more popular in different engineering fields, because of their advantages compared with metal heat exchangers.

Due to the corrosive resistant feature polymeric heat exchangers can be used in aggressive media for metals, for example, in chemical industry. Jia et al. [21] present an experimental study on the heat transfer performance of wet flue gas heat recovery system using a plastic longitudinal spiral plate heat exchanger.

Production of polymeric heat exchangers uses much less energy than the production of metal one, it is another important advantage of these devices. Liu et al. [22] tested two types of heat exchanger (tube-and-shell and immersed tube) made manufactured either from high temperature nylon or cross-linked polyethylene for solar water heating systems. Authors reported that the polymer heat exchangers can provide thermal outputs equivalent to conventional copper heat exchangers at lower

cost. The cost of a nylon tube-and-shell heat exchanger was about 80% of that of a copper tube in shell heat exchanger.

Other significant advantages of plastic heat exchangers are low weight, smooth surface, simplicity of shaping and producing and resistance to fouling [23].

All these features allow polymeric heat exchangers to be applied in different fields, such as heat recovery system, evaporative cooling system, desiccant cooling system, electronic device cooling and water desalination system [24]. Rousse et al. [25] presented the theoretical and experimental analysis for using plastic heat exchanger as a dehumidifier in greenhouse for agriculture industry. Most commercially available polymer heat exchangers can be used in low temperature applications [26]. These heat exchangers can be used for solving water distillation problems. For example, the membrane distillation module [27], which was designed and manufactured in the Heat Transfer and Fluid Flow Laboratory in collaboration with CZ ZENA s.r.o.

Polymeric hollow fiber heat exchangers [28] described and investigated in this work are the type of polymer heat exchanger. Using thin-wall polymeric hollow fibers as heat exchanger tubes was first proposed by Zarkadas & Sirkar [29] as a new type of heat exchanger for lower temperature/pressure applications. This heat exchanger utilizes polymeric microchannels as the heat transfer surface. The outer diameter of these microchannels is smaller than 1.5 mm and the wall thickness is about 0.1 mm. The heat exchanger is made of hundreds of such fibers, which result in a very large heat transfer area compared to the size of the entire heat exchange Fig. 13.

*Fig. 13 Overall view of a PHFHE with a straight hollow fiber bundle*

Polymeric materials are not good heat conductors, but very thin wall and large heat transfer area allows PHFHE to compete with metal heat exchangers in terms of heat transfer intensity. Krasny et al. [30] conducted comparative tests of PHFHE and a conventional automobile aluminum finned-tube radiator and observed that heat transfer rates (up to 10.2 kW), overall heat transfer coefficients (up to 335 $W/m^2K$) of PHFHE were competitive with the metal heat exchanger. Despite the wall thickness of about 0.1 mm the hollow fibers can accommodate a big pressure due to small diameter of microchannel. In Fig. 14 a wall defect on the polypropylene hollow fiber PP-RCT can be seen. This defect occured at environmental temperature 80 °C and pressure inside the hollow fiber was equal 40 bar. So, it says that PHFHE can be applied and for high pressure applications.

*Fig. 14 The defect of PP-RCT fiber occurred at the temperature 80°C and the pressure 40 bar*

## 4.1 Heat exchanger based on three hollow fiber bundles

A PHFHE made of twisted hollow fiber bundle with chaotic and semi-chaotic structure (shown in Fig. 15) was designed and manufactured in Heat Transfer and Fluid Flow Laboratory. Compared with straight hollow fibers bundels (presented in Fig. 13) this kind of bundle is more efective in water-air application becouse fibers can uniformly fill the volume of heat exchanger ensuring a homogenium hydraulic resistanse in the cross section. It means that air passes through all hollow fibers and whole heat transfer surface is involved in heat transfer process.

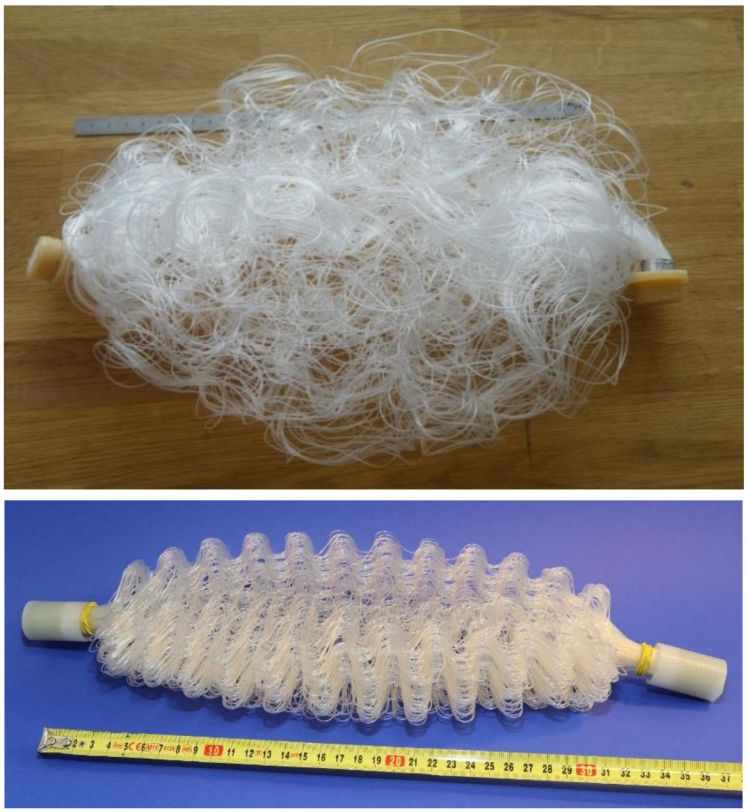

*Fig. 15 Overall view of polymeric hollow fiber bundle with chaotic (top) and semi-chaotic (bottom) structure*

Experimental research of natural convection in PHFHE based on polymeric hollow fibers bundle with chaotic structure, also called twisted hollow fibers bundle, is presented in this work. Overall view of first heat exchanger prototype is shown in Fig. 16. Three twisted hollow fiber bundles with chaotic structure were placed inside the duct. Distance between bundles was equal to 250 mm. From the both sides of each hollow fiber bundle a metal net was placed to prevent bundles from dipping and to uniformly distribute the hollow fibers over the cross section of the heat exchanger. A cross-section area of the heat exchanger was equal to 0.044 $m^2$ and height was 1.2 m. Resistance thermometers Pt100 RTD were used to measure the temperature distribution inside the heat exchanger. Sensor 1 was placed in the inlet of the heat exchanger. Sensors 2, 3 and 4 were placed 70 mm above each hollow fiber bundle. Top view of three hollow fiber bundles heat exchanger is shown in Fig. 17.

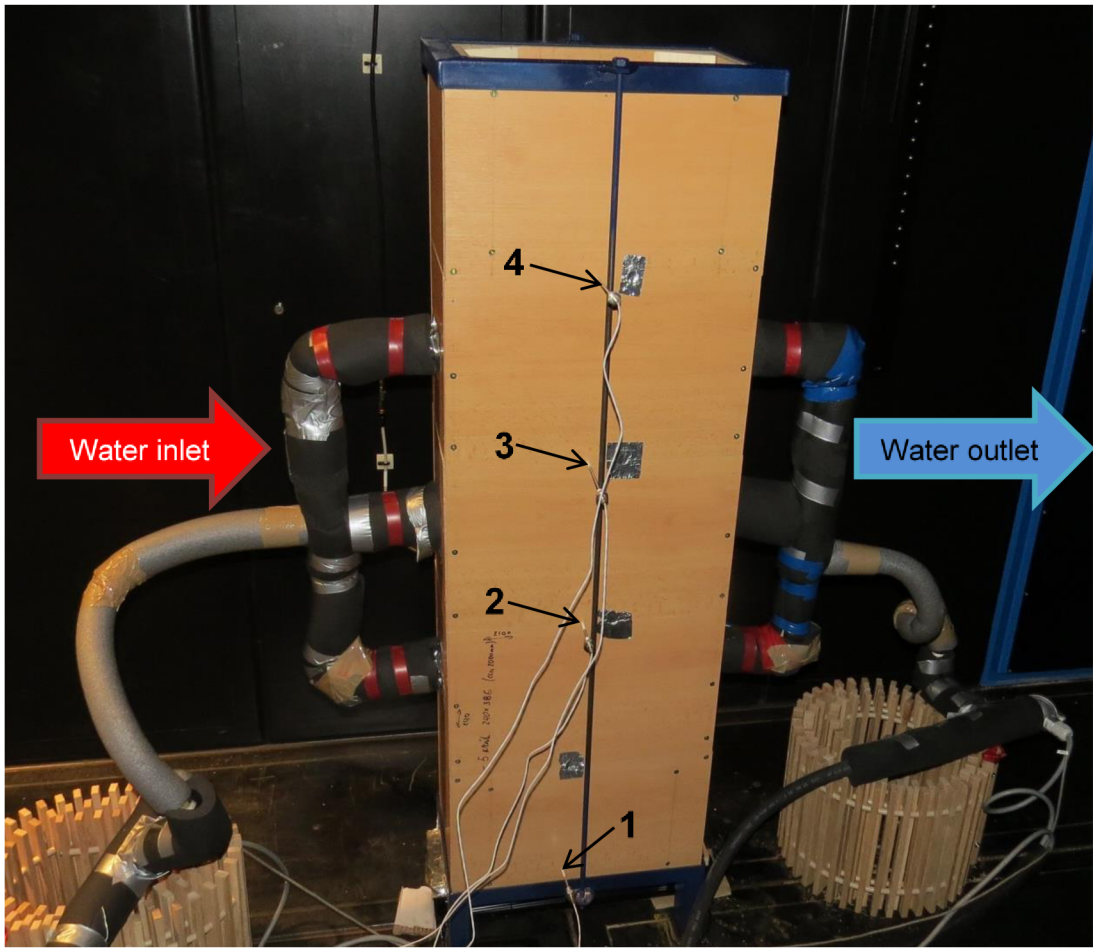


*Fig. 16 Overall view of a three hollow fiber bundles heat exchanger (1, 2, 3, 4 – Pt100 RTD sensors)*

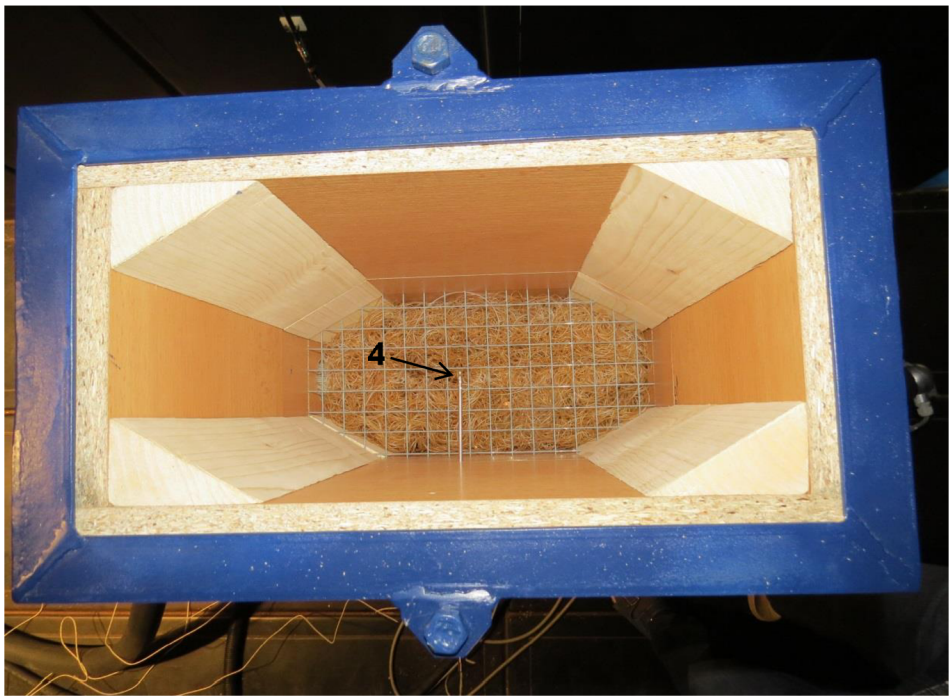


*Fig. 17 Top view of the three hollow fiber bundles heat exchanger (4 – Pt100 RTD sensor)*

Five experiments were conducted in calorimeter chamber with this heat exchanger. The testing conditions for the first experiment were chosen as the inlet water temperature of 45 ˚C, the outlet water temperature of 35 ˚C and the ambient temperature of 20 ˚C. Required water flow rate was adjusted based on temperature values. When the steady state was reached temperatures at each the heat exchanger section was measured and the heat transfer rate was calculated. Values of temperatures and heat transfer rates are given in Tab. 5. In the second experiment the initial conditions were the following: the inlet water temperature was equal to 75 ˚C, the outlet water temperature was equal to 65 ˚C and the ambient temperature was 20 ˚C.

Experiments № 3, 4 and 5 were conducted at the same initial conditions that experiment 2, but a fan installed from the bottom side of heat exchanger was used. The air flow velocity through the heat exchanger was set with the help of a voltage regulator. Experiments were conducted at air flow velocities equal to 0.5, 0.9 and 2 m/s.

*Tab. 5 Experimental results*

| Experiment number | | 1 | 2 | 3 | 4 | 5 |
|---|---|---|---|---|---|---|
| Inlet/Outlet/Room temp. | ˚C | 45/35/20 | 75/65/20 | 75/65/20 | 75/65/20 | 75/65/20 |
| Temp. 1 | ˚C | 20.0 | 20.0 | 20.5 | 20.0 | 19.5 |
| Temp. 2 | ˚C | 34.5 | 64.0 | 59.0 | 52.5 | 48.5 |
| Temp. 3 | ˚C | 39.4 | 68.0 | 69.5 | 66.7 | 61.2 |
| Temp. 4 | ˚C | 35.6 | 60.0 | 70.5 | 70.3 | 68.5 |
| Air velocity | m/s | - | 0.2* | 0.5 | 0.9 | 2 |
| Heat transfer rate | W | 145 | 550 | 1260 | 2020 | ≈ 4000 |
| Heat transfer coefficient | $W/m^2K$ | 16.5 | 34.6 | 65.3 | 77.8 | 134.1 |

* air flow rate at natural convection, the value was calculated.

From the table it can be seen that heat transfer rates for the experiments conducted at natural convection are quite low, especially for the case when the inlet water temperature was equal to 45˚C, the outlet water temperature was 35˚C and the ambient temperature was 20 ˚C. With increasing of water temperatures, the air velocity also increases and achieves the value of 0.2 m/s. Fig. 18 presents a dependence of the heat transfer rate on the air velocity inside the heat exchanger. It can be seen that the heat transfer rate increases linearly with the air velocity increasing and reaches a value of 4000 W at the air velocity of 2 m/s.

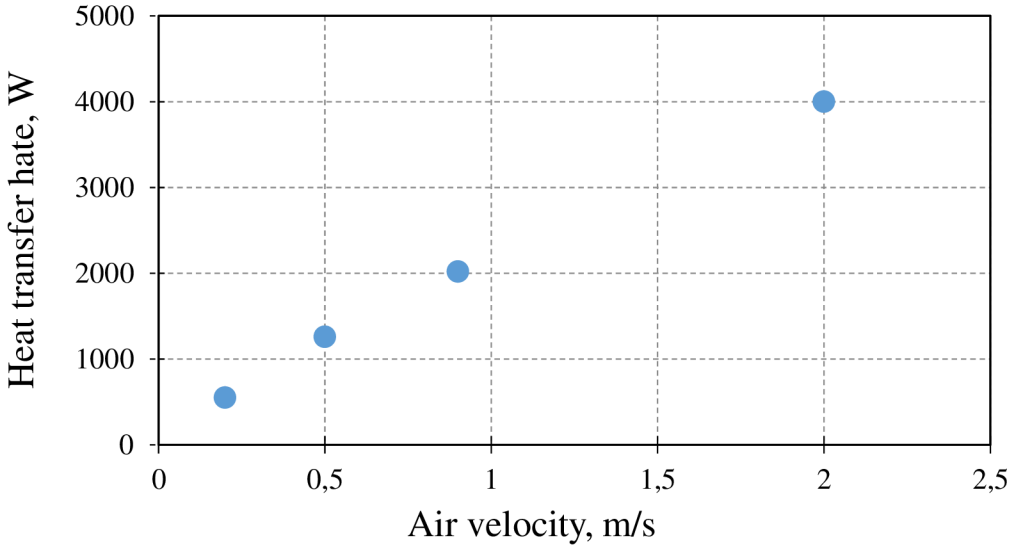


*Fig. 18 Dependence of the heat transfer rate of PHFHE on the air velocity through the three hollow fiber bundles heat exchanger*

Fig. 19 presents a temperature distribution inside the heat exchanger for different air flow velocities. It can be seen that at air velocity equal to 0.9 and 2 m/s a substantial contribution to the air heating is made only by the first two bundles. The use of the third bundle is unreasonable. At natural convection and forced convection with the air velocity of 0.5 m/s the main air heating is realized by the first bundle. In the case of natural convection, can be seen that air after third bundle had a lower temperature than air after first one. It can be explained by very slow air flow rate through the third bundle and by the mixing of the surrounded air above the third bundle with lower temperature with the hot air after third bundle in the top of the heat exchanger. It means that is no need to use second and third bundles because they almost don't participate the air heating but provide an additional hydraulic resistance in the system.

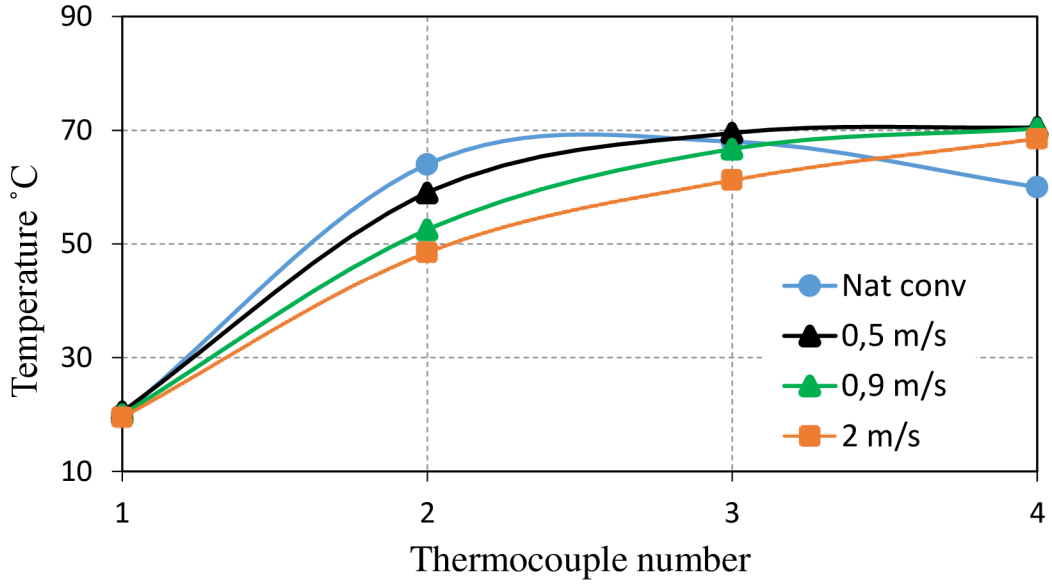


*Fig. 19 Temperature distribution inside the three hollow fiber bundles heat exchanger*

## 4.2 Heat exchanger based on one hollow fiber bundles

Based on experimental results with three bundle heat exchanger, tests of the heat exchanger consisting of one hollow fiber bundle were carried out. At the experiment № 6 a free hollow fiber bundle was tested. The initial conditions during experiment were the following: the inlet water temperature was equal to 75 ˚C, the outlet water temperature was equal to 65 ˚C and the ambient temperature was 20˚C. Heat was transferred by natural convection. Pt100 RTD sensor № 1 registered temperature on the bottom side of the bundle, sensors № 2-4 measured temperature above the bundle.

At the experiment № 7 the heat exchanger containing one hollow fiber bundle was tested. Bundle was placed between two metal nets, protecting it from dipping. Pt100 RTD sensor № 1 registered temperature on the bottom of the heat exchanger, sensor № 2 - on the bottom side of the bundle, sensors № 3-4 measured temperature above the bundle. Experiment № 7 was conducted at the same conditions as experiment № 6.

The overall view of both experimental setups is shown in the Fig. 20.

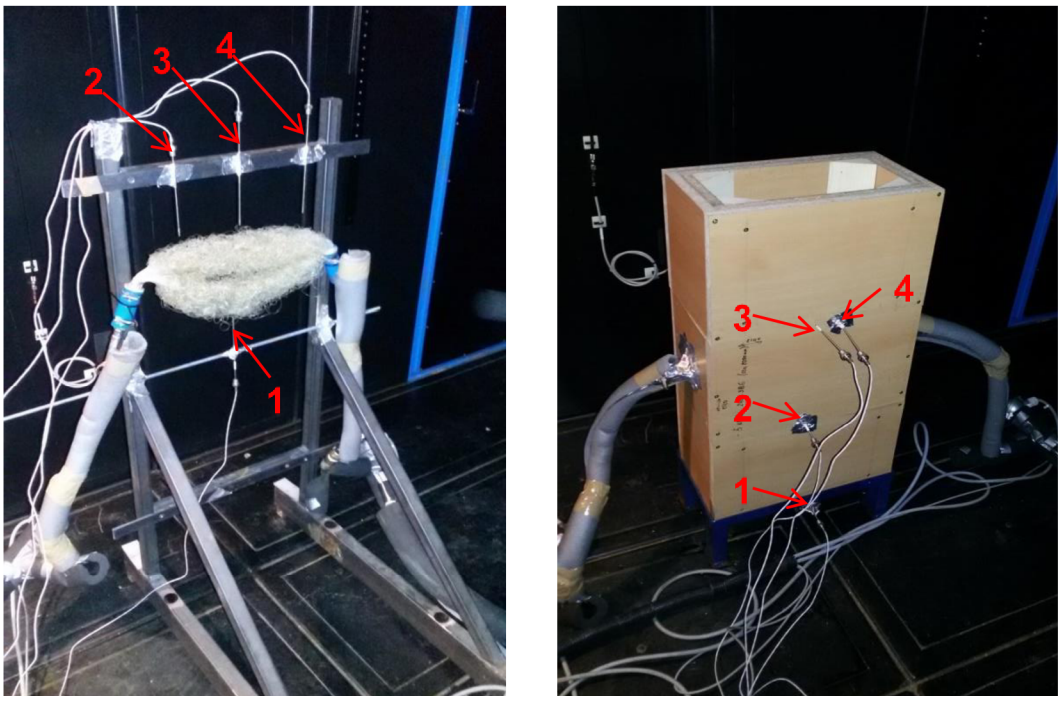


*Fig. 20 Overall views of experimental setup for a free hollow fiber bundle (left) and for the heat exchanger with one hollow fiber bundle (right)*

Values from resistance thermometers and heat transfer rates are given in Tab. 6. Base on the equation of thermal balance values of air velocities for each type of experiment were calculated. Can be seen that in experiment with free hollow fiber bundle values of temperature sensors 2-4 are differ. It indicates nonuniformity of the air flow, the air flow rate is small. Experimental data for one hollow

fiber bundle heat exchanger show that the use of a case results in air flow rate increase by 60%. Heat transfer rate also increased by 54%. It can be explained by the chimney effect.

*Tab. 6 Experimental results*

| Experiment number | | 6 | 7 | 8 |
|---|---|---|---|---|
| Inlet/Outlet/Room temp. | ˚C | 75/65/20 | 75/65/20 | 75/65/20 |
| Temp. 1 | ˚C | 19.1 | 19.3 | 18.6 |
| Temp. 2 | ˚C | 65.8 | 20.4 | 19.4 |
| Temp. 3 | ˚C | 65.6 | 56.5 | 64.6 |
| Temp. 4 | ˚C | 31.7 | 60.0 | 62.4 |
| Heat transfer rate | W | 292 | 450 | 1085 |
| Heat transfer coefficient | $W/m^2K$ | 21.2 | 29.7 | 75.9 |
| Air velocity | m/s | 0.13 | 0.21 | 0.48 |

Air velocities for each type of experiment are demonstrated in Fig. 21.

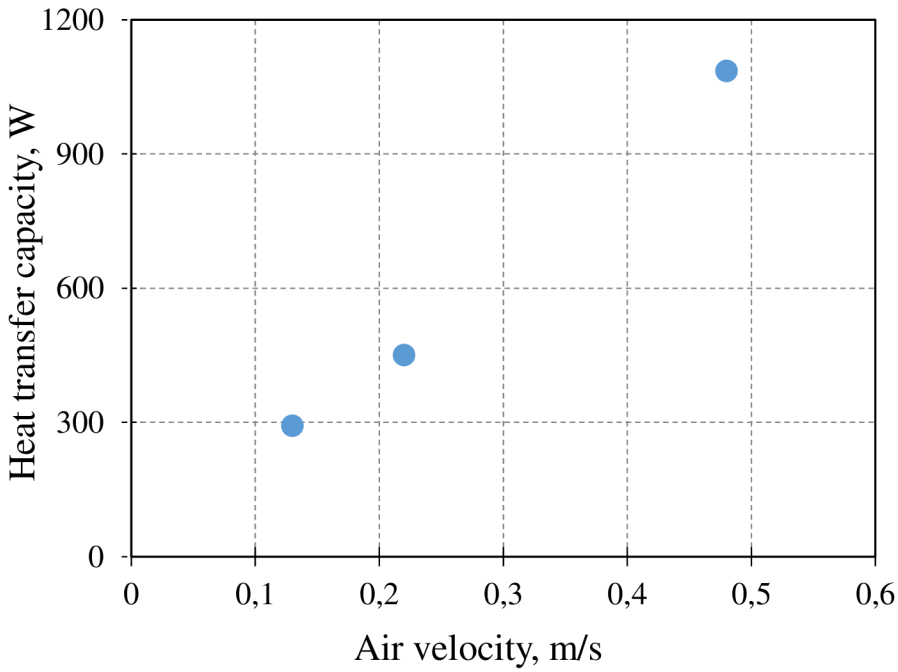


*Fig. 21 Dependence of the heat transfer rate on the air velocity for one hollow fiber bundle*

In order to increase the chimney effect one hollow fiber heat exchanger equipped with a 1.6 m tube installed on the top was tested. Experiment № 8 was conducted at the same conditions like experiments № 6 and 7. The use of a tube strengthened the chimney effect and resulted in the heat transfer rate increase by 2.5 times and reached a value of 1085 W. Results obtained for one hollow fiber bundle heat exchanger with tube on the top are compared with a heat transfer rate of series-produced metal radiators.


*Fig. 22 Overall view of the heat exchanger with one hollow fiber bundle and a tube.*

## *Intermediate conclusion*

Experiments conducted show that the use of twisted hollow fiber bundles in water-air application is perspective. For vertical heat exchangers with a natural convection does not make sense to use several hollow fiber bundles. One bundle is enough to obtain high values of the heat transfer rate. Chimney effect can significantly increase the heat transfer rate of the heat exchanger.

# 5. OPTIMIZATION OF SHELL-AND-TUBE PHFHE

For water-water applications one of the most frequent type of heat exchanger is shell-and-tube heat exchangers. This kind of heat exchangers usually are made in the form of a case with several tubes inside. During the operation of such devices one working fluid flows inside the shell, from the outer surface of tubes. And the second working fluid flows inside the tubes. Heat exchange process takes place due to deference between working fluid temperatures.

In this work the ways of shell-and-tube PHFHE optimization were studied. Such devices usually consist of hundreds of polymeric hollow fibers placed in the shell. During their operation one working fluid flows inside the polymeric hollow fibers and another working fluid flows inside the heat exchanger shell, flowing from the outside of the fibers.

## 5.1 PHFHE with parallel hollow fibers PA-72

The first object of study was a plastic shell-and-tube type heat exchanger PA-72, shown in Fig. 23. The heat exchanger 240 mm long had an external transparent shell with a diameter of 50 mm, made of plastic. Inside the shell 1700 parallel polyamide hollow fibers 180 mm long with outer diameter of 0.8 mm were placed. The maximum internal pressure of this heat exchanger was 3 bar.

*Fig. 23 Overall view of PA-72 PHFHE*

Water was used as working fluids. The experiment was carried out under the following conditions: water flow inside the fibers had a temperature of 11 °C, shell water flow had a temperature of 50 °C and 70 °C. The measurements were carried out for two values of water flow rate inside the fibers equal to 338 l/h and 675 l/h. Shell water flow rate varied from 50 to 240 l/h with the step of 50 l/h. During the experiments, temperatures at the inlet and outlet of the fibers, as well as at the inlet and outlet of the shell were measured. The differential manometer was used to measure the water pressure loss in the heat exchanger shell.

The dependence of the PA-72 heat transfer rate on the shell water flow rate is shown in Fig. 24. Data are given for the shell water temperature of 50 °C. From the graph it can be seen that at low

shell water flow rates the heat transfer rate of heat exchanger does not depend on the flow rate of the liquid inside the fibers. Only with an increase in the shell water flow rate more than 150 l/h, the difference in heat transfer rate becomes more than 10%. The maximum heat transfer rate reached for a PA-72 heat exchanger with a shell water temperature of 50°C is 3.8 kW and maximum flow rates for both working fluids.

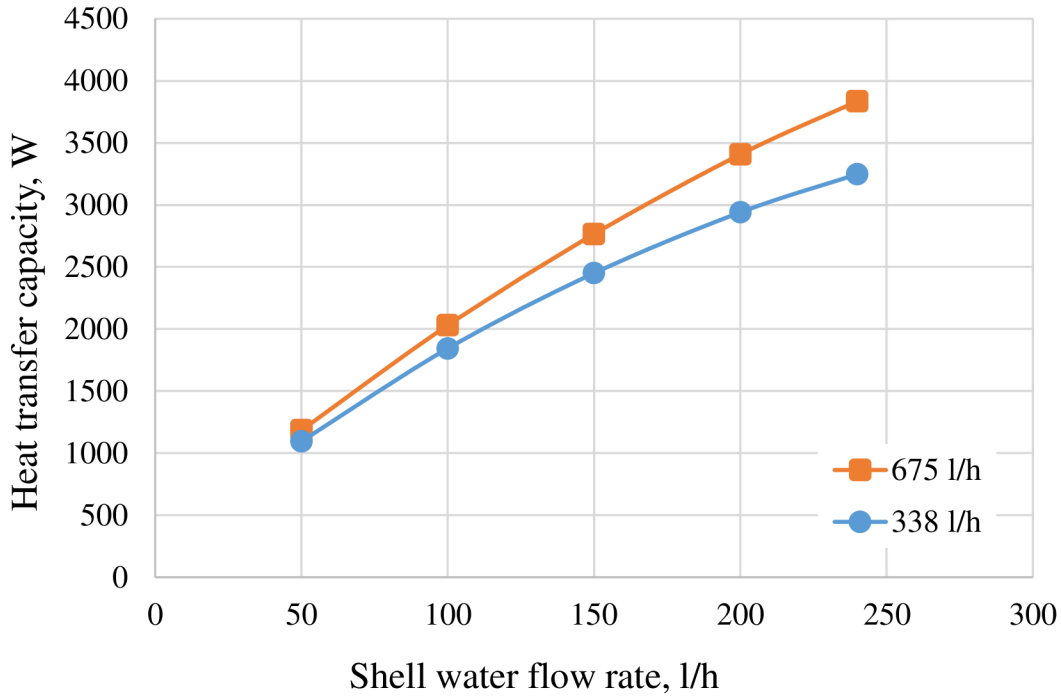


*Fig. 24 Dependence of the PA-72 heat transfer rate on the shell water flow rate for the shell water temperature of 50 °C*

Fig. 25 shows the dependence of the PA-72 heat transfer rate on the shell water flow rate for the shell water temperature of 70 °C. It is seen that the nature of the thermal rate change with the increase in the water flow rate inside the fibers is similar to that observed at 50 °C. The maximum value of the heat transfer rate reaches 4.3 kW with a shell water temperature of 70°C and maximum flow rates for both working fluids.

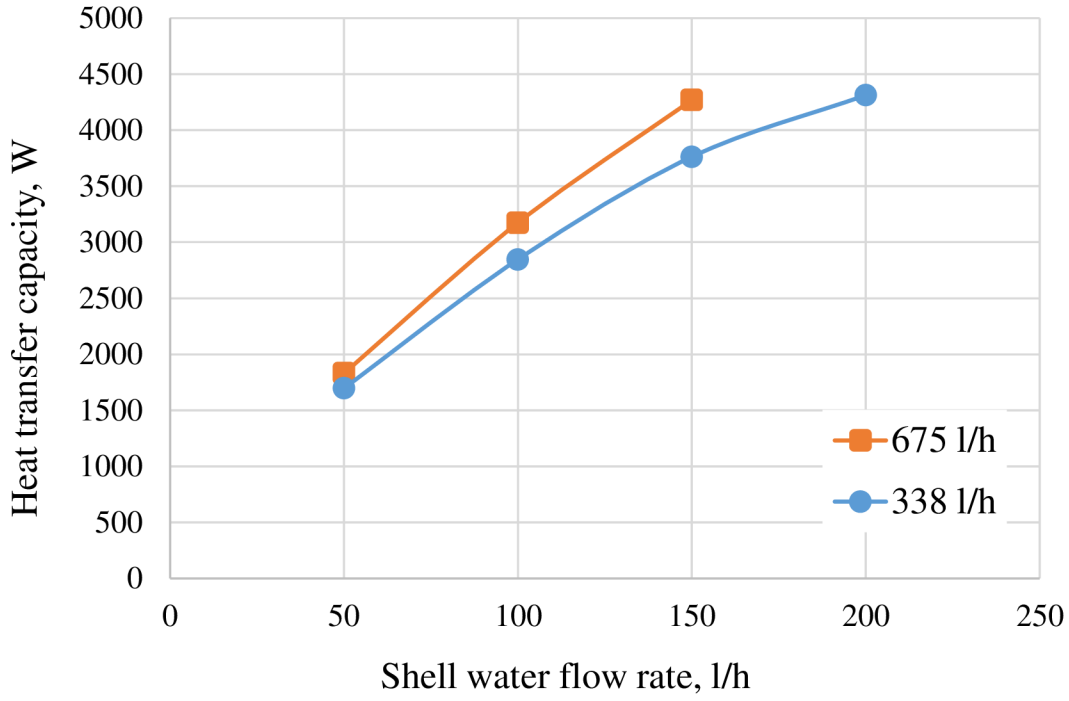


*Fig. 25 Dependence of the PA-72 heat transfer rate on the shell water flow rate for the shell water temperature of 70 °C*

Fig. 26 presents a dependence of the pressure losses in the PA-72 heat exchanger shell on the shell water flow rate. It can be noted that already at relatively small flow rates of 200 l/h the pressure loss is 50 kPa. This happen due to the fact that a large number of fibers inside the heat exchanger create a significantly hydraulic resistance to fluid flow. However, with this manufacturing technology it is impossible to reduce the number of fibers keeping the uniformity of their distribution in the volume of the heat exchanger.

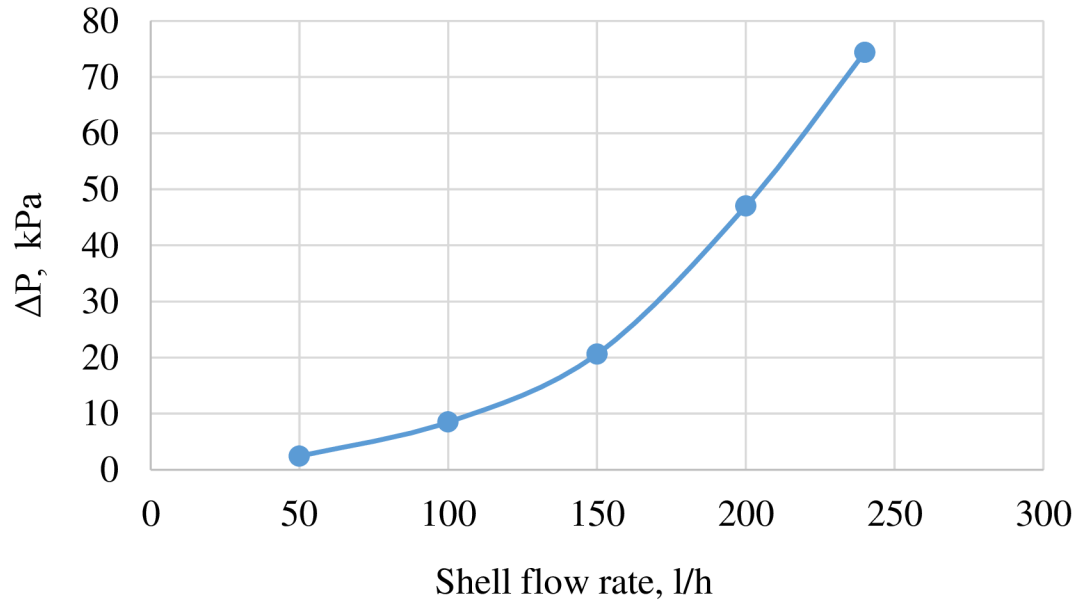


*Fig. 26 Dependence of the pressure drop in the heat exchanger shell on the shell water flow rate*

If you pay attention to the graph of the overall heat transfer coefficients of the heat exchanger (Fig. 27), it is clear that $h_{overall}$ for both water shell temperatures are quite low. The maximum $h_{overall}$ was equal to 180 W/m$^2$K at the shell water temperature of 50 °C and the water flow rate inside the fibers of 675 l/h. It can be explained by the large number of fibers in the shell and specialty of hollow fibers location along each other. In this case the fibers can easy overlap and adhere to each other, reducing the active heat transfer area.

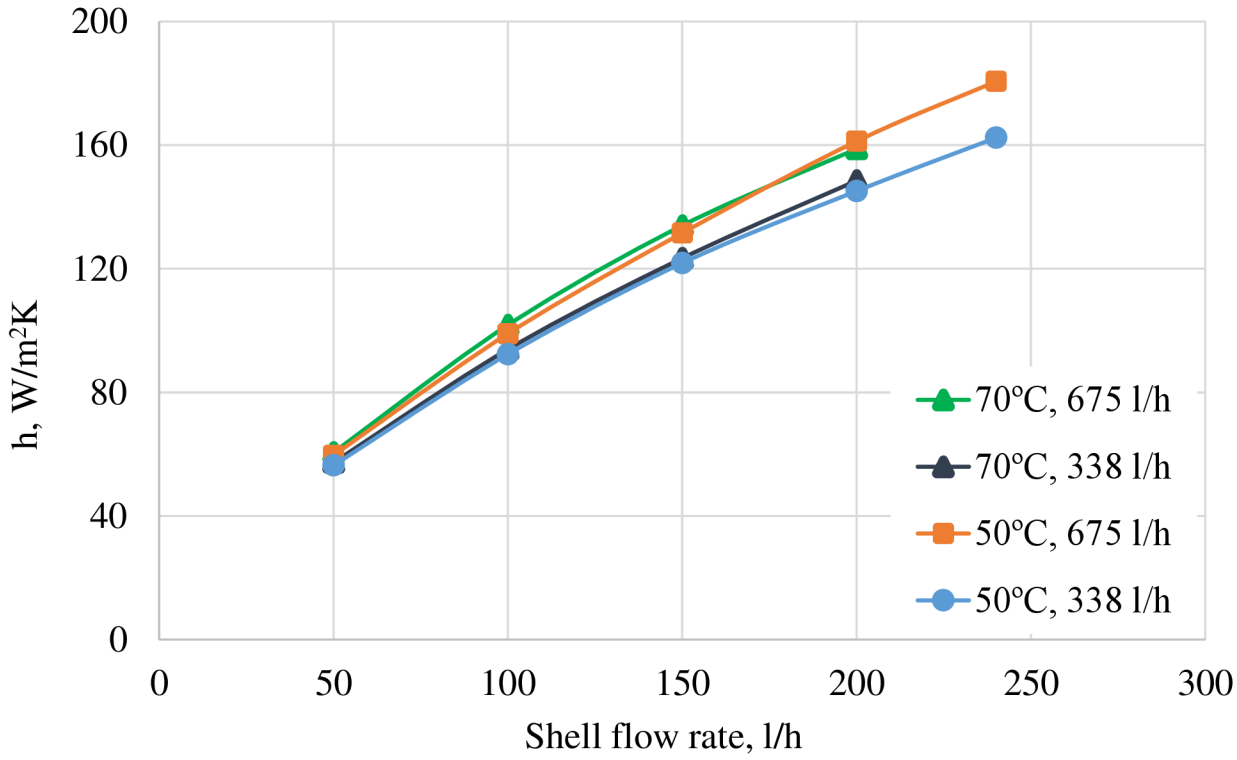


*Fig. 27 Dependence of the overall heat transfer coefficient of the PA-72 heat exchanger on the shell water flow rate*

Changes in the heat exchanger structure connected with adhesion of hollow fibers can be seen in Fig. 28 presenting a photo of the heat exchanger PA-72 after experiments. Fibers stick to each other, blocking the active area of heat transfer. It can also be noted that separate compact structures were formed from the fibers. Gaps with a low hydraulic resistance appeared between these structures. So, the part of shell water goes through these gaps and does not penetrate between the fibers. Than this working fluid almost not participate in heat transfer. Both of these factors leads to a significant decrease in the overall heat transfer coefficient of the PA-72 heat exchanger.

*Fig. 28 External view of PA-72 PHFHE after tests*

### *Intermediate conclusion*

Plastic heat exchanger PA-72 showed a quite good thermal performance for compact heat exchangers. However, the problems with fibers sticking and their irregular spacing in the shell due to the formation of compact structures forced us to search ways for optimizing the fibers arrangement in the volume of the heat exchanger and ways for increasing the intensity of heat transfer on the hollow fibers outer surface.

## 5.2 Main methods of heat- and mass- transfer modeling

To avoid sticking of the fibers during operation of the heat exchanger, was considered a method of optimizing the design of the heat exchanger by placing fibers in the shell at an angle (Fig. 29). Supposed that such a change in the heat exchanger structure will allow the fibers to be evenly positioned and to avoid sticking of the fibers. Fiber will have a contact to each other only in one point and not in the whole length. It can lead to a uniform fluid flow in the volume of the heat exchanger shell and the whole entire surface will participate heat transfer processes. Also, when hollow fibers will lay at an angle to each other it may lead to an increasing in the thermal performance of the device due to intermixing of the liquid flow and avoiding of laminar flow forming inside the shell.

Before making a prototype, a numerical simulation of the heat exchange process on the outer surface of polymeric fibers was carried out. The main purpose of such a modeling was to optimize the heat exchanger geometry and to determine the best hollow fibers position inside the heat exchanger. For this purpose, a program ANSYS was used.

### 5.2.1 Classification of modeling methods

Nowadays, with the intensive development of computer technology a modeling of various physical processes becomes more popular. In problems of heat and mass transfer a numerical experiment now is comparable with the importance of a natural experiment.

As known, processes of heat- and mass- transfer from the continuum mechanics viewpoint can be described by a system of nonlinear differential equations in partial derivatives. This equation system is called Navier-Stokes equations. For non-isothermal flow of an incompressible fluid it will contain the equations of continuity, momentum and energy:

$$\frac{\partial U_i}{\partial x_i} = 0 \tag{20}$$

$$\frac{\partial U_i}{\partial \tau} + U_j \frac{\partial U_i}{\partial x_j} = f_i - \frac{1}{\rho}\frac{\partial P}{\partial x_i} + \nu \frac{\partial}{\partial x_j}\left(\frac{\partial U_i}{\partial x_j}\right) \tag{21}$$

$$\frac{\partial T}{\partial \tau} + U_j \frac{\partial T}{\partial x_j} = \chi \frac{\partial}{\partial x_j}\left(\frac{\partial T}{\partial x_j}\right) + \frac{q_v}{\rho c_p} \tag{22}$$

where $\nu = \frac{\mu}{\rho}$ - is a kinematic viscosity of the medium and $\chi = \frac{\lambda}{\rho c_p}$ is a thermal diffusivity.

Unfortunately, this system of equations has no general analytical solution. The analytical solution of this system exists only in a few specific examples and with a number of specific assumptions. At the same time numerical methods for solving Navier-Stokes equations are developed quite well and have found wide application in various fields of science and technology.

There are three basic methods for numerical solution of the Navier-Stokes equations. The first method is called the Finite Difference Method. Its essence is that partial derivatives are replaced by discrete analogues. The solution is sought in nodes of the mesh, into which the computational area is divided. The advantage of this method is a relative simplicity, but at the same time, specific requirements for the mesh construction are imposed, that often complicates the decision process.

The second method is called the Finite Elements Method [31], [32], [33]. The method is about the fact that the problem of finding some function is replaced by the problem of finding a finite number of its approximate values in individual nodes. The Finite Elements Method, as well as other numerical methods, in essence approximately replaces the continual problem by a discrete. In the Finite Elements Method, the whole procedure of such replacement has a simple physical meaning. It allows more fully imagining of the whole process of solving the problem, avoidance of many possible mistakes and properly assessment of the obtained results. The Finite Elements Method is convenient to apply for geometrically and physically complex systems due to the fact that this method uses an algorithm of transition from individual elements to their full set.

The third method is called the Finite Volumes Method [34]. In this method the calculated area is divided to an aggregate of finite volumes with the help of the mesh. Nodes, in which the solution is sought, are located in centers of these volumes. For each volume laws of mass, momentum and

energy conservation are maintained. This method is widely used in different hydrodynamic packages (CFD).

There are also methods that combine features of the Finite Volumes Method and the Finite Elements Method [35]. The combination of these methods makes it possible to use a wide range of computational meshes that is very important in solving problems with complex geometry. This approach is used in such programs like Ansys CFX and Ansys Fluent.

In the Finite Volume Method solution to each of the system equations (20),(21),(22) is reduced to the solution of linear algebraic equations. The number of these equations is equal to the number of cells in the computational mesh. Each of these equations systems can be solved conjointly with all other or separately. Separate solution requires fewer resources, however in this case a number of problems may arise. When using a separate decision, it is necessary to apply special techniques in order that decisions obtained for pressure and velocity fields meet each other, to use so-called pressure-velocity coupling. For this purpose, special formulas for adjustment of the pressure and velocity are introduced.

One of the most popular methods of separate solution is called Semi-Implicit Method for Pressure-Linked Equations (SIMPLE) [36], [37].

### 5.2.2 Turbulent flow modeling

***Reynolds Averaged Navier-Stokes equations***

Turbulent flow can be described by the Navier-Stokes equations. For the direct numerical solution of the equations systems there is a method called Direct Numerical Simulation. However, this method is extremely resource-intensive and is not suitable for problems with complex geometry. For the case of turbulent flow high quality meshes with a very small step are necessary. The time step also has to be very small. All this requires very powerful computers with a large memory capacity. In this connection for engineering calculations, a need to simplify the Navier-Stokes equations arises thereby reducing the computational power demand.

For a quantitative description of the developed turbulent flow Reynolds suggested that the value of any parameter dependent on time can be represented as the sum of averaged and fluctuating components. It means that the considered value is the value varying according to some definite law, to which accidental pulsation are added.

Then the system of equations (20), (21), (22)can be rewritten as follows

$$\frac{\partial \bar{U}_i}{\partial x_i} = 0 \tag{23}$$

$$\rho\left(\frac{\partial \bar{U}_i}{\partial \tau} + \frac{\partial\left(\bar{U}_i \cdot \bar{U}_j\right)}{\partial x_j}\right) = \rho f_i - \frac{\partial \bar{p}}{\partial x_i} + \frac{\partial}{\partial x_j}\left(\mu \frac{\partial \bar{U}_i}{\partial x_j} - \rho\overline{U_j' U_i'}\right) \tag{24}$$

$$\rho c_p\left(\frac{\partial \bar{T}}{\partial \tau}+\bar{U}_j\frac{\partial \bar{T}}{\partial x_j}\right)=\frac{\partial}{\partial x_j}\left(\frac{\partial \bar{T}}{\partial x_j}-\rho c_p\overline{U_j^{'}T_i^{'}}\right)+q_v \quad (25)$$

The term $-\rho\overline{U_j^{'}U_i^{'}}$ represents Reynolds stress tensor. The term $-\rho c_p\overline{U_j^{'}T_i^{'}}$ is an additional heat flow due to turbulent transfer. In order to calculate these terms, additional equations are required. These equations are called models of turbulence.

***Boussinesq hypothesis***

Boussinesq hypothesis is not a model of turbulence, it only states that turbulent stresses, as well as common friction stresses are proportional to the velocity gradient.

For the general case of an incompressible fluid Boussinesq hypothesis is written as follows:

$$-\rho\overline{U_j^{'}U_i^{'}}=\mu_T\left(\frac{\partial \bar{U}_i}{\partial x_j}+\frac{\partial \bar{U}_j}{\partial x_i}\right)-\frac{2}{3}\delta_{ij}\rho k \quad (26)$$

where $\delta_{ij}$ is a Kronecker symbol and $k=\frac{\overline{U_i^{'}U_i^{'}}}{2}$ is a kinetic energy of turbulence.

For the energy equation Boussinesq hypothesis would look like this:

$$-\rho c_p\overline{U_j^{'}T^{'}}=\lambda_T\cdot\frac{\partial \bar{T}}{\partial x_j} \quad (27)$$

Then the system of equations (23), (24), (25)can be rewritten as:

$$\frac{\partial \bar{U}_i}{\partial x_i}=0 \quad (28)$$

$$\rho\left(\frac{\partial \bar{U}_i}{\partial \tau}+\frac{\partial\left(\bar{U}_i\cdot\bar{U}_j\right)}{\partial x_j}\right)=\rho f_i-\frac{\partial P}{\partial x_i}+\frac{\partial}{\partial x_j}\left((\mu+\mu_T)\frac{\partial \bar{U}_i}{\partial x_j}\right) \quad (29)$$

$$\rho c_p\left(\frac{\partial \bar{T}}{\partial \tau}+\bar{U}_j\frac{\partial \bar{T}}{\partial x_j}\right)=\frac{\partial}{\partial x_j}\left(\lambda+\lambda_T\frac{\partial \bar{T}}{\partial x_j}\right)+q_v \quad (30)$$

where $P=\bar{p}+\frac{2}{3}\rho k$ is a pressure with the consideration of turbulent pulsations.

However, approaches using the Boussinesq hypothesis have one major drawback. In this method the viscosity is represented as a scalar, thus Boussinesq theory assumes that the turbulence is isotropic that is not always in real life.

***Models of turbulence***

One of the most popular differential models of turbulence is a k-ε model. Two parameters are entered for its building. The first parameter is a kinetic energy of turbulence $k = \frac{\overline{U_i' U_i'}}{2}$, the second one is a dissipation of turbulent energy$\varepsilon = \nu \overline{\frac{\partial U_i'}{\partial x_j} \frac{\partial U_i'}{\partial x_j}}$. Then the model equations will look like this

$$\frac{\partial k}{\partial \tau} + \bar{U}_j \frac{\partial k}{\partial x_j} = \frac{\partial}{\partial x_j}\left((\nu + \nu_T)\frac{\partial k}{\partial x_j}\right) + \left(\frac{\partial \bar{U}_i}{\partial x_j} + \frac{\partial \bar{U}_j}{\partial x_i}\right) \cdot \frac{\partial \bar{U}_i}{\partial x_j} - \varepsilon \tag{31}$$

$$\frac{\partial \varepsilon}{\partial \tau} + \bar{U}_j \frac{\partial \varepsilon}{\partial x_j} = \frac{\partial}{\partial x_j}\left(\left(\nu + \frac{\nu_T}{a}\right)\frac{\partial \varepsilon}{\partial x_j}\right) + b\frac{\varepsilon}{k}\left(\frac{\partial \bar{U}_i}{\partial x_j} + \frac{\partial \bar{U}_j}{\partial x_i}\right) \cdot \frac{\partial \bar{U}_i}{\partial x_j} - c\frac{\varepsilon^2}{k} \tag{32}$$

where $\nu_T = a_\mu \frac{k^2}{\varepsilon}$ is a turbulent kinematic viscosity and $a_\mu$is an empirical constant approximately equal to 0.09. The k-ε model is a high Reynolds model and describes developed turbulence well. This model is most commonly used in the first calculation.

In addition to this turbulent model, there is a k-ω model, it is one of the very first differential models with two differential equations. This model contains transfer equations of the turbulent kinetic energy k and the dissipation energy specific rate ω. The dissipation energy specific rate is connected with k and ε by the following equation $\omega = \frac{\varepsilon}{a_\mu k}$. This is a low Reynolds model and describes well the near-wall flow, but not very well describes the developed turbulence.

In this respect a much more universal model is the Shear Stress Transport model (SST). It is a combination of k-ε and k-ω models. The k-ω model is used for the near-wall layer and turbulence in the volume is described by the k-ε model. SST model is also extremely popular as a k-ε model and is included in many packages of computational fluid dynamics.

In addition to these three described models there are many different models, including more complex such as LES [38] and DES, and the list continues to grow.

## 5.3 Description of PHFHE domain

This study was already published in Materiali in tehnologije journal in 2018 [39]

Usually PHFHE heat exchanger contains more than 1500 hollow fibers. Described above heat exchanger with parallel hollow fibers PA-72 had about 1700 fibers. Due to the large number of fibers the simulation of the whole internal volume of the heat exchanger will take a lot of computing power. Therefore, a rectangular parallelepiped domain with a square cross section of 10x10 mm and length of 100 mm was selected as the object of investigation. Fibers in the model, which were considered as hollow cylinders, pass through the cooling medium's domain. The outer diameter of each fiber was 0.8 mm and the interaxial distances between adjacent fibers was 2.4 mm. As the fiber wall temperature at this length changes slightly in reality, in the model it was set as a constant and

were equal to 60 °C. Water was chosen as a cooling medium with the velocity equal to 0.3 m/s. The pressure inside the domain was 1 bar. Plastic fibers have a low surface roughness (less than 1 μm), therefore it was not considered in this model.

The model of model makes possible to change the orientation of the hollow fibers inside the heat exchanger. The hollow fiber position with respect to the direction of the shell water flow, determined by the angle α, was concerned as a variable parameter.

Angle α in the model was set according to Fig. 29 (left). The largest value of the angle α is restricted by opportunities of production equipment and is equal to 45°. Therefore, in this simulation, this parameter varied from 0° to 45°. Fig. 29 (right) shows angle α determination in a real PHFHE.

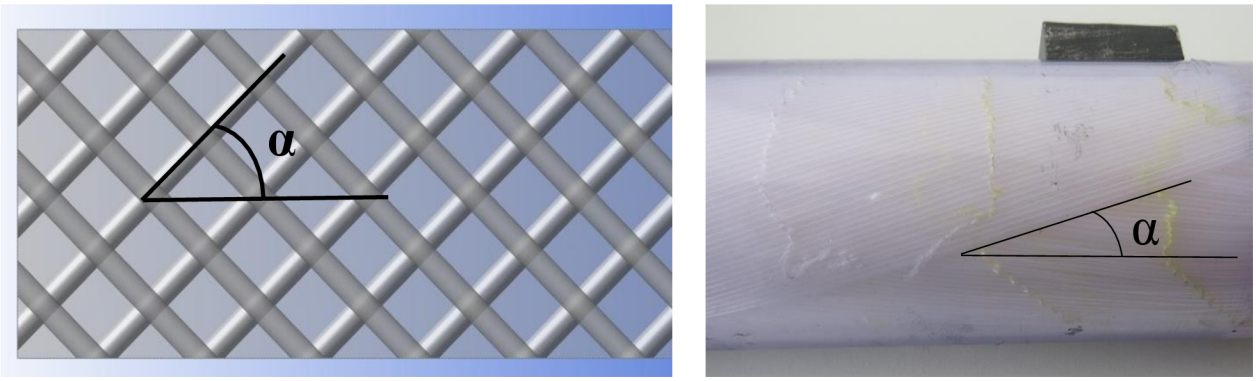


*Fig. 29 Angle α in in the model (left) and a real PHFHE (right)*

The overall view of the whole PHFHE domain with hollow fibers placed at the angle to the cooling water flow is shown in Fig. 30.

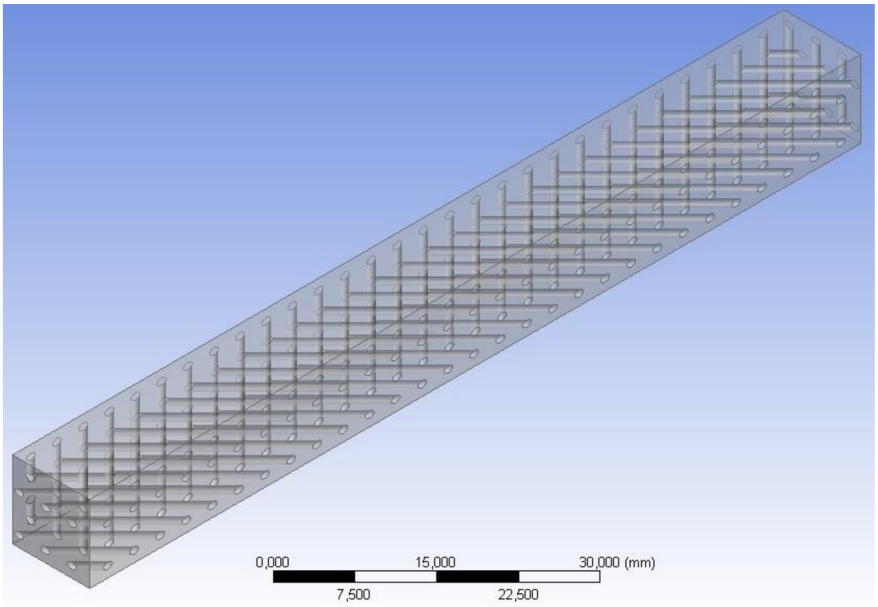


*Fig. 30 Overall view of the PHFHE domain*

The heat exchange process was simulated using the finite volume method in ANSYS CFX [31], [35]. Because the aim of the work was to compare the heat transfer coefficients on the hollow fiber surface, the domain size and boundary conditions for each case of α were identical.

The mesh was set using the ANSYS Meshing program. For α = 0°, the mesh had quadro elements. The number of these elements was equal to 3.7 ml. One of the main parameters of mesh quality is the Y+ coefficient. It represents the non-dimensional wall distance for a wall-bounded flow and can be described by the following equation:.

$$Y^+ = \frac{u \cdot y}{\upsilon} \tag{33}$$

where u is the friction velocity at the wall, y is the distance to the wall $y$ is the distance to the wall and $\upsilon$ is the local kinematic viscosity of the fluid. For a heat transfer calculation, Y+ near the wall usually must be less or equal to 1. When α = 0°, Y+ max was equal to 0.94.

When α > 0°, a mesh with tetra elements was used in the volume and the near-wall layer was defined by quadro elements. For different values of α, the number of elements varied from 5 to 7 million and the Y+max never exceeded 0.98. General views of each mesh are shown in Fig. 31.

At angle α = 0° Re < 1000 and the water-cooling flow regime was a laminar. A laminar model for modelling this flow was used for this case. The heat from the fiber outer surface transferred to the cooling medium only by the thermal conductivity of water.

For α > 0° the SST-turbulence model was selected as a combination of k-ε and k-ω models. The k-ω model was used for simulating the near-wall layer turbulence. The turbulence in the flow volume is described by the k-ε model [34]. Certainly, LES and DES tabulating models enable to simulate the turbulence flow more detail, but they require significant computing power resources and for case under discussion are redundant [38].

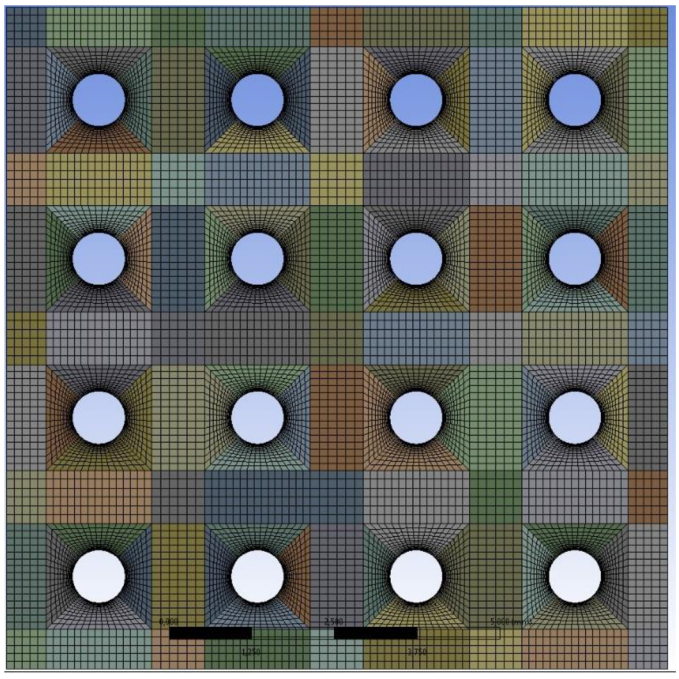

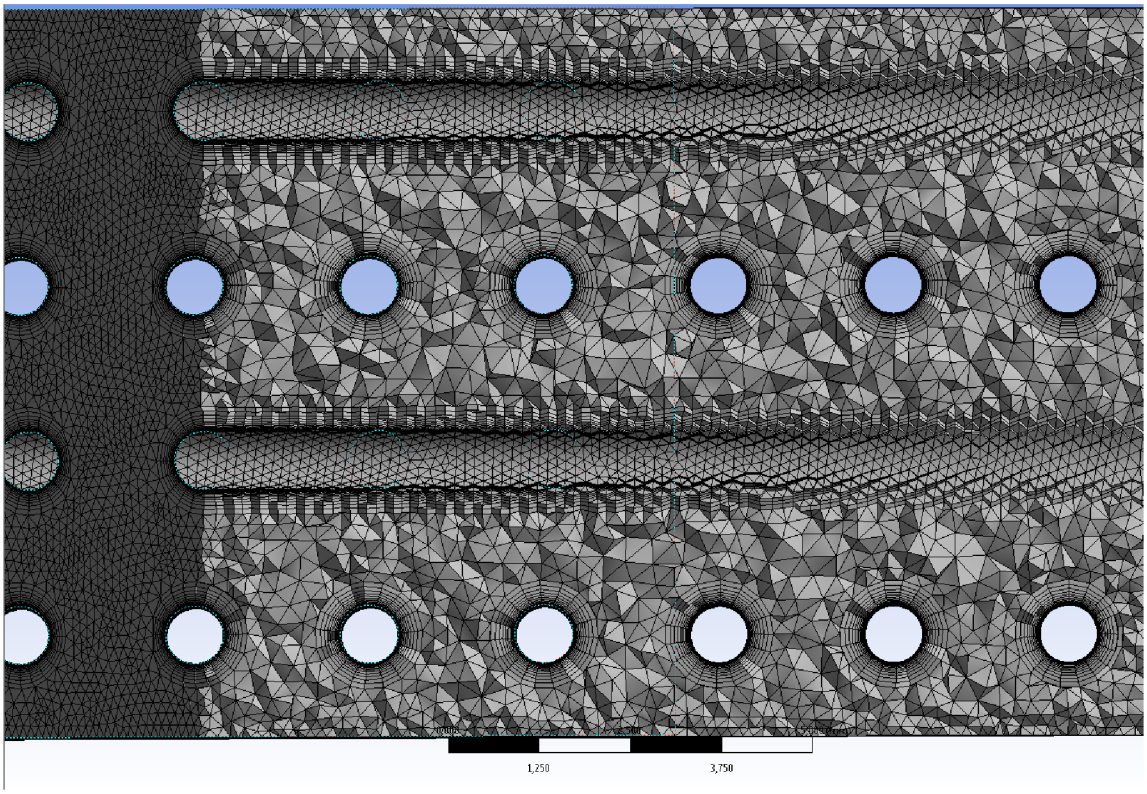


*Fig. 31 Computational mesh for the case of α =0° (a) and α=45° (b)*

## 5.4 Results of PHFHE modeling

Equation (34) was used in a calculation relating the heat transfer coefficient and thermal resistance inversely proportional

$$R = \frac{1}{h} \tag{34}$$

where h is the heat transfer coefficient. Overall thermal resistance of heat exchanger can be presented as a sum of the resistances:

$$R_{overall} = R_{in} + R_{wall} + R_{out} \tag{35}$$

where $R_{in}$ is the thermal resistance of the heat transfer from the hot fluid inside the fiber to its wall, $R_{wall}$ is the thermal resistance of the fiber wall, $R_{out}$ is the thermal resistance of the heat transfer from the fiber wall to the cooling medium outside the fiber.

Each fiber is a capillary tube and the heat exchange inside the tubes with a small diameter is very intensive (Fig. 32). It is obvious that heat exchangers with hollow fibers works in laminar area where heat transfer is independent from liquid velocity (constant Nu). $R_{in}$ is a relatively small part of the $R_{overall;}$ and attempts to its further reducing will not have a significant impact on the $R_{overall}$.

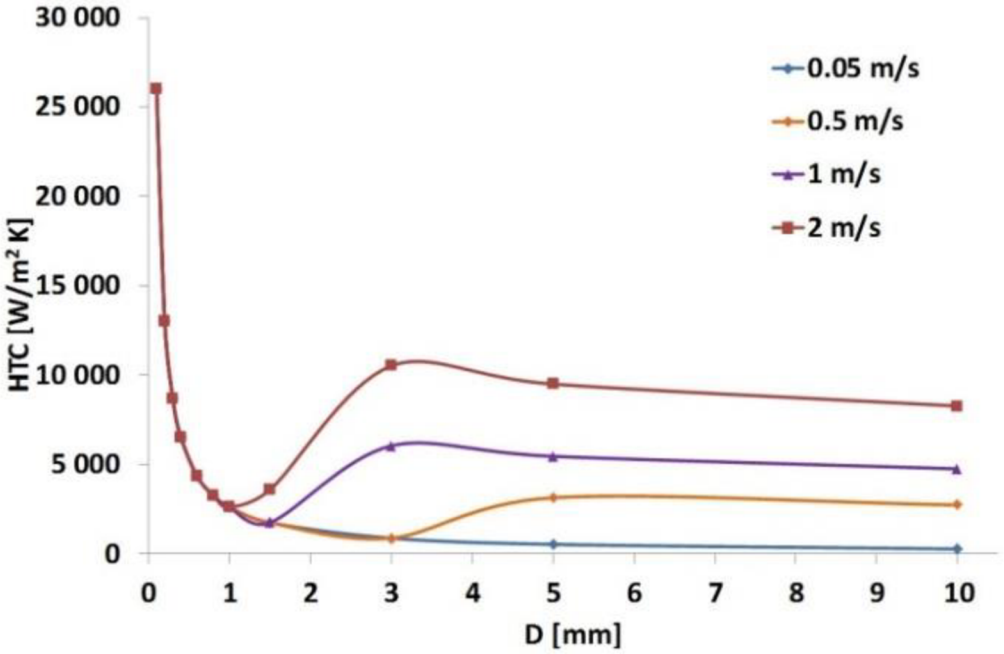


*Fig. 32 Dependence of heat transfer coefficients inside the tubes on the tube diameter for water with variable velocity [40].*

$R_{wall}$ depends on wall thickness. For this PHFHE hollow fibers with a wall thickness of 0.1 mm were used. Such a value was determined by the strength properties of the fibers. Further reduction in wall thickness will adversely affect the reliability of the heat exchanger. So, for this type PHFHE the value $R_{wall}$ can be considered as a constant.

That is why the main attention in this analyze was focused on the intensity of the heat transfer in the outer surface of the fibers $R_{out}$. Contribution of $R_{out}$ to the total thermal resistance of the heat exchanger at $\alpha = 0°$ is about 35% - 40%.

The computer simulation results in the view of the dependence of the heat transfer coefficient on the outer fibers surface on the angle α between the cooling flow direction and the fibers is shown on the. Fig. 33 The graph shows that even an increase in angle α up to 5° results in the heat transfer coefficient increase by two times. This fact is explained by the change of the laminar cooling flow regime in the heat exchanger with the angle $\alpha=0$ to the turbulent cooling flow regime for the exchangers with $\alpha > 0$. Hollow fibers cross the water flow and water starts to intermix, leading to intensification of heat exchanging on the outer surface of hollow fibers.

It can be seen from the graph that heat transfer coefficients increase almost linearly when angle α changes from 0° to 30°. Further increases in α, from 30° to 45°, lead to very slight increase in heat transfer coefficients. Decrease in the growth rate of heat transfer coefficients can be explained by the achievement of the regime of advanced turbulence. The maximum heat transfer coefficient was equal to 10 563 $W/m^2K$.

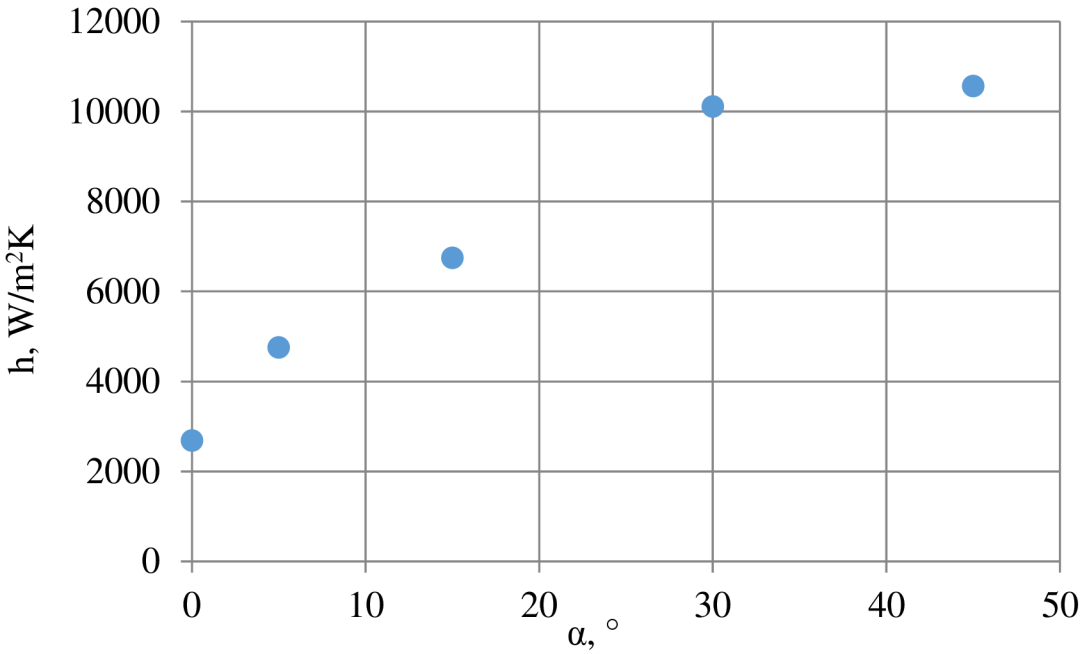


*Fig. 33 Heat transfer coefficient on the outer surface of hollow fiber vs the angle α.*

Fig. 34 illustrates the dependence of the total heat transfer coefficient of the whole heat exchanger on angle α. Even an increase in α to 5° increases the heat transfer coefficient by nearly 20%. At the maximum angle α= 45°, the heat transfer coefficient is increased by 35% and is equal to 1267 W/m$^2$K.

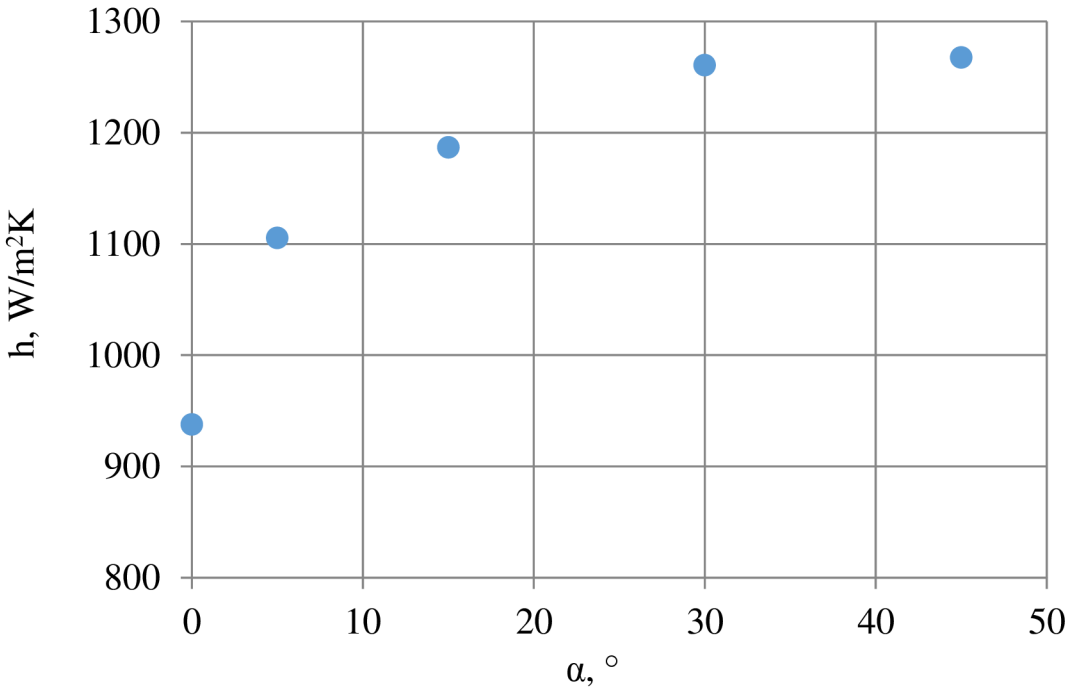


*Fig. 34 Overall heat transfer coefficient of the PHFHE vs the angle α.*

### *Intermediate conclusion*

It was found that hollow fibers placing at the angle to water cooling flow leads to increase in heat transfer coefficient on the outer surface of hollow fibers. A sharp overall heat transfer coefficient increase was observed as angle α increases to 20°. Further angle α changing to 45° had no significant effect on the $h_{overall}$. Angle 20° can be considered as a minimum optimal angle for manufacturing of PHFHEs with crossed hollow fibers.

## 5.5 PHFHE with crossed hollow fibers

Based on computer modeling results two similar PHFHEs shown in Fig. 35 were produced. Heat exchangers were constructed as shell-and-tube with a water as a working fluid [41]. Hollow fibers with the diameter of 0.8 mm were made of polycarbonate. Potting area diameter of the shell was equal to 40 mm and the effective length of the PHFHEs was 280 mm.

In PHFHE-1 hollow fibers were placed parallel to the liquid flow. PHFHE-2 had hollow fibers crossed at the angle of 22.5°. Such hollow fibers orientation was realized by hollow fibers interweaving by a synthetic filament and its further twisting, see Fig. 36 and Fig. 29 (right). Fibers amount of potting area for PHFHE-1 was 30% and the heat transfer area was 0.52 $m^2$, for PHFHE-2 these values were equal to 33% and 0.54 $m^2$ correspondently.

In comparative experiments the water temperature inside the fibers was equal to 27 ºC and the shell water temperature was set as 80 ºC. The liquid flow rate inside the fibers was 660 l/h, and the shell water flow rate varied from 200 to 1000 l/h.

*Fig. 35 PHFHE-1 and PHFHE-2 in stainless steel shell*

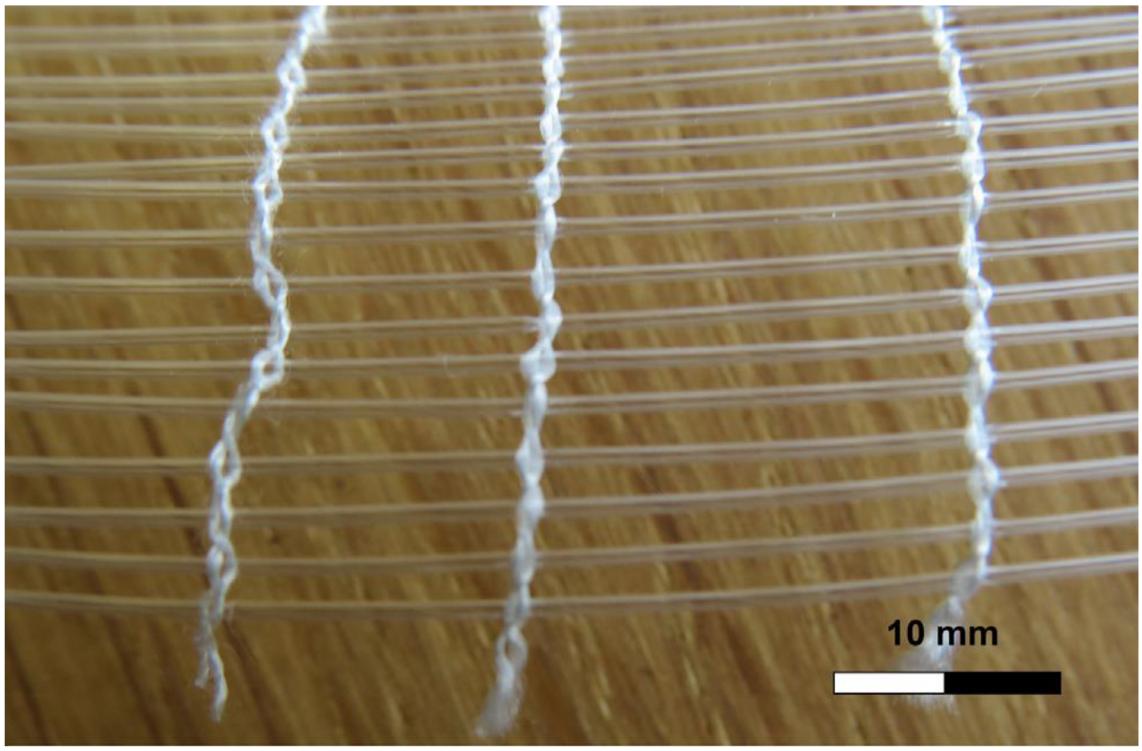


*Fig. 36 Layer of hollow fibers separated by weaving technology [42].*

The dependence of the PHFHE overall heat transfer coefficients on the shell water flow rate is presented in the Fig. 37. It can be seen, that at low flow rates heat transfer coefficients are almost the same for both of heat exchangers. However, the heat transfer coefficients for the PHFHE-2 with crossed hollow fibers are more than 10% higher compared with the PHFHE-1 with parallel fibers at the shell water flow rate increasing over 800 l/h. At the shell water flow rate of 1000 l/h $h_{overall}$ for PHFHE-2 achieves the maximum value of 1091 W/m$^2$K, wherein the maximal heat transfer coefficient of the PHFHE-1 was 970 W/m$^2$K.

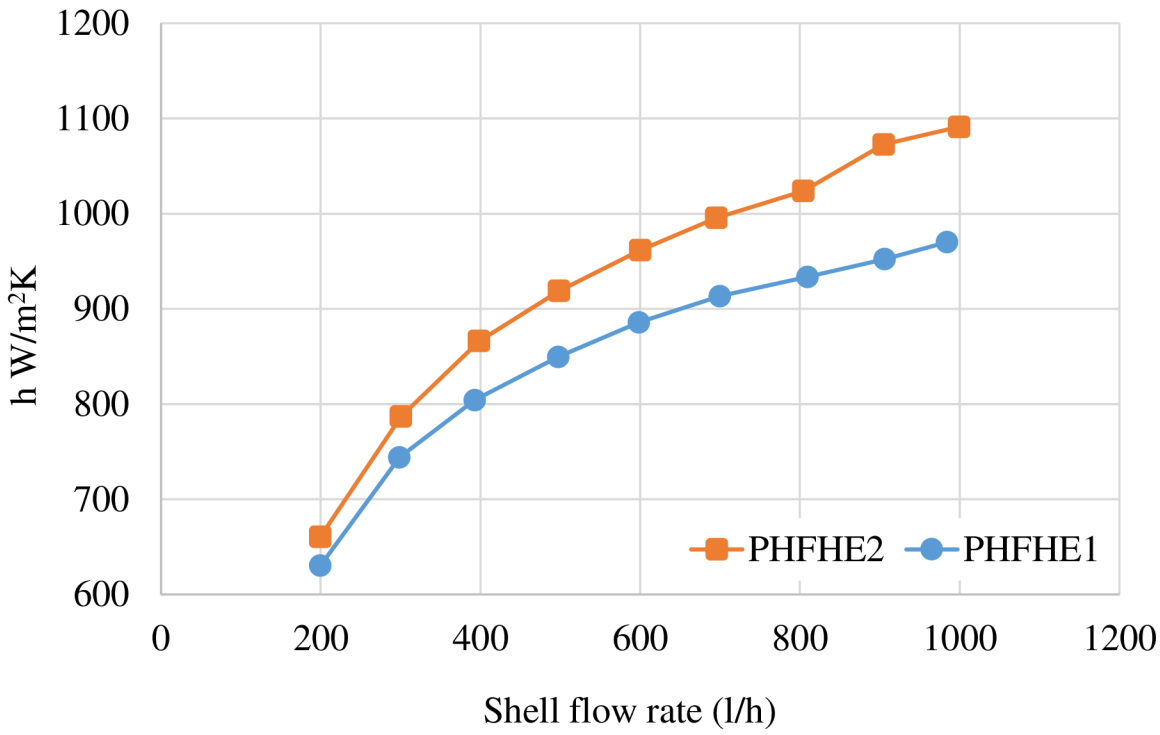


*Fig. 37 Dependence of the PHFHE-1 and PHFHE-2 overall heat transfer coefficients on the shell water flow rate.*

Such an increase in $h_{overall}$ for the PHFHE-2 with crossed hollow fibers can be explained by the fact that the declination of the hollow fiber axis with respect to the shell water flow leads to the its turbulization and as a consequence to the heat transfer coefficients on the hollow fibers outer surface increase.

Moreover, despite hollow fibers crossing the pressure losses for both of heat exchangers were identical as can be seen from the Fig. 38. Such a PHFHE design doesn't affect the device hydraulic resistance.

It should be noted that active heat transfer areas were almost the same for both heat exchangers. So, the method of hollow fibers crossing inside the PHFHE results on the heat exchanger efficiency increase and can be applied for producing the shell-and-tube PHFHEs.

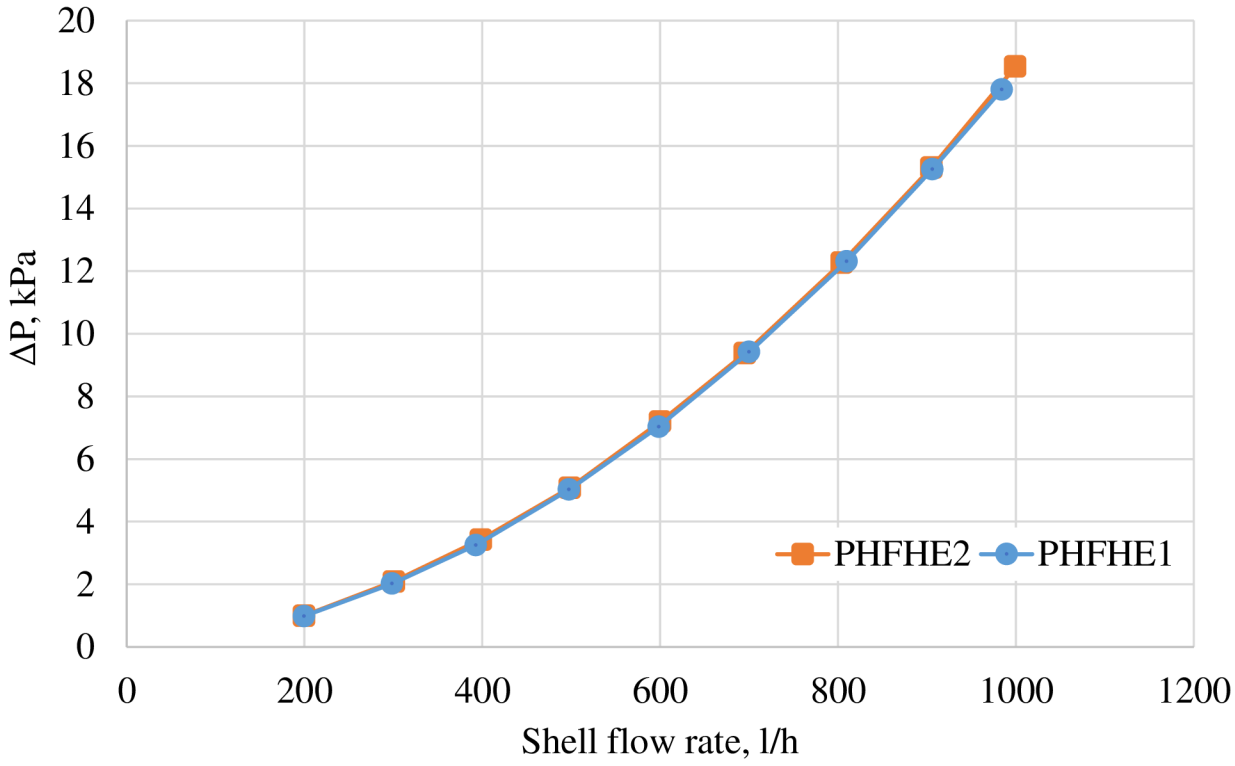


*Fig. 38 Dependence of the hydraulic losses inside the PHFHE-1 and PHFHE-2 shell on the shell water flow rate*

## *Intermediate conclusion*

Tests of heat exchanger with hollow fibers interweaved by synthetic filament showed that a strict arrangement of the fibers in the heat exchanger and their crossing gives a significant positive effect on the thermal characteristics of the device. However, the use of such a synthetic filament is a quite expensive technology. Besides, during the operation of the heat exchanger, there is a possibility of the fibers wiping in the contact point with the filament. So, it was necessary to find another method for manufacturing of plastic heat exchangers with a specified arrangement of fibers and their number.

# 6. DEVELOPMENT OF TECHNOLOGY FOR PRODUCING PHFHE WITH OPTIMIIZED STRUCTURE

The requirements for manufacturing methods of polymeric hollow fiber heat exchangers and for pilot machine itself can be summed up as follows:

1. should allow automated production of the PHFHE;
2. should be easily adapted for mass production;
3. should allow to set the dimensions of the heat exchanger (length, diameter and so on);
4. should allow to regulate angle of slope of the hollow fibers and their number.

Taking into account these requirements, the pressure tanks manufacturing technology was taken into account. The winding principle on these machines was adapted and adjusted for the needs of PHFHEs manufacturing.

## 6.1 Winding setup X-Winder and its modernization

For the production of PHFHE with crossed fibers, the X-Winder was used. This machine is a smaller version of the filament winding machines, which were invented during the 1960's and were used to winding of airframes and missiles [43]. These machines are typically the size of a school bus and are very expensive. The X-Winder considered as a desktop version of these machines and it is mainly used to create small pressure tanks by winding technology. The main advantage of this device is the ability to simulate the process of manufacturing a product on real production capacity for reasonable price.

External view of the X-Winder is shown in Fig. 39. It consists of several functional blocks:

1. A block for fixing a wound device equipped with an electric motor with the possibility of changing the direction and the speed of rotation.
2. The block for the wound material, which included the holder for the spool with the wound material - a hollow fiber for the creation of the internal structure of the heat exchanger and fiberglass for wounding the outer surface of the device. It also contains a container for adhesive material, knife for removing excess glue, a feeding head and two electric motors that control turning and moving of the feeding head along the Y axis.
3. Guide for moving the unit with the wound material, equipped with an electric motor for moving along the X-axis and a belt drive.
4. Motors and end sensors of the control system.


*Fig. 39 External view of the X-Winder*

Thus, the X-Winder had four moving axes. This machine is controlled by special program that allows to set diameter, length and other parameters of the winding device. After setting these parameters, the program generates a G-code that controls the movement of all four axes of the system in the winding process. A program window with customizable device parameters is shown in Fig. 40. In the left side of the window is possible to choose a number of rotation axes, a type of wound sample (with flat ends or beveled ends), a number of winding layers, a diameter and a thickness of winding material, a winding rate. In the central part the following parameters can be specified: winding sample sizes (length and diameter that can differ on the opposite ends of the sample), a diameter of the central tube, an offset from the central axis to determine start position of feeding head, an angle of the winding material. In the right part of the program window button *Home* returns winding head to the initial position which is calculated by the program based on adjusted parameters. Button *Manual* allows to manually set the speed of each motor. Button *Trace* allows to check the offset distance of the winding head. Button *Build* starts the winding process.

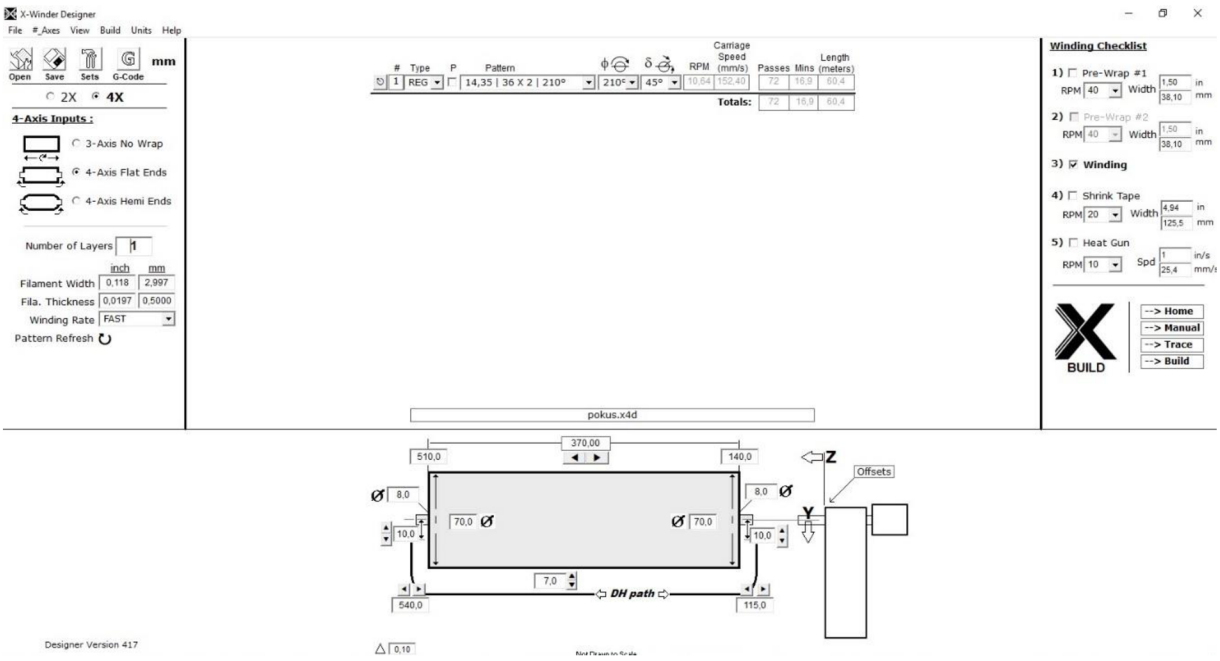


*Fig. 40 Working window of the X-Winder Designer*

To use this system for the shell-and-tube heat exchanger production, changes were made to its design. New feeding heads have been designed and manufactured using 3D printer shown in Fig. 41: the lower one was used for winding plastic fiber, the upper one - for winding glass fiber for the PHFHE shell. New heads made it possible to more accurately set the position of the plastic fiber in the finished product and prevent the glass fiber of slipping during the winding of the outer shell.

*Fig. 41 Improved feeding heads*

In order to avoid slipping of the plastic fibers at the ends of the PHFHE during their winding, as well as to set the exact location of the fibers in the necessary positions, special sprockets were designed and manufactured. They were fixed at the ends of the device. During the winding process the fiber lays in the groove and due to this remains fixed in the right position. The use of different number of a sprocket beam allowed to create a constant volume of fibers with increasing winding

diameter. The External view of the sprockets and their use in the pilot machine are shown in Fig. 42 and Fig. 43. For different diameters of the winding samples, various sprockets were used. These sprockets allowed their reuse for production of the next piece of the PHFHE.

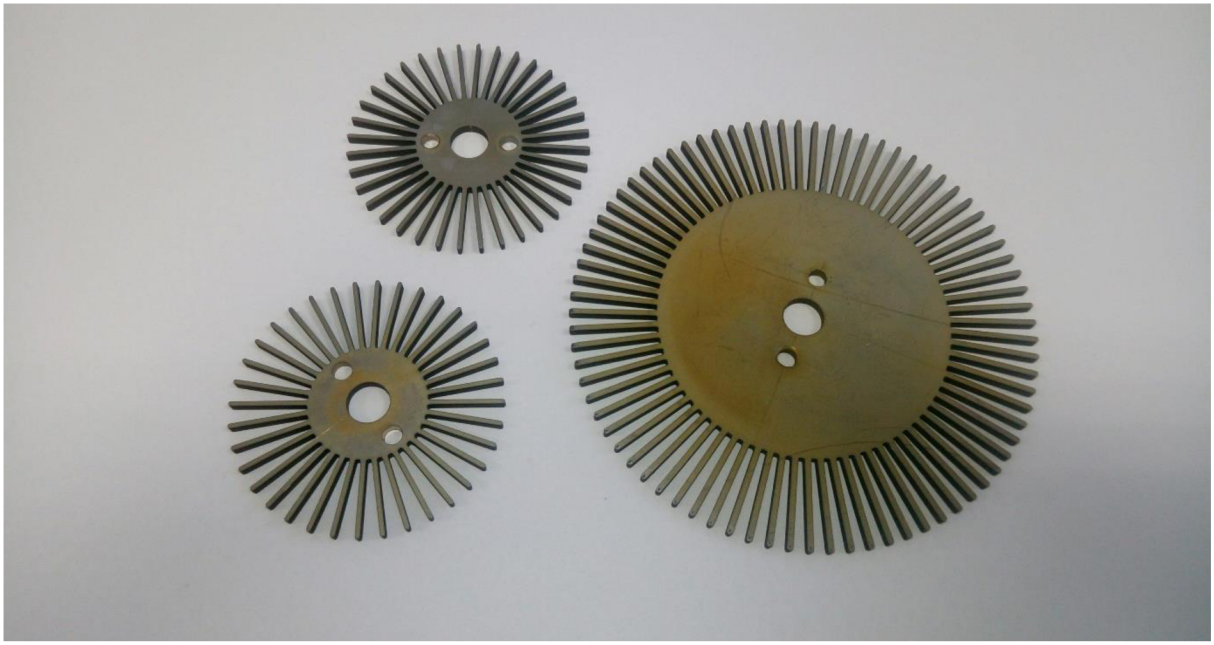

*Fig. 42 External view of the sprockets with different diameters.*

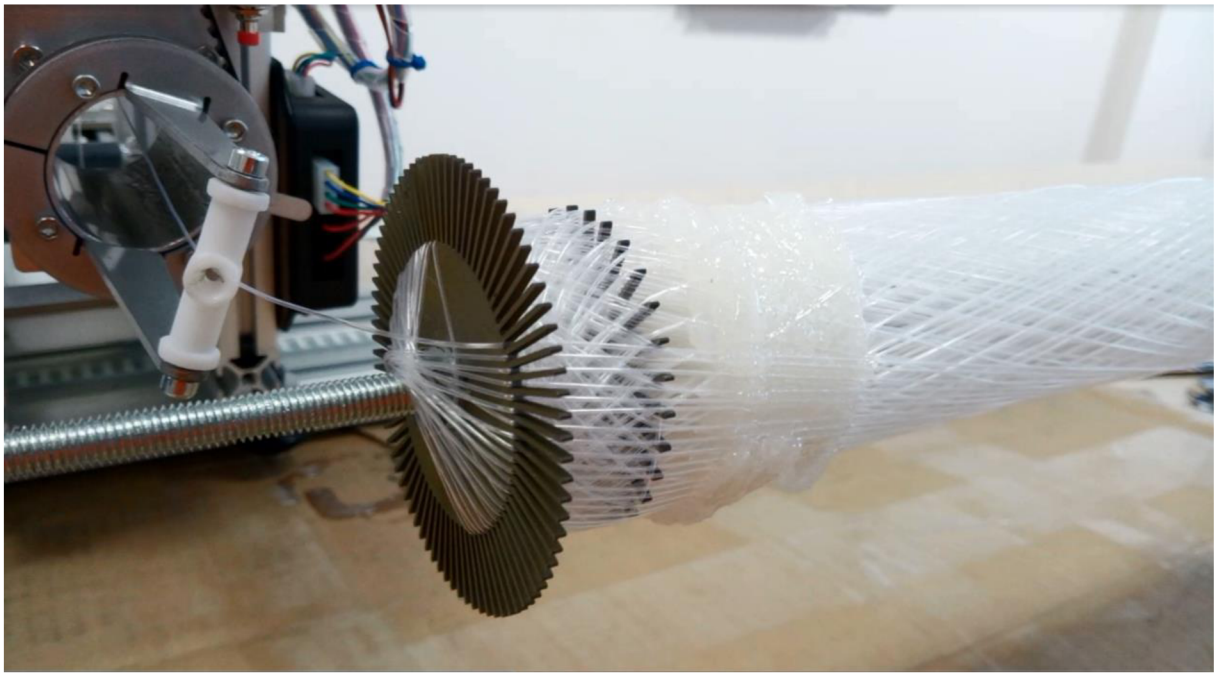

*Fig. 43 Using of sprockets at the PHFHE winding with the diameter increasing*

The third change concerned the management program. It was necessary to keep the fiber volume at the end sections constant and to fit each hollow fiber to exact sprocket groove. So, the G-code was completely rewritten. It took into account different speeds of feeding head movement while

forming the linear and ends sections, turns of the feeding head, the speed of the created PHFHE rotation and so on. An example of a G-code part is shown in Fig. 44. Each line of code corresponds to one action. For example, line 34 responds for the feeding head movement to the left end and during that movement the winding sample will be rotated at the angle of 80º.

```
[G-CODE GENERATED BY X-WINDER DESIGNER v417 on 11.30.2018 16:08]
[FileName= pokus.X4G ]
[Units are in MILLIMETERS ]
[FilePath= C:\Program Files (x86)\X-Winder\X-Winder40\XW_G-Code_Files\ ]
[GENERAL PART DESCRIPTION: LeftDia=70,0 RightDia=70,0 ]
[GENERAL PART DESCRIPTION: TotLen=370,00 FilaWidth=0,118 ]
[GENERAL PART DESCRIPTION: FilaThickness=0,0197 ]


[INITIALIZE WINDING SESSION -------------------------------- ]
C C1 [DECIMAL COMMA FORMAT = YES]
G21 [Units are Millimeters]
G90 [Absolute Positioning]
X V417,000 T4 Z47,752 [X-WINDER DESIGNER VERSION NUMBER, FILE TYPE, AND Z-AXIS MEAS. OFFSET DISTANCE]
M711 H0 M17 S0 [Estimated Total Build Time]

[ENABLE STEPPERS AND MOVE TO STARTING POSITION --------------- ]
M17 [Enable Steppers]
G1 I10 J10 K10 N10 O10 T10 [Linear and Angular Acceleration Settings of Axes]
G28 E50,800 R4 F25,400 C0,00 [Move Axes to Limit Switches]
G4 P10000 [Pause 1s at Carriage Limit Switch]
G1 J1,250 K1,250 O1,250 T10 [Set Axes Accels]
G4 Z P10000 [Pause 1000ms]
G1 F25,400 Z316,81 Y42 E25,400 B75,65 R10 S0

[BEGIN 4-AXIS WINDING WITH FLAT ENDS ---------------------------------------------------- ]
D0 ST=Winding Schedule
M0 [Wait for Button Press to Begin  Winding Schedule]
M601 [MARK THE MANDREL REFERFENCE ANGLE]

[START LAYER #1 ------------------------------------------------]
[Layer 1: Group 1/2 : Pass 1/36]
D0 LA=1_of_1 PA=1_of_72 RPM=10,64 CS=152,40 WA=14,35 WM=4AX TI=0 LD=70 FW=0,118 HL= [Display Layer Properties]
G1 F152,40 Z510,00 S10,64 C80,91 A154,95  [MOVE LEFT END]
G2 K40,00 F12,00 Z540,00 E73,30 Y10,00 R4,79 B40,60 U32,00 V30,00 H510,00 W10,00 S10,00 C165,00 A319,95 [CW ELLIPSE AT LEFT END]
G5 K2,00 F18,46 Z510,00 E19,69 Y42,00 R14,31 B-75,65 U32,00 V30,00 H510,00 W10,00 S4,00 C45,00 A364,95 [DH G5 WITHDRAWL LEFT END]
G1 F152,40 Z140,00 S10,64 C154,95 A519,91  [MOVE RIGHT END]
G3 K40,00 F10,00 Z115,00 E73,30 Y10,00 R5,48 B-35,54 U32,00 V25,00 H140,00 W10,00 S10,00 C165,00 A684,91 [CCW ELLIPSE AT RIGHT END]
G6 K2,00 F15,38 Z140,00 E19,69 Y42,00 R13,68 B75,65 U32,00 V25,00 H140,00 W10,00 S4,00 C45,00 A729,91 [DH G6 WITHDRAWL RIGHT END]

[Layer 1: Group 1/2 : Pass 2/36]
D0 LA=1_of_1 PA=2_of_72 RPM=10,64 CS=152,40 WA=14,35 WM=4AX TI=0 LD=70 FW=0,118 HL= [Display Layer Properties]
G1 F152,40 Z510,00 S10,64 C154,95 A884,86  [MOVE LEFT END]
G2 K40,00 F12,00 Z540,00 E73,30 Y10,00 R4,79 B40,60 U32,00 V30,00 H510,00 W10,00 S10,00 C165,00 A1049,86 [CW ELLIPSE AT LEFT END]
<
Ln 1 : 687  Col 1  Sel 0        58,2 kB        ANSI        CR+LF  INS  Default Text
```

*Fig. 44 Part of the G-code which controls motors of the X-Winder.*

The production of the heat exchanger is divided into three stages. The first is polymeric fibers winding and its sealing at the ends of the device. At this stage it was possible to set the number of fibers in the heat exchanger and the angle of their inclination relative to the axis of the heat exchanger. Simultaneously with the winding process, flooding of the hollow fibers took place to create the end sections. This method of casting is highly effective, because epoxide is applied to the end sections of the fiber gradually and evenly, better fills all cavities between the fibers. It prevents the formation of through microcracks between the fibers and epoxy, which can damage the tightness of the device. Also, one of the most important advantages of this manufacturing method is that during the entire cycle of heat exchanger winding one continuous filament is used. Appropriately, when the hollow fibers are flooded with epoxide, the penetration of the epoxide into the fibers is impossible, and when cutting off the ends of the heat exchanger, 100% of the fibers are open. Overall view of the heat exchanger inner part at the end of the first creation stage is shown in Fig. 45.

*Fig. 45 Inner part of PHFHE after first stage of creation*

At the second stage a shell of the heat exchanger is wound. The shell is created by winding fiberglass strip directly onto polymer hollow fibers. The fiberglass strip from the supply coil passes through the bath with epoxide, extra amount of epoxide is cut off with a special knife, and glass fiber is wound onto the heat exchanger through the delivery head. Winding of the heat exchanger shell is realized by several layers of winding fiberglass strip. The first layer consists of fiberglass wound at an angle close to 90° to the axis of the heat exchanger. This layer ensures the tightness of the heat exchanger. The next layer is wound at an angle of 20-30° to the axis of the heat exchanger and ensures rigidity and strength of the shell. At the end of the PHFHE shell production it consists of 3-4 layers of fiberglass interchanging each other. The heat exchanger shell made in such way is very durable and quite thin, about 2-3 mm. The main advantage of this method is to ensure reliable adhesion of the shell structure with the end-filled areas of the heat exchanger that eliminated a possible leak. External view of the PHFHE at the end of the second stage of creation is shown in Fig. 46.

*Fig. 46 External view of the PHFHE at the end of the second creation stage*

At the third stage the side sections are cut, and side flanges are glued. Side flanges have holes for the input and output of working fluids. The overall view of the PHFHE at the end of the third stage of creation is shown in Fig. 47.

*Fig. 47 External view of PHFHE in the end of the third part of the creations*

A scheme of the PHFHE wound by X-Winder is shown in Fig. 48. The first working fluid, passing through the central hole in the PHFHE side flange flows into the central tube, around which PHFHE was wound. The tube had special holes inside the heat exchanger. Separation walls preventing liquid to flow inside the tube were made. Thus, the shell water flows through the side flange hole inside the shell of the heat exchanger, flows around the fibers from the outside and goes out from the other end of the heat exchanger. The second working fluid, passing through an additional hole in the PHFHE side flanges, flows inside the polymeric hollow fibers.

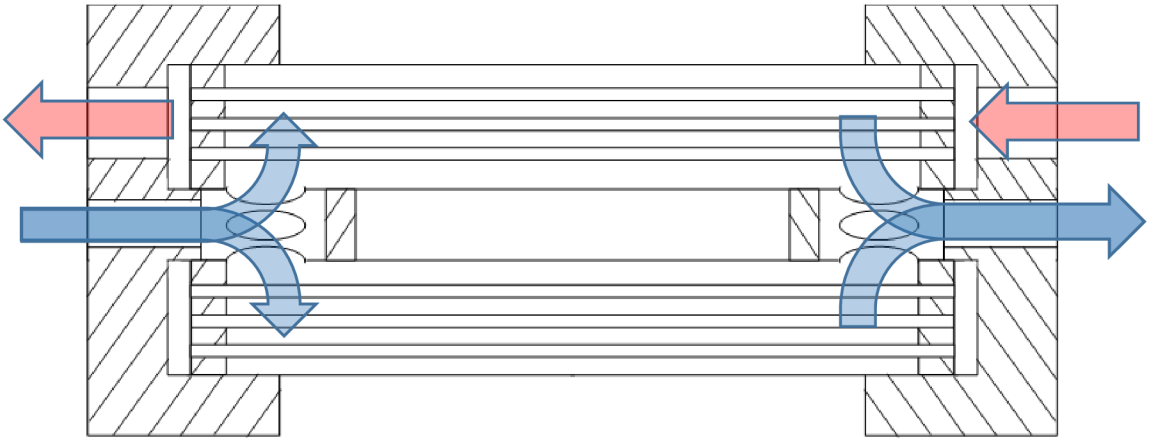

*Fig. 48 Scheme of the PHFHE*

The main advantage of the described method of polymeric heat exchanger creating is the following: based on this principle, it is possible to create serial production of shell and tube PHFHE. This production method can be fully automatized and one winding machine can create several heat exchangers at a once.

## 6.2 Strength pressure tests of prototype Wind-1

Before conducting a heat transfer experiments, it was necessary to verify the reliability of the created heat exchanger and evaluate its performance in terms of leak tightness. The heat exchanger shell was made of 4-layers of fiberglass strip. The main purpose of tests was to check whether this number of layers is capable to ensure sufficient body strength. PHFHE pressure tests were carried out with static and cyclic loading of increased pressure. For these purposes, a special stand was designed and created, the scheme of which is shown in Fig. 49. The stand allowed pressure testing with air or water at the given pressure. The Wind-1 connected to the stand is showed on the scheme by the number 10. The stand allows multiple samples to be connected at the same time. On the scheme 1 indicates an electromagnetic valve that serves as the main water shut-off in case of a leak, 2 represents a valve for manual closing of the water inlet, 3 indicates a manometer, 4 represents a three-stage water filtration, 5 corresponds to electromagnetic valve used for automatic water level filling, 6 is a pressure reducing valves and the pressure behind the reducing valve is indicatively monitored by means of a manometer 7, the testing itself is carried out by electromagnetic valves marked as 8 and 9, the exact pressure value is recorded by means of a manometer 11, 12 is a heater for heating the water bath in which the samples are tested, the temperature of the bath is recorded using Pt100 (13).

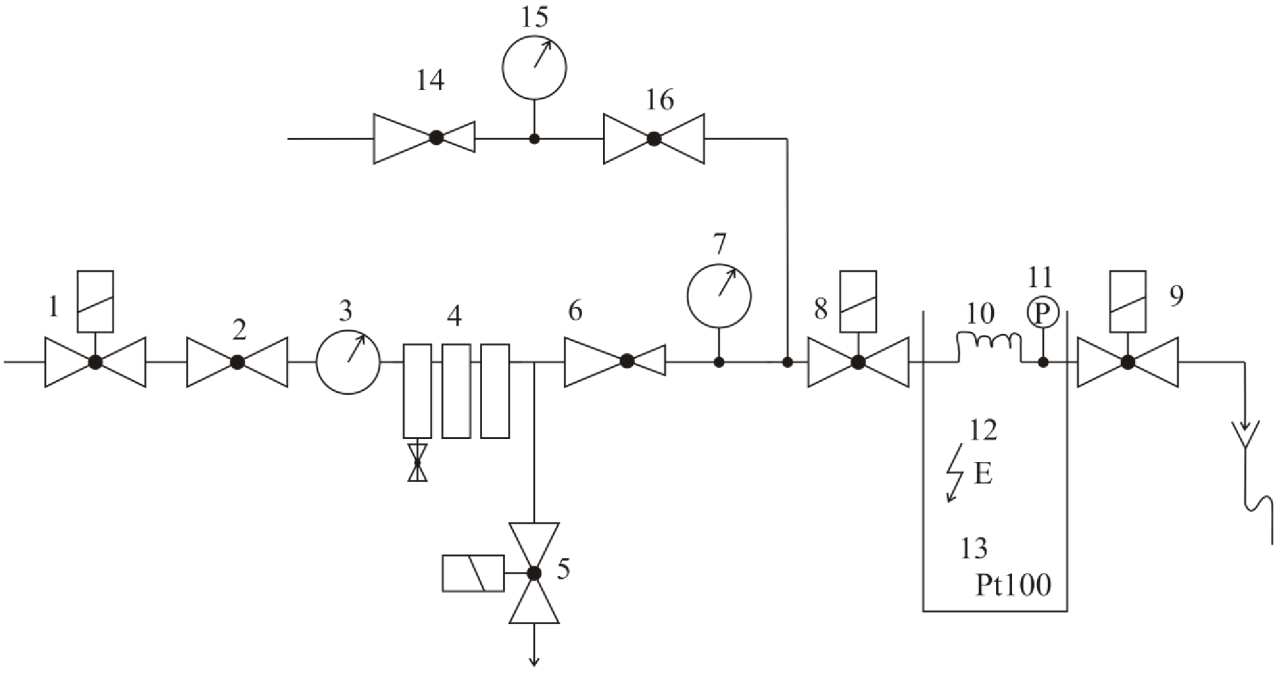


*Fig. 49 Scheme of the cycling testing facility [44]*

The typical pressure profile during the cycle tests in dependence on time is shown in Fig. 50. At point ①, the valve 9 was opened, the output valve 10 was closed. At this moment, the pressure increases inside the heat exchanger, it can be seen in ②. At point ③, the inlet valve 9 closes. After

a pause specified in the program, valve 10 opens and the pressure in the heat exchanger drops sharply to point ④.

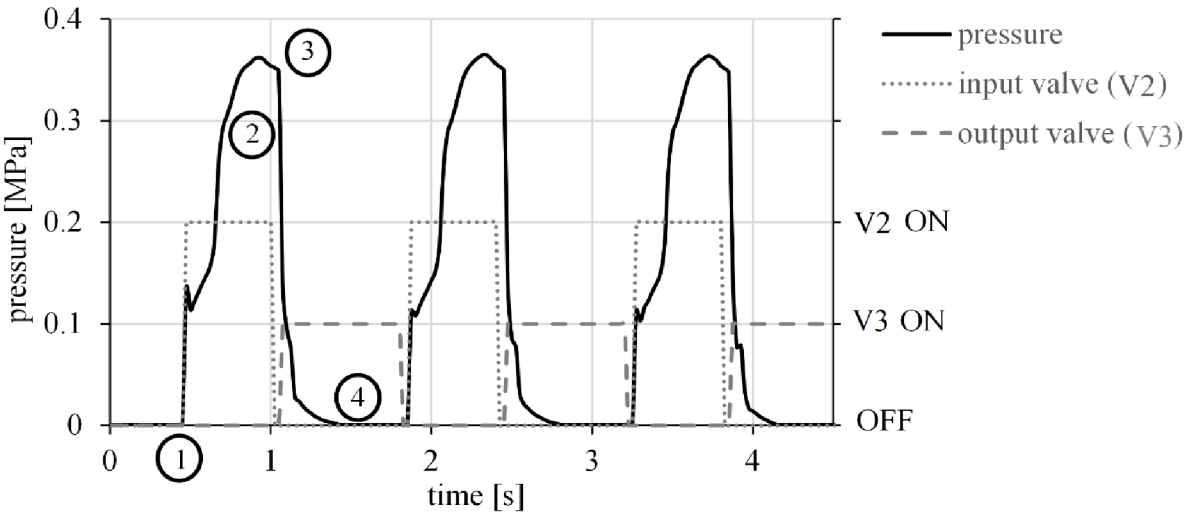


*Fig. 50 Sample of pressure test cyclogam [44]*

Pressure values, number of cycles, duration of one cycle, and other parameters were set via special program made in LabVIEW. General view of the stand is presented in Fig. 51.

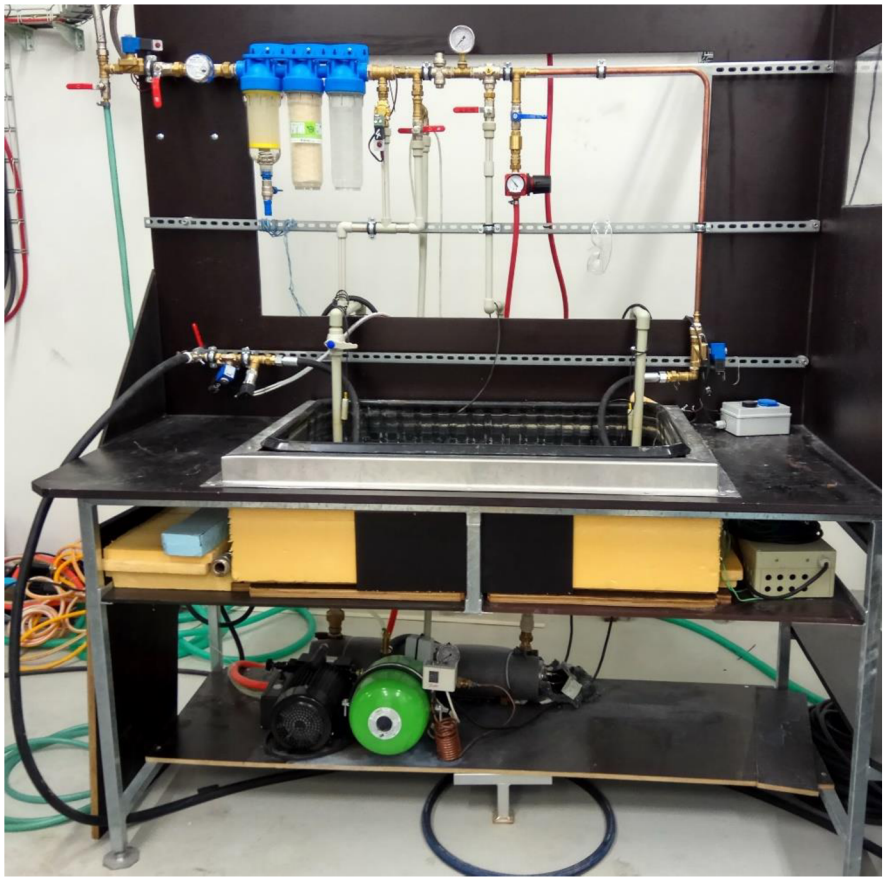

*Fig. 51 General view the cycling testing facility.*

This stand also allows pressure tests during thermal heating of the measured sample. For these purposes, the stand is equipped with a tank, containing water of the required temperature, which maintained constant during the entire test cycles. The water tank is equipped with sensors for registration the internal water level. During the experiment with high water temperature, water evaporates from the tank and automatic refiling system using these sensors keeps a water level constant during all experiment.

The stand was also equipped with a security system. In the case of test sample leaking this system immediately de-energizes the entire stand and releases pressure from the heat exchanger.

The cycling testing facility also can be used for static pressure tests of heat exchanger. It means that a constant pressure will be maintained in the sample throughout the experiment.

Prototype Wind-1 was made with the help of the modified winding system X-Winder especially for pressure test aiming to check the shell reliability and PHFHE leak tightness. A 350 mm long heat exchanger with a diameter of 80 mm was made of polyamide hollow fibers that were crossed at the angle of 22.5° to the axis of the heat exchanger. The flanges of PHFHE were made of metal, one of them did not have holes for the input/output of the working fluid, so that it was possible to make a pressure tests of the heat exchanger. The first pressure test was carried out at the air constant pressure of 3 bar, while the heat exchanger was immersed in a water tank with the water temperature of 60 °C, as shown in Fig. 52.

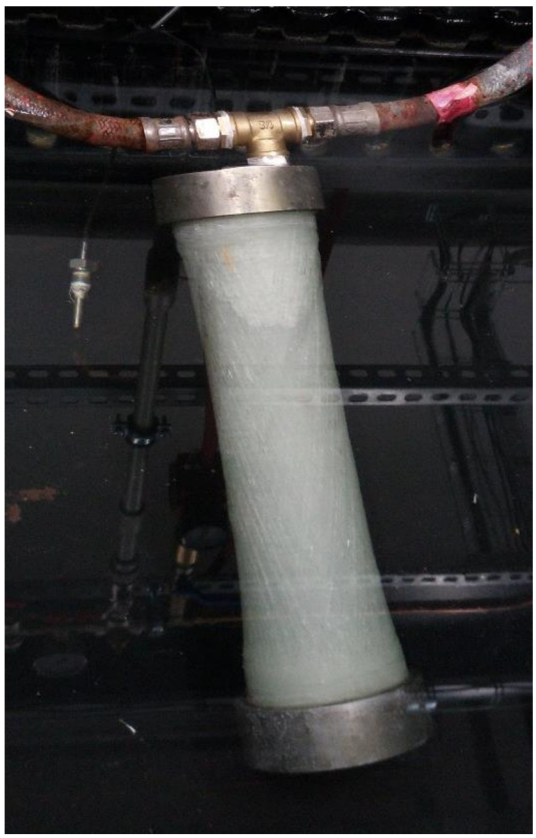

*Fig. 52 Prototype Wind-1 during the pressure tests.*

After 10 hours of Wind-1 testing at the junction of the shell and the metal flange a leak occurred (Fig. 53). This can be explained by the difference in the metal and fiberglass expansion coefficients. When Wind-1 was heated, in the junction of the shell and the flange can be form microcracks, which disrupted the tightness of the device. Based on this experiment, it was concluded that flanges of the PHFHE should be made of a material with a similar coefficient of expansion, like the fiberglass.

*Fig. 53 Leak location in PHFHE Wind-1 after static pressure tests*

Since one of the tests purposes was to check the fiberglass shell reliability, so the leak was resealed, and the heat exchanger was tested again. In this case, water was used as the test fluid, and the pressure inside the heat exchanger was 3.5 bar throughout the test. Wind-1 was no longer placed in water but was in air at a temperature of about 20 °C to avoid leak occurred due to the different expansion coefficient of materials. After 287 hours of testing, no leaks were detected. The test was stopped, and the test results were regarded as successful.

The next step was cyclic pressure tests. Tests were carried out at the air pressure with the peak value of 3 bar. The Wind-1 was immersed in water with a temperature of 20 °C. The heat exchanger was tested for a week, during this time 1747364 cycles were made, and no leaks were identified.

After this, a test was carried out with Wind-1 immersed in water with temperature of 60 °C and air pressure inside was equal to 6 bar in the maximum peak. After 100 cycles a small leak was found in the same place as shown in Fig. 53. Since the heat exchanger shell was still leak-proof, the tests were continued, and only after 7609 cycles, when more leaks between the shell and the metal side sections began to occur, the tests were stopped. No leaks were found in the shell.

These tests showed that the shell is reliable and ruggedized enough to withstand an impact of internal pressure in 6 bar. In this regard, it can be concluded that 4 layers of fiberglass provide the necessary strength and tightness of the PHFHE shell. The same tests showed that even at the prototype stage it is impossible to use metal flanges, due to the difference in expansion coefficients of the metal and fiberglass which leads to the occurrence of microcracks at the junction of the shell and the flanges and the leakage of the heat exchanger.

## 6.3 Prototype Wind-2 and its testing

With the help of the modified winding system X-Winder the second shell-and-tube PHFHE prototype Wind-2 shown in Fig. 54 was made. The outer diameter of the heat exchanger body was equal to 80 mm, length was equal to 350 mm. Inside the heat exchanger were 2200 PA fibers 206 mm long with an outer diameter of 0.8 mm, that were crossed at angle of 22.5 ° to the axis of the heat exchanger. Despite the relative compactness of devise, the heat exchange surface of the Wind-2 was 1.14 m².

Considering the negative test results of the prototype Wind-1 with metal flanges, for prototype Wind-2 they were made from fiberglass.

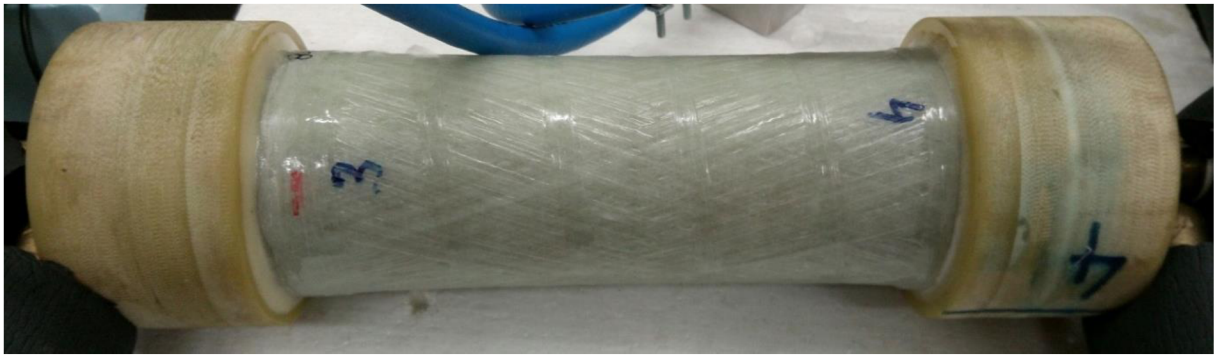

*Fig. 54 Hollow fiber heat exchanger prototype Wind-2*

The experiments were carried out under the following conditions: water flows into fibers with a temperature of 13°C and with a constant flow rate of 2160 l/h. The shell water flow rate varied from 390 l/h to 800 l/h with a step of 200 l/h. Experiments were carried out at two shell water temperatures - 70°C and 50°C. During the test, temperatures at the inlet and outlet of the heat exchanger shell, as well as at the inlet and outlet of the fibers, were measured. Pressure losses in the heat exchanger shell were measured by a differential manometer. Fig. 55 shows the PHFHE prototype Wind-2 installed in calorimeter chamber, where 1 is the heat exchanger itself, 2 is the inlet and outlet of warm water that will flow inside the fibers, 3 is the inlet of cold liquid into the heat exchanger shell, 4 is the outlet of cold water from the heat exchanger. Temperatures were measured using Pt-100

resistance thermometers installed inside the water inlet and outlet channels, that make it possible to achieve a measurement error of +/- 0.1 °C.

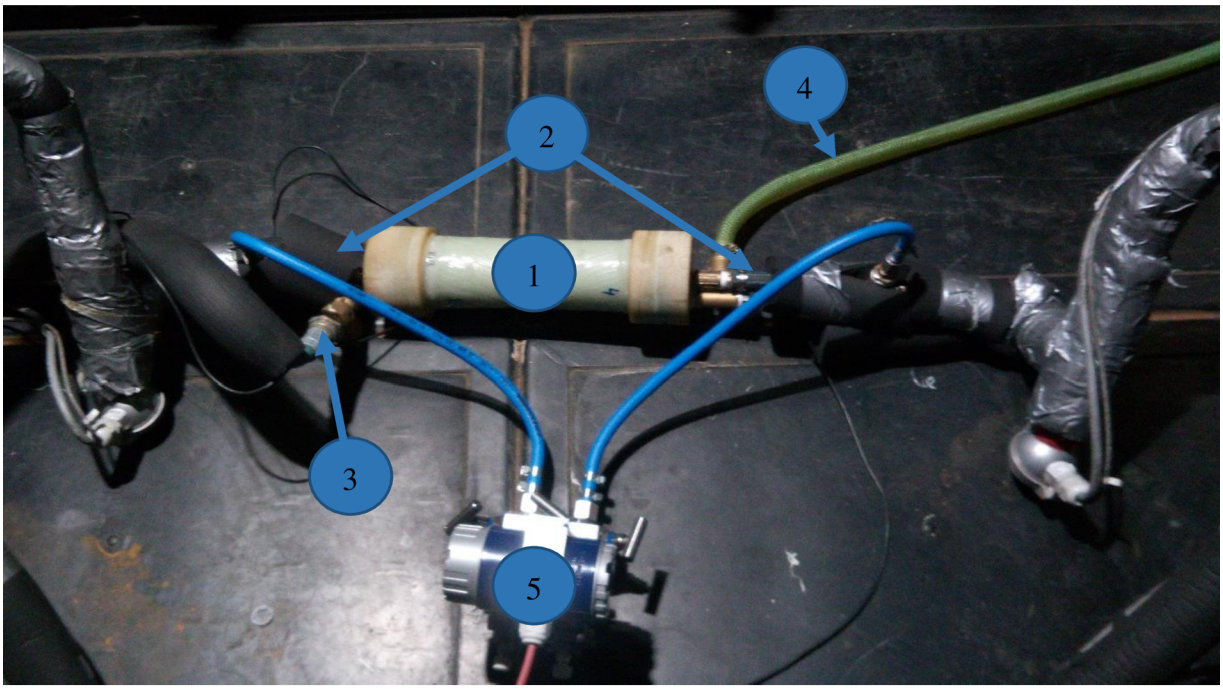


*Fig. 55 Hollow fiber heat exchanger Wind-2 installed in calorimeter chamber.*

Differential manometer is marked in Fig. 55 as a number 5 and it was used to measure the hydraulic losses inside the heat exchanger shell. The dependence of the pressure drop inside the heat exchanger on the shell water flow rate is shown in Fig. 56.

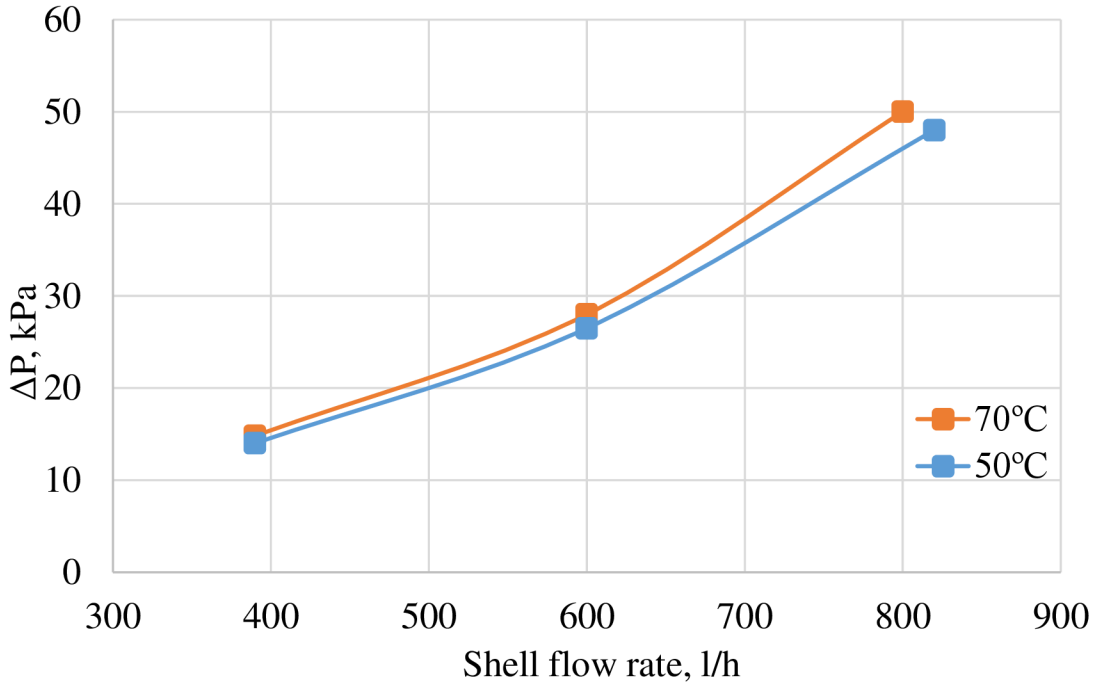


*Fig. 56 Dependence of the pressure drop inside the shell of Wind-2 on the shell water flow rate.*

It can be seen from Fig. 56 that pressure drop does not depend on the temperature of the liquid inside the fibers and at a maximum shell water flow rate of 800 l/h reaches a value of 0.5 bar. This is an acceptable value for shell-and-tube heat exchangers. The pressure drop in the Wind-2 heat exchanger is higher than in the previously tested PHFHE-2 (Fig. 38), in which polymeric hollow fibers were located at an angle of 22.5° to the axis of the heat exchanger and were fixed with the help of threads. However, it should be noted that the active heat transfer area in Wind-2 is more than two times higher than in the heat exchanger PHFHE-2. It means that inside the shell of Wind-2 is a greater amount of fibers and, correspondingly, a greater hydraulic resistance. However, this production method allows percussive setting of fibers amount inside the heat exchanger to achieve the optimal number for each application.

Fig. 57 shows the dependence of the Wind-2 heat transfer rate on the shell water flow rate. Curves are given for shell water temperature of 50°C and 70°C. Difference in heat transfer rate values for both water temperatures is about 27% and a maximum reached at shell water temperature of 70 °C is equal to 38 kW at shell water flow rate of 800 l/h.

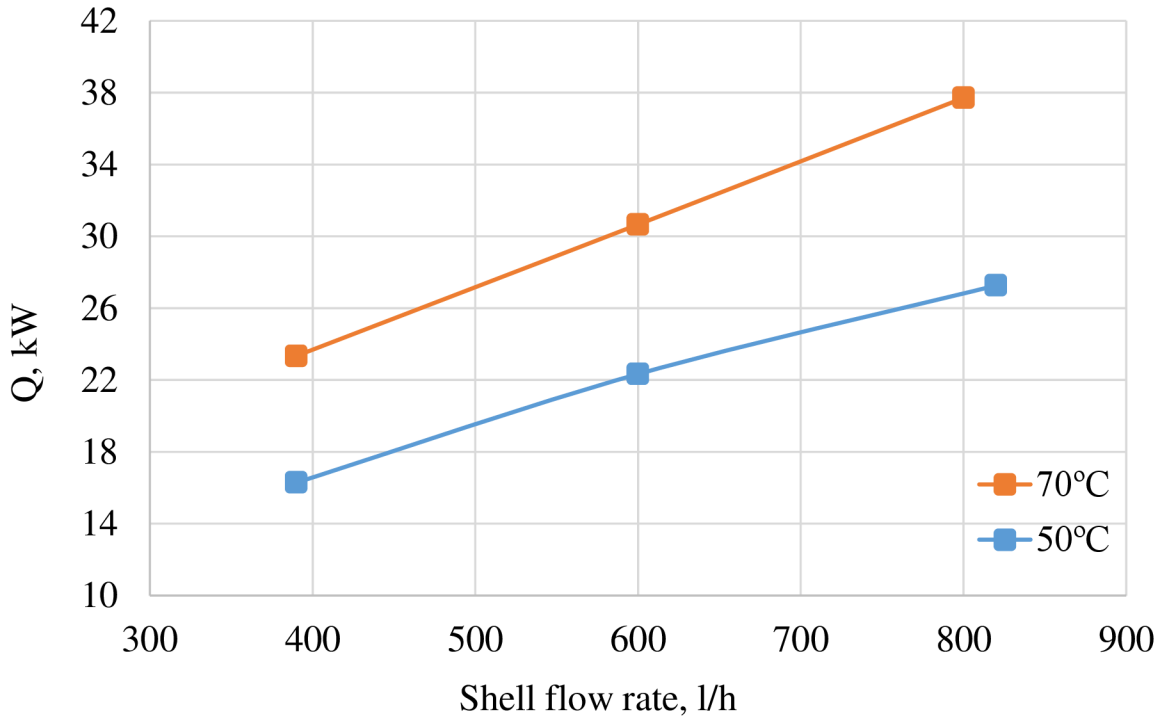


*Fig. 57 Dependence of the heat transfer rate of Wind-2 on the shell water flow rate.*

Fig. 58 shows dependence of the Wind-2 heat transfer coefficient on the shell water flow rate. It can be seen that heat transfer coefficients do not depend on shell water temperature and reach a maximum value of 1950 W/m²K at maximum shell water flow rate 800 l/h. This is a relatively high value. It means that the whole surface of hollow fibers in the shell is involved in heat transfer

process. Moreover, hollow fibers crossing inside the shell leads to better shell water intermixing and allows to achieve better heat transfer coefficients on an outer surface of hollow fibers.

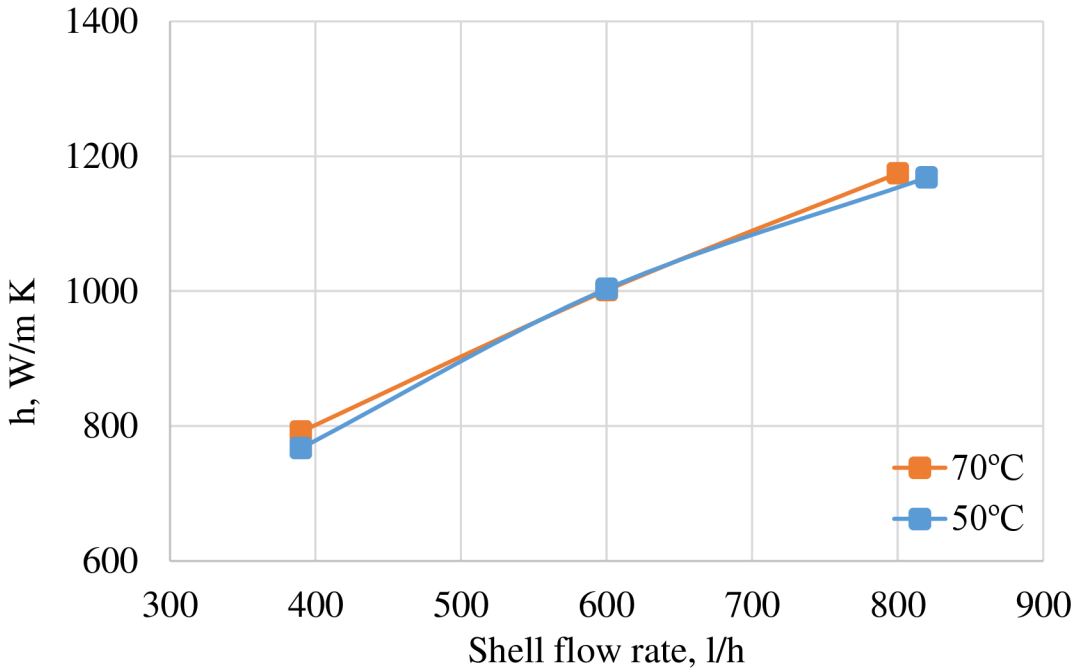


*Fig. 58 Dependence of the heat transfer coefficient of Wind-2 on the shell water flow rate.*

## *Intermediate conclusion*

PHFHE produced by the developed winding technology have shown very good results. At relative compactness such devices have a large heat transfer area that leads to a high heat transfer performance of the PHFHE. The use of materials with similar expansion coefficients allows PHFHE to withstand pressure up to 6 bar. This value can be increased by increase in number of shell layers during winding.

The possibilities of assembled equipment make it possible to wind several heat exchangers at the same time. So, this technology can by applied for PHFHE mass production.

# CONCLUSION

This thesis is dedicated to the optimization of heat exchangers in order to increase their thermal performance. Metal and polymeric heat exchangers intended for operation in air-water and water-water systems were considered.

The influence of heat pulses on the efficiency reduction of the commercial heat exchanger in fancoil used in building air-conditioning systems was investigated. The metal finned tube heat exchanger consisting of copper coil pipe with pressed aluminum fins as a working body of the fancoil was thermally cycled to simulate its actual operating conditions and find out a potential deterioration of the contact between the fins and the coil pipe. Test have shown that even 100 000 cycles of metal heat exchanger heating and its subsequent rapid cooling did not have a negative impact on the fancoil heat transfer rate. Has been confirmed that the contact between fins and the tube remains constant during heat exchanger's useful life and the vibration of finning is excluded. In this regard, the technology of manufacturing metal-heat exchangers with a copper coil pipe with pressed aluminum fins can be considered as optimal.

Most of the work is devoted to the optimization of a relatively new type of polymeric heat exchangers - polymeric hollow fiber heat exchangers (PHFHEs). These heat exchangers utilize hundreds of polymeric microchannels with the outer diameter smaller than 1.5 mm and the wall thickness about 0.1 mm as the heat transfer surface.

Experimental investigation has shown that the use of twisted hollow fiber bundles in water-air applications is perspective. For vertical heat exchangers with natural convection even the use of one twisted hollow fiber bundle can be enough to obtain high values of the heat transfer rate. Chimney effect can significantly increase the heat transfer rate of the heat exchanger.

Wide investigation of PHFHEs design of shell-and-tube type used for water-water application and their optimization were conducted. Study of PHFHE with parallel hollow fibers brought to light problems with fibers sticking and their irregular spacing in the shell due to the formation of compact structures. Such changes in the heat exchanger structure had led to decrease in the heat transfer efficiency of the PHFHE. Computer modeling with the help of ANSYS was used for searching the optimal hollow fiber arrangement inside the PHFHE. Modeling results have shown that the hollow fiber placement at the angle about 20°-30° leads to heat exchange intensification on the outer surface of the hollow fibers. Another advantage of such an arrangement of fibers consist in their volume separation what prevents fibers from sticking.

Tests of PHFHE with hollow fibers placed at the angle to the heat exchanger axis and interweaved by synthetic filament have shown that a strict arrangement of the fibers in the heat exchanger and the possibility of crossing them gives a significant positive effect on the thermal characteristics of the device. However, the use of such a synthetic filament is a quite expensive technology. Besides, during the operation of the heat exchanger, there is a possibility of the fibers wiping in the contact point with the filament.

To solve this problem the technology of pressure tanks winding was modified for producing crossed-wound hollow fiber heat exchanger – a new type of the PHFHE. The prototype produced by the developed winding technology with hollow fibers placed at the angle to heat exchanger axis have shown very good results. At relative compactness this device had a large heat exchange surface that led to a high heat transfer performance of the PHFHE. The prototype shell wound by this technology had withstood the pressure up to 6 bar. This value can be increased by increase in number of shell layers during winding.

The possibilities of assembled winding setup make it possible to wind several heat exchangers at the same time. The developed technology can by applied for crossed-wound PHFHEs mass production.

# REFERENCE


[1] LUKAKIN, Valentin, Michail SHATOV a Georgy KAMFER. *Teplotechnika*. Moscow: Vyshaja Shkola, 2000, 671 s.

[2] TANDA, Giovanni. Experiments on natural convection from two staggered vertical plates. *International Journal of Heat and Mass Transfer*. 1995, **38**(3), 533-543.

[3] TADIE FOGAING, M., L. NANA, O. CRUMEYROLLE a I. MUTABAZIA. Wall effects on the stability of convection in an infinite vertical layer. *International Journal of Thermal Sciences*. 2016, **100**, 240-247.

[4] PIS'MENNYI, E. An asymptotic approach to generalizing the experimental data on convective heat transfer of tube bundles in crossflow. *International Journal of Heat and Mass Transfer*. 2011, **54**(19–20), 4235–4246. DOI: doi:10.1016/j.ijheatmasstransfer.2011.05.021.

[5] WON, S., N. BURGESS, S. PEDDICORD a P. LIGRANI. Spatially resolved surface heat transfer for parallel rib turbulators with 45 deg orientations including test surface conduction analysis. *Journal of Heat Transfer*. 2004, **126**(2), 193-201. DOI: doi:10.1115/1.1668046.

[6] WEI, Ping, Tak-Shing CHAN, Rui NI, Xiao-Zheng ZHAO a Ke-Qing XIA. Heat transport properties of plates with smooth and rough surfaces in turbulent thermal convection. *Journal of Fluid Mechanics*. 2014, **740**, 28-46. DOI: 10.1017/jfm.2013.638. available from: http://www.journals.cambridge.org/abstract_S0022112013006381

[7] KIATPACHAI, Parinya, Santi PIKULKAJORN a Somchai WONGWISES. Air-side performance of serrated welded spiral fin-and-tube heat exchangers. *International Journal of Heat and Mass Transfer*. 2015, **89**, 724–732. DOI: doi:10.1016/j.ijheatmasstransfer.2015.04.095.

[8] MORI, Y., A. SHEĬNDLIN a A. KHALATOV. Heat transfer in high temperature heat exchanger channels with inlet flow swirling. *High temperature heat exchangers*. Washington, D.C.: Hemisphere Pub., 1986. ISBN 978-089116565-1.

[9] GVOZDIć, Biljana, Elise ALMÉRAS, Varghese MATHAI et al. Experimental investigation of heat transport in homogeneous bubbly flow. *Journal of Fluid Mechanics*. 2018, **845**, 226-244. DOI: 10.1017/jfm.2018.213. ISSN 0022-1120. available from: https://www.cambridge.org/core/product/identifier/S0022112018002136/type/journal_article

[10] NGUYEN, Tuyen, Subhasish MITRA, Mayur SATHE, Vishnu PAREEK, J.B. JOSHI a G.M. EVANS. Evaporation of a suspended binary mixture droplet in a heated flowing gas stream. *Experimental Thermal and Fluid Science*. 2018, **91**, 329-344. DOI:

10.1016/j.expthermflusci.2017.10.025. ISSN 08941777. available from: https://linkinghub.elsevier.com/retrieve/pii/S089417771730331X

[11] LATOUR, Benjamin, Pascale BOUVIER a Souad HARMAND. Convective heat transfer on a rotating finned cylinder with transverse airflow. *International Journal of Heat and Mass Transfer*. 2011, **54**(21-22), 4710–4718. DOI: doi:10.1016/j.ijheatmasstransfer.2011.06.006.

[12] FLORYAN, J. a Sahab ZANDI. Reduction of pressure losses and increase of mixing in laminar flows through channels with long-wavelength vibrations. *Journal of Fluid Mechanics*. 2019, **864**, 670-707. DOI: 10.1017/jfm.2019.21. ISSN 0022-1120. available from: https://www.cambridge.org/core/product/identifier/S0022112019000211/type/journal_article

[13] KHARVANI, H., F. DOSHMANZIARI, A. ZOHIR a D. JALALI-VAHID. An experimental investigation of heat transfer in a spiral-coil tube with pulsating turbulent water flow. *Heat and Mass Transfer*. 2015, , 1-11. DOI: 10.1007/s00231-015-1697-x. available from: http://link.springer.com/10.1007/s00231-015-1697-x

[14] XU, Hang, I. POP a Q. SUN. Fluid flow driven along microchannel by its upper stretching wall with electrokinetic effects. *Applied Mathematics and Mechanics*. 2018, **39**(3), 395-408. DOI: 10.1007/s10483-017-2307-7. ISSN 0253-4827. available from: http://link.springer.com/10.1007/s10483-017-2307-7

[15] LEI, Juanmian, Qingyang LIU a Tao LI. Suction control of laminar separation bubble over an airfoil at low Reynolds number. *Proceedings of the Institution of Mechanical Engineers, Part G: Journal of Aerospace Engineering*. 2017, **233**(1), 81-90. DOI: 10.1177/0954410017727025. ISSN 0954-4100. available from: http://journals.sagepub.com/doi/10.1177/0954410017727025

[16] REHMAN, Sajid, M. IDREES, Rehan SHAH a Zeeshan KHAN. Suction/injection effects on an unsteady MHD Casson thin film flow with slip and uniform thickness over a stretching sheet along variable flow properties. *Boundary Value Problems*. 2019, **2019**(1). DOI: 10.1186/s13661-019-1133-0. ISSN 1687-2770. available from: https://boundaryvalueproblems.springeropen.com/articles/10.1186/s13661-019-1133-0

[17] VILEMAS, Yu., G. VORONIN, B. DZUBENKO a G. DREICER. *Uspehi teploperedaci 2: Itentifikacia teploobmena*. Vilnius: Mokslas, 1988, 188 s.

[18] DOU, Hua-Shu, Gang JIANG a Lite ZHANG. A Numerical Study of Natural Convection Heat Transfer in Fin Ribbed Radiator. *Mathematical Problems in Engineering*. 2015, **2015**, 1-13. DOI: 10.1155/2015/989260. ISSN 1024-123x. available from: http://www.hindawi.com/journals/mpe/2015/989260/

[19] *Calorplast Waermetechnik* [online]. b.r. [cit. 2016-05-15]. Available from: www.calorplast-waermetechnik.de

[20] *Mersen* [online]. b.r. [cit. 2016-05-15]. Dostupné z: www.mersen.com

[21] JIA, L., X.F. PENG, J.D. SUN a T.B. CHEN. An experimental study on vapor condensation of wet flue gas in a plastic heat exchanger. *Heat Transfer Asian Research*. 2001, **30**(7), 571-580. DOI: 10.1002/htj.10000. ISSN 1099-2871. Available from: http://doi.wiley.com/10.1002/htj.10000

[22] LIU, Wei, Jane DAVIDSON a Susan MANTELL. Thermal Analysis of Polymer Heat Exchangers for Solar Water Heating: A Case Study. *Journal of Solar Energy Engineering*. 2000, **122**(2), 84-91. DOI: 10.1115/1.1288027. ISSN 01996231. Available from: http://SolarEnergyEngineering.asmedigitalcollection.asme.org/article.aspx?articleid=1455995

[23] ASTROUSKI, Ilya, Miroslav RAUDENSKÝ a Mirko DOHNAL. Fouling of polymeric hollow fiber heat exchanger by wastewater. *Chemical Engineering Transactions* [online]. 45. Italian Association of Chemical Engineering - AIDIC, 2015, **45**, 949-954 [cit. 2016-12-05]. DOI: 10.3303/CET1545159. ISBN 978-889560836-5. ISSN 22839216.

[24] CHEN, Xiangjie, Yuehong SU, David REAY a Saffa RIFFAT. Recent research developments in polymer heat exchangers – A review. *Renewable and Sustainable Energy Reviews*. 2016, **60**, 1367-1386. DOI: 10.1016/j.rser.2016.03.024. ISSN 13640321. Available from: https://linkinghub.elsevier.com/retrieve/pii/S1364032116002598

[25] ROUSSE, D.R., D.Y. MARTIN, R. THÉRIAULT, F. LÉVEILLÉE a R. BOILY. Heat recovery in greenhouses: a practical solution. *Applied Thermal Engineering*. 2000, **20**(8), 687-706. DOI: 10.1016/S1359-4311(99)00048-4. ISSN 13594311. Available from: http://linkinghub.elsevier.com/retrieve/pii/S1359431199000484

[26] MALIK, T a C BULLARD. Suitability of polymer heat exchangers for air conditioning applications. *College of Engineering, University of Illinois at Urbana-Champaign*. 2005, , 1-22.

[27] BROŽOVÁ, T.; RAUDENSKÝ, M.; BARTULI, E.; SLADKÁ, E.; DOHNAL, M. *Modul pro membránovou destilaci.* 32427. utility model 2018. Brno University of Technology, CZ ZENA s.r.o., Ostopovice, CZ

[28] ASTROUSKI, Ilja a Miroslav RAUDENSKY. The study of polymeric hollow fiber heat exchangers. *18th International Conference ENGINEERING MECHANICS, Svratka, Czech Republic*. 2012, , 47-57.

[29] ZARKADAS, Dimitrios, Baoan LI a Kamalesh SIRKAR. Polymeric Hollow Fiber Heat Exchangers (PHFHEs): A New Type of Compact Heat Exchanger for Lower Temperature Applications. *Heat Transfer: Volume 4*. ASME, 2005, , 429-438. DOI: 10.1115/HT2005-72590. ISBN 0-7918-4734-9. Available from: http://proceedings.asmedigitalcollection.asme.org/proceeding.aspx?articleid=1586589

[30] KRÁSNÝ, Ivo, Ilya ASTROUSKI a Miroslav RAUDENSKÝ. Polymeric hollow fiber heat exchanger as an automotive radiator. *Applied Thermal Engineering*. 2016, **108**, 798-803. DOI: 10.1016/j.applthermaleng.2016.07.181. ISSN 13594311. Available from: http://linkinghub.elsevier.com/retrieve/pii/S1359431116313254

[31] LEWIS, R., P. NITHIARASU a K. SEETHARAMU. *Fundamentals of the finite element method for heat and fluid flow*. Hoboken, NJ: Wiley, 2004, xi, 341 p. ISBN 978-0-470-84789-3.

[32] CONNOR, J a C BREBBIA. *Finite element techniques for fluid flow*. Boston: Newnes-Butterworths, 1976, 310 s. ISBN 04-080-0176-3.

[33] ZIENKIEWICZ, O. a R. TAYLOR. *The finite element method: Fluid Dynamics Vol.3*. Boston: Butterworth-Heinemann, 2000, 334 s. ISBN 07-506-5050-8.

[34] VERSTEEG, H. *An introduction to computational fluid dynamics: the finite volume method*. Harlow: Longman, 1995, 257 s. ISBN 05-822-1884-5.

[35] FERZIGER, Joel a Milovan PERIć. *Computational methods for fluid dynamics*. 3rd rev. ed. Berlin: Springer-Verlag, 2002, xiv, 423 s. ISBN 35-404-2074-6.

[36] DYSON, R.W., S.D. WILSON, R.C. TEW a R. DEMKO. Stirling analysis comparison of commercial VS. High-order methods. *Collection of Technical Papers - 3rd International Energy Conversion Engineering Conference*. 2005, **2**, 668-719.

[37] LI, Jie, Quan ZHANG a Zhi-qiang(John) ZHAI. An efficient segregated algorithm for two-dimensional incompressible fluid flow and heat transfer problems with unstructured grids. *International Journal of Heat and Mass Transfer*. 2019, **133**, 1052-1064. DOI: 10.1016/j.ijheatmasstransfer.2018.12.039. ISSN 00179310. Available from: https://linkinghub.elsevier.com/retrieve/pii/S0017931018341589

[38] GANESAN, T. a M. AWANG. Large Eddy Simulation (LES) for Steady-State Turbulent Flow Prediction. *Engineering Applications of Computational Fluid Dynamics*. 2015, , 17-32. DOI: 10.1007/978-3-319-02836-1_2. Dostupné také z: http://link.springer.com/10.1007/978-3-319-02836-1_2

[39] BARTULI, E. a M. RAUDENSKY. Numerical investigation of heat transfer on the outer surface of polymeric hollow fibers. *Materiali in tehnologije*. 2018, **52**(4), 459-463. DOI: 10.17222/mit.2016.221. ISSN 15802949. Available from: http://mit.imt.si/Revija/izvodi/mit184/bartuli.pdf

[40] ASTROUSKI, Ilja. *Polymeric Hollow Fiber Heat Exchanger Design*. Heat Transfer and Fluid Flow Laboratory, 2016, 91 s. PhD thesis. Faculty of Mechanical engineering, Brno University of Technology. Supervisor of doctoral thesis: Prof. Ing. Miroslav Raudenský, CSc.

[41] BARTULI, E., T. BROZOVA a M. RAUDENSKY. The Influence of Hollow Fibers Orientation Inside the Polymeric Hollow Fiber Heat Exchanger on the Heat Transfer Intensity. *Engineering Mechanics 2018*. Prague, 2018, , 61-64.

[42] RAUDENSKÝ, Miroslav, Ilya ASTROUSKI a Miroslav DOHNAL. Intensification of heat transfer of polymeric hollow fiber heat exchangers by chaotisation. *Applied Thermal Engineering* [online]. 2017, **113**, 632-638 [cit. 2016-11-23]. DOI: 10.1016/j.applthermaleng.2016.11.038. ISSN 13594311. Available from: http://linkinghub.elsevier.com/retrieve/pii/S1359431116330770

[43] *X-Winder* [online]. b.r. [cit. 2019]. Dostupné z: http://www.xwinder.com/

[44] BROŽOVÁ, Tereza. *Fázové změny na povrchu tepelných výměníků s dutými vlákny*. Heat Transfer and Fluid Flow Laboratory, 2018, 106 s. PhD thesis. Faculty of Mechanical Engineering, Brno University of Technology. Supervisor of doctoral thesis: Prof. Ing. Miroslav Raudenský, CSc.

# NOMENCLATURE

| | | |
|---|---|---|
| h | [W/m²K] | Heat transfer coefficient |
| $C$ | [-] | Constant |
| P | [kg/(m·s$^2$)] | Pressure |
| T | [K] | Temperature |
| $S$ | [m$^2$] | Area |
| $c$ | [J/K] | Heat capacity |
| $f$ | [N] | Mass forces |
| g | [m/s$^2$] | Acceleration of gravity |
| k | [J/kg] | Kinetic energy of turbulence |
| $l$ | [m] | Length |
| $q$ | [J] | Heat transfer rate |
| $w, U$ | [m/s] | Velocity |
| d | [m] | Diameter |

**Greek symbols**

| | | |
|---|---|---|
| $\beta$ | [K$^{-1}$] | Coefficient of volume expansion |
| δ | [m] | Thickness |
| $\varepsilon$ | [-] | Correction factor |
| $\lambda$ | [W/(m·K)] | Thermal conductivity |
| $\rho$ | [kg/m$^3$] | Density |
| $\varphi$ | [ ° ] | Angle |
| α, $\psi$ | [ ° ] | Flow attack angle |
| $\nu$ | [m$^2$/s] | Kinematic viscosity |
| μ | [kg/m·s] | Dynamic viscosity |
| $\chi$ | [m$^2$/s] | Thermal diffusivity |
| ω | [s$^{-1}$] | Specific turbulence dissipation rate |

**Indices**

| | |
|---|---|
| *f* | Fluid/Ambient |
| *p* | Pressure |
| w | Surface/Wall |
| *i/j* | Number |
| x,y,z | Axes |

# LIST OF FIGURES

# LIST OF TABLES

# AUTHOR PUBLICATIONS RELATED TO THE TOPICS OF THE THESIS

1) BROŽOVÁ, T.; BARTULI, E.; RAUDENSKÝ, M. Condensation on the Outer Surface of Polymer Hollow Fiber Heat Exchangers and its Influence to the Heat Transfer. *Engineering Mechanics 2018.* 2018. Praha: ITAM CAS, p. 117-120. ISBN: 978-80-86246-88-8.
2) BROŽOVÁ, T.; BARTULI, E. Influence of Condensation on the Outer Surface of Polymer Hollow Fiber Heat Exchangers during Heat Transfer. *ASME 2018 16th International Conference on Nanochannels, Microchannels, and Minichannels.* American Society of Mechanical Engineers, 2018. 1-6. ISBN: 978-0-7918-5119-7.
3) BARTULI, E.; BROŽOVÁ, T.; RAUDENSKÝ, M. The Influence of Hollow Fibers Orientation Inside the Polymeric Hollow Fiber Heat Exchanger on the Heat Transfer Intensity. *Engineering Mechanics 2018*. 2018. 61-64. ISBN: 978-80-86246-88-8.
4) BARTULI, E. a M. RAUDENSKY. Numerical investigation of heat transfer on the outer surface of polymeric hollow fibers. *Materiali in tehnologije*. 2018, **52**(4), 459-463. DOI: 10.17222/mit.2016.221. ISSN 15802949. Available from: http://mit.imt.si/Revija/izvodi/mit184/bartuli.pdf
5) RAUDENSKÝ, M.; BROŽOVÁ, T.; BARTULI, E. Flexible heat exchangers with polymeric hollow fibres. *Scientific Tracks and Abstracts*. *Journal of Applied Mechanical Engineering*. Paris, Francie: 2017. 31-31. ISSN: 2168-9873.
6) BARTULI, E.; RAUDENSKÝ, M. Numerical Investigation of Heat Transfer on the Outer Surface of Polymeric Hollow Fibers. 24th INTERNATIONAL CONFERENCE ON MATERIALSAND TECHNOLOGY. Ljubljana, Slovenia: Inštitut za kovinske materiale in tehnologije, 2016. p. 37-37. ISBN: 978-961-94088-0-3.
7) RAUDENSKÝ, M.; ASTROUSKI, I.; BROŽOVÁ, T.; BARTULI, E. Flexible Polymeric Hollow Fiber Heat Exchangers for Electronic Systems. *Thermal and Thermomechanical Phenomena in Electronic Systems ITherm 2016*. 2016. 2010 IEEE. USA: IEEE1143-1147. ISBN: 978-1-4799-5266-3. ISSN: 1087-9870.

**UTILITY MODEL**

1) BROŽOVÁ, T.; RAUDENSKÝ, M.; BARTULI, E.; SLADKÁ, E.; DOHNAL, M. *Modul pro membránovou destilaci.* 32427. utility model 2018. Brno University of Technology, CZ ZENA s.r.o., Ostopovice, CZ

# OTHER AUTHOR PUBLICATIONS


1) BARTULI, E.; GUZEJ, M.; KOMÍNEK, J.; HORSKÝ, J. Experimental Investigation of a Heat Transfer Coefficient for Aluminum Alloys. *Heat Pipes, Heat Pumps, Refrigerators, Power Sources*. Minsk: A.V. Lykau Institute of Heat and Mass Transfer of the National Academy of Sciences of Belarus, 2015. 56-62. ISBN: 978-985-6456-99-5.
2) LUKS, T.; HORSKÝ, J.; BARTULI, E. Experimentální stanovení teplotních a silových poměrů ve válcovací mezeře. *Hutnické listy*, 2015, vol. LXVIII, no. 4, 9-14. ISSN: 0018-8069.
3) GUZEJ, M.; BARTULI, E.; KRIŠTOF, O. Water jet cooling of aluminium alloy. *IMETAL 2015, 24rd International Conference on Metallurgy and Materials, Conference Proceedings.* Ostrava: TANGER Ltd., 2015. p. 1439-1444. ISBN: 978-80-87294-58- 1.
4) BARTULI, E., S. VERSHININ a Yu. MAYDANIK. Visual and instrumental investigations of a copper–water loop heat pipe. *International Journal of Heat and Mass Transfer*. 2013, **61**, 35-40. DOI: 10.1016/j.ijheatmasstransfer.2013.01.074. ISSN 00179310. Available from: https://linkinghub.elsevier.com/retrieve/pii/S0017931013001051
5) BARTULI, E. Investigation of water condensation in a flap gap condenser of a loop heat pipe. *Proc. of XIX school-seminar of young scientists and specialists under the guidance of the academic RAS A.I. Leontiev "The problems of gas dynamics and heat and mass transfer in power installation"*. 2013. Orehovo-Zyevo, Russia, 239-240.
6) BARTULI, E. Film condensation in a flap gap condenser of a copper-water loop heat pipe. *Proc. of XIII Russian Youth School-Seminar on Physics of Condensed State of Matter.* 2012. Ekaterinburg, Russia, 79.
7) BARTULI, E., CHERNYSHEVA, M., VERSHININ, S., MAYDANIK, Yu. Heat transfer during condensation in a flat gap condenser of a loop heat pipe with the guide inserts. *Thermal processes in engineering*. 2012. **9**, 413-417.
8) BARTULI E. Visual and instrumental investigations of a copper-water loop heat pipe. *Proc. of II Information school of the young scientist*. 2012. Ekaterinburg, Russia, 238-247.
9) BARTULI, E., VERSHININ, S., MAYDANIK, Yu. Visual and instrumental investigations of a copper-water loop heat pipe. *Proc. of 16th International Heat Pipe Conference.* 2012. Lyon, France, 111-116.
10) BARTULI, E., CHERNYSHEVA, M., VERSHININ, S., MAYDANIK, Yu. Investigation of the guide insertions influence on the condensation of water in a narrow gap condenser of a loop heat pipe. *Proc. of 8th Minsk International Seminar "Heat Pipes, Heat Pumps, Refrigerators, Power Sources".* 2011. Minsk, Belarus, **2**, 11-17.
11) CHERNYSHEVA, M, BARTULI, E., MAYDANIK, Yu. Thermal processes in gap condenser of a copper-water LHP. *Thermal processes in engineering.* 2010. **2(8)**, 354-363.

12) BARTULI, E., VERSHININ, S., MAYDANIK, Yu. Investigation of the influence of guide inserts on the intensity of heat transfer during condensation in a flat gap condenser of a loop heat pipe. *Proc. of XI Russian Youth School-Seminar on Physics of Condensed State of Matter*. 2010. Ekaterinburg, Russia, 63.

13) BARTULI, E., CHERNYSHEVA, M., VERSHININ, S., MAYDANIK, Yu. Investigation of a vapor condensation in a flat gap condenser of a loop heat pipe. *Proc. of 5th Russian National Conference on Heat Exchange*. 2010. Moscow, Russia, **4**, 202-205.

14) CHERNYSHEVA, M, BARTULI, E., VERSHININ, S., MAYDANIK, Yu. Investigation of heat transfer in the condenser of a loop heat pipe. *Proc. of 15th International Heat Pipe Conference*. 2010. Clemson, USA.

15) BARTULI, E., VERSHININ, S., MAYDANIK, Yu. Investigation of the effect of the heat sink temperature on the intensity of heat exchange during water condensation in a flat gap condenser of a loop heat pipe. *Proc. of X Russian Youth School-Seminar on Physics of Condensed State of Matter*. 2009. Ekaterinburg, Russia, 198.

16) BARTULI, E., VERSHININ, S., Investigation of the structural properties of nickel capillary-porous structures. *Proc. of IX Russian Youth School-Seminar on Physics of Condensed State of Matter*. 2008. Ekaterinburg, Russia, 55.

**PATENTS**

2) VERSHININ, S., BARTULI, E., MAYDANIK, Yu. Patent RU 124377 U1 “Condenser of a loop heat pipe”, 2012.

3) MAYDANIK, Yu., BARTULI, E., VERSHININ, S. Patent RU 141207 U1 “Condenser of a loop heat pipe”, 2014.